

Guided Wave Optics Laboratory

Report No. 61

Active Antennas with Periodic Structures

by

Kuang Yi Chen

October 1994

19941227 071

Report No. 61

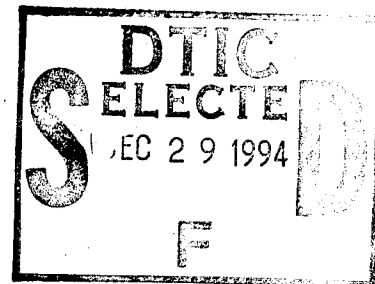
Active Antennas with Periodic Structures

by

Kuang Yi Chen

October 1994

Guided Wave Optics Laboratory
Department of Electrical and Computer Engineering
University of Colorado at Boulder
Boulder, Colorado 80309-0425



This document has been approved
for public release and sale; its
distribution is unlimited.

This work was supported by the Army Research Office under Grant #DAAL-03-92-G-0289 and by the Office of Naval Research under Grant #DOD-ONRN00014-92-J-1190.

unclassified

SECURITY CLASSIFICATION OF THIS PAGE

REPORT DOCUMENTATION PAGE

Form Approved
OMB No. 0704-0188

1a. REPORT SECURITY CLASSIFICATION unclassified		1b. RESTRICTIVE MARKINGS none	
2a. SECURITY CLASSIFICATION AUTHORITY DISCASS		3. DISTRIBUTION / AVAILABILITY OF REPORT unrestricted	
2b. DECLASSIFICATION / DOWNGRADING SCHEDULE N/A			
4. PERFORMING ORGANIZATION REPORT NUMBER(S) ECE/GWOL/61		5. MONITORING ORGANIZATION REPORT NUMBER(S) DOD-ONRN00014-92-J-1190	
6a. NAME OF PERFORMING ORGANIZATION University of Colorado	6b. OFFICE SYMBOL (if applicable)	7a. NAME OF MONITORING ORGANIZATION Office of Naval Research Attn: Dr. Arthur Jordan, Code 1114 SE	
6c. ADDRESS (City, State, and ZIP Code) Electrical & Computer Engineering Dept. Boulder, CO 80309-0425		7b. ADDRESS (City, State, and ZIP Code) 800 N. Quincy Avenue Arlington, VA 22217-5000	
8a. NAME OF FUNDING / SPONSORING ORGANIZATION Office of Naval Research	8b. OFFICE SYMBOL (if applicable)	9. PROCUREMENT INSTRUMENT IDENTIFICATION NUMBER	
8c. ADDRESS (City, State, and ZIP Code) 800 N. Quincy Avenue Arlington, VA 22217-5000		10. SOURCE OF FUNDING NUMBERS	
		PROGRAM ELEMENT NO.	PROJECT NO.
		TASK NO.	WORK UNIT ACCESSION NO.
11. TITLE (Include Security Classification) (u) Active Antennas with Periodic Structures			
12. PERSONAL AUTHOR(S) Kuang Yi Chen			
13a. TYPE OF REPORT technical (PhD thesis)	13b. TIME COVERED FROM _____ TO _____	14. DATE OF REPORT (Year, Month, Day) October 1994	15. PAGE COUNT 130
16. SUPPLEMENTARY NOTATION			
17. COSATI CODES		18. SUBJECT TERMS (Continue on reverse if necessary and identify by block number)	
FIELD	GROUP		
19. ABSTRACT (Continue on reverse if necessary and identify by block number) Integration of a solid-state transistor oscillator with a radiative element has many advantages: it eliminates the feed network, replaces the expensive waveguide transition, reduces the size of the antenna system, and provides active impedance matching. Active devices also offer promise for optical control of beam steering antenna arrays. The objective of this thesis is to determine the physical characteristics of an active antenna and understand its operational principles.			
20. DISTRIBUTION / AVAILABILITY OF ABSTRACT <input checked="" type="checkbox"/> UNCLASSIFIED/UNLIMITED <input type="checkbox"/> SAME AS RPT. <input type="checkbox"/> DTIC USERS		21. ABSTRACT SECURITY CLASSIFICATION unclassified	
22a. NAME OF RESPONSIBLE INDIVIDUAL Alan R. Mickelson		22b. TELEPHONE (Include Area Code) 303/492-7539	22c. OFFICE SYMBOL

THIS DOCUMENT IS UNCLASSIFIED

ACTIVE ANTENNAS WITH PERIODIC STRUCTURES

By

Kuang Yi Chen

B.S., South China Institute of Technology, 1982

M.S., South China Institute of Technology, 1986

M.S., Idaho State University, 1989

A thesis submitted to the
Faculty of the Graduate School of the
University of Colorado in partial fulfillment
of the requirement for the degree of
Doctor of Philosophy
Department of Electrical Engineering

1994

This thesis for the Doctor of Philosophy degree by

Kuang Yi Chen

has been approved for the Department of Electrical Engineering

By

Accession For	
NTIS CRA&I	<input checked="" type="checkbox"/>
DTIC TAB	<input type="checkbox"/>
Unannounced	<input type="checkbox"/>
Justification	
By	
Distribution/	
Availability Codes	
Dist	Avail and/or Special
A-1	

Alan R. Mickelson

Alan R. Mickelson

Jon R. Sauer

Jon Sauer

Date 7/15/99

Chen, Kuang Yi (Ph.D., Electrical Engineering)

Active Antennas with Periodic Structures

Thesis directed by Professor Alan R. Mickelson

Integration of a solid-state transistor oscillator with a radiative element has many advantages: it eliminates the feed network, replaces the expensive waveguide transition, reduces the size of the antenna system as well as providing active impedance matching. active devices also offer promise for optical control of beam steering antenna arrays. The objective of this thesis is to determine the physical characteristics of an active antenna and understand its operational principles.

In our investigation of the active antenna, a noninvasive in-situ optical sampling measurement technique is applied. Several active antennas and antenna arrays were fabricated on GaAs substrates. HEMTs and MESFETs in the chip form were used as the active elements for these devices. The real time potential distributions on the active antenna structure were obtained. A Green's function for the charge on a thin dielectric substrate was developed for interpreting the experimental results. Numerous simulations of the antenna operation were performed and compared to the measurements. The operation mode of the antenna is identified within some degree of certainty.

An optical sampling technique is developed to determine the guided-wave circuit parameters which are inaccessible to other microwave measurements. Sampling an active radiating structure provides us with the opportunity to analyze the active antenna. A single active antenna with the same geometry as a single array element was built and experimentally characterized. It was found that the single

active antenna has the same form of potential distribution, same stability condition, and the difference in oscillation frequency are within the locking range (which is about 0.4 % of the oscillation frequency in our case). The same bias dependency is also found in a single antenna and an array. Sampling data on various sizes of the active array indicated that there is no edge effect for the finite array. The evaluations of the optical sampling combined with microwave measurements indicate that the oscillation condition of the antenna is determined by the geometry within the spacing of the grid elements, which are periodic. Coherent operation of the array is achieved by mutual coupling between the neighboring active elements. In short, the active antenna in the periodic structure is found to behave as a coupled oscillator array. Even though there is a lack of a ground in the back side of the antenna, an open cavity formed by placing a mirror in front of the array functions as an external cavity. As long as the mirror is further than half a wavelength away, the presence of the mirror would not affect the oscillation condition of the antenna. Thereby, the optimization procedure of the active array can start with optimization of a single active antenna. The performance of the array can be analyzed through coupled oscillator theory.

An experimental technique for determining the Van der Pol parameters of a single active antenna is derived. A simple analytical formula is presented for obtaining a damping constant of the active antenna. Experimental results agree with the analytical solution. With the aid of the Van der Pol coupled oscillator theory, the fundamental limit of the size and output power of the active antenna array can be defined. The approach should be useful for future design of active antenna arrays.

ACKNOWLEDGMENTS

Many people have assisted in this work. First and foremost, I would like to express my gratitude to Prof. Alan Mickelson, whose unwavering support and guidance in the ever changing frontier of science and technology has been essential to this work. I also wish to acknowledge the Army Research Office and Office of Naval Research for the financial support and interest in this project.

Many thanks go to the people who have assisted in this project; Dr. Dag Hjelme, for his precious work of the optical sampling system and excellent technical assistance during the experiments; Dr. Zoya Popovic for the valuable suggestion during the first stage of the fabrication of the devices; Mr. David Pannan of the Ball Aerospace company for his help with device bounding; and Mr. Steve Buchheit and Mr. Stephen Kwiatkowski for helpful discussions and suggestions.

Special thanks to Dr. Jon Sauer, for his advice, support and introducing me into the world of optics; Ms P. Bowman for her friendship and English editing and Dr. D. Lenschow for proofreading this thesis.

I am also grateful for the members of my thesis committee Dr. J. Pankove, Dr. F. Barnes, Dr. Y. C. Lee for their time and interest in this work.

My study in this country could not possible without the encouragement, and support from my uncle and aunt Mr. & Mrs. Chan Chart Man. Thanks also go to friends that I can not individually name here. Finally, I would like to thank my husband Dr. Mark Hanna for his love, companionship and helping me stick to the bitter and yet sweet end of this graduate study.

CONTENTS

CHAPTER

1. INTRODUCTION

1.1. Statement of Purpose.....	1
1.2. History of Active Antennas.....	5
1.3. Self-resonant Active Antennas in the Periodic structures.....	10
1.4. Organization of the Thesis.....	15

References.....	17
-----------------	----

2. APPLICATION OF ACTIVE PHASED ARRAYS

2.1. Introduction.....	21
2.2. Beam Steering for Passive Arrays.....	21
2.3. Optical Control Beam Steering for Active Arrays.....	22

References.....	28
-----------------	----

3. INVESTIGATIONS OF ACTIVE ANTENNAS AND ACTIVE PHASED ARRAYS

3.1 Introduction.....	30
3.2. Optical Sampling and What It Measures.....	32
3.3. Mathematical Relations between the Potential and Charge Distributions.....	34
3.4. Device Fabrication and Electrical Characteristics.....	37
3.5. Optical Sampling Measurements.....	48
3.6. Summary.....	60

References.....	62
-----------------	----

4. ANALYSIS OF OPTICAL SAMPLING DATA	
ON RADIATIVE STRUCTURES	
4.1. Introduction.....	63
4.2. Potential Distribution of a Single Active Antenna.....	64
4.3. Models of Operation Mode of an Antenna array.....	84
4.4. Summary.....	85
References.....	88
5. AN EXPERIMENTAL TECHNIQUE FOR DETERMINATION OF	
VAN DER POL PARAMETERS OF A TRANSISTOR OSCILLATOR	
5.1. Introduction.....	89
5.2. VDP Equation for a Self-Sustained Transistor Oscillator.....	92
A) Instability of a Radiating Oscillator.....	92
B). Saturation of a Radiating Oscillator.....	94
5.3. Theory for Determination of the VDP Parameters Experimentally...	103
5.4. Results and Discussion.....	110
5.5. Summary.....	116
References.....	118
6. CONCLUSION AND SUGGESTIONS FOR FUTURE WORK.....	120
BIBLIOGRAPHY.....	124

Tables

Table

4.1. Comparison of calculated potential distribution fromthe measured distribution.	70
---	----

FIGURES

Figure

Figure 1.1. Small antenna with wideband coupling tube, used in a broadcast receiver.	6
Fig. 1.2. The active transmitting antenna. (a) Fed-base emitter loop (FBEL) and (b) Fed-emitter base loop (FEBL).	6
Fig. 1.3. Schematic illustration of a two-dimensional active array antenna (a), and side view of the array (b).	12
Fig. 1.4. Sketch of surface emitting lasers. (a), the surface distributed feedback (SEDFB). (b), the grating surface emitting laser (GSEL) in top and side view.	14
Figure 2.1. Block diagrams of control schemes for the active phased array.	23
Figure 2.2. Diagram of complete electronic beam steering of active array antennas.	24
Figure 2.3. The schematic diagram of optical beam steering for an active phased array.	27
Figure 3.1. Schematic depiction of the device under test defining the coordinate system and sampling geometry.	33
Figure 3.2. Schematic depiction of the device under test of Figure 3.1, with the surfaces upon which $\sigma(x)$ and $V_1(x)$ (top surface) and $V_3(x)$ are labeled.	35
Figure 3.3. The structure of single active antenna.	38
Figure 3.4. The structure of an archetypal active antenna array.	39
Figure 3.5. Illustration of a experimental set up for measuring the microwave characteristics of active antennas.	41
Figure 3.6a. The radiated power of the single active antenna versus bias voltages.	42
Figure 3.6b. The effect of the bias voltages on the oscillation frequency of the active antenna.	43

Figure 3.6c. The comparison of the radiated power between the 25 HEMT element array and a single active HEMT antenna as it changes with the mirror distance.	44
Figure 3.7a. The comparison of the radiated power of two active antennas \ with different active elements.	46
Figure 3.7b. The oscillation frequencies of single active antenna versus mirror distance.	47
Figure 3.8. The optical sampling arrangement for measuring (a) the amplitude and (b) the phase of potential distribution.	49
Figure 3.9. A schematic diagram of two-dimensional optical sampling for measuring the amplitude potential distribution.	52
Figure 3.10(a-f). Some of the measured potential distributions along a column of the active HEMT array are obtained from non-invasive optical sampling. A potential distribution along (a) a gate radiating lead; (b) a drain radiating lead between two active elements;(c) a gate radiating lead between two active elements;(d) a drain radiating lead; (e) a source bias line of two active elements, and (f) a gate bias line of two active elements.	53
Figure 3.10g. A two-dimensional distribution of the potential in an elementary cell of the 25-HEMTs arrays.	56
Figure 3.11a. Measurements of the potential distribution of a single MESFET active antenna. (a), potential distribution along (a) the drain radiating lead; (b) the gate radiating lead, and (c) the source bias line.	58
Figure 4.1. Assumed potential distribution of V_1 in case 1. Case 2 has the same distribution profile except the value on the source bias lines are set to equal to -1.25V.	67
Figure 4.2. Assumed potential distribution of V_1 in case 4. Case 3 has a similar distribution profile except the value on the gate, drain and source bias lines are set to equal to 0 V.	68
Figure 4.3. Assumed potential distribution of V_1 in case 5.	69

Figure 4.4. Comparison of measured potential dV with calculated potentials dV (a) on radiating leads at both sides of the active device; (b) on a source bias line; (c) on a gate bias line, and (d) on a drain bias line.	71
Figure 4.5a. Measured potential dV obtained from optical sampling.	76
Figure 4.5b The calculated potential dV from case 5.	77
Figure 4.6. The comparison of the potential V_1 and potential $dV = V_1 - V_3$ in a radiative structure (a) in case 5, and (b) in case 1.	78
Figure 4.7. The schematic diagrams of the potential distributions and the main field lines presented (a) in case 3; (b) in case 4, and (c) in case 5.	82
Figure 4.8a. Schematic depiction of the global potential distribution on a column of active antenna array in cases 3 and 5.	86
Figure 4.8b. Schematic depiction of the global potential distribution on a column of active antenna array in case 4.	86
Figure 5.1. Equivalent circuit model of a common source transistor oscillator.	93
Figure 5.2. The I-V curves of the HEMT fhx35x.	95
Figure 5.3. The effect of the amplitude of a.c. gate-source voltage to direct drain-source current in the channel.	97
Figure 5.4. The effect of the amplitude of a.c. gate-source voltage to transconductance from nonlinear computation.	99
Figure 5.5. The effect of the amplitude of a.c gate-source voltage to the input resistance (a), and the input reactance (b) of a transistor.	100
Figure 5.6. Power spectrum of the transistor oscillator.	105
Figure 5.7. Power spectrum of the VDP equation with a periodic coefficient calculated from a numerical simulation. Simulation parameters $\epsilon = 0.01$, $\gamma=0.01$, $\omega_0= 1$ Hz, $\omega_f = 0.1$ Hz.	111
Figure 5.8. Power spectrum of the VDP equation with a periodic coefficient calculated from analytical solution. Simulation parameters $\epsilon = 0.01$, $\omega_0 = 1$ Hz, $\omega_f = 0.1$ Hz.	112

Figure 5.9. Experimental set-up for a measurement of the VDP parameter.	114
Figure 5.10. Power spectra of a self-sustained active antenna at different external modulation frequencies. Center oscillation frequency $\omega_0 = 3.5$ GHz; (a), $\omega_f = 7.5$ MHz; (b), $\omega_f = 11.07$ Mhz.	115
Figure 5.11. Power spectrum of a self-sustained active antenna with external modulation frequency $\omega_f = 0.91$ Mhz; which is less than the bandwidth of the phase noise.	117

CHAPTER 1

INTRODUCTION

1.1 Statement of Purpose

As solid-state transistors technology becomes more sophisticated, the idea of integrating transistors in radiative microwave structures has become more attractive. The use of diodes or transistors as active elements in free space microwave devices has been demonstrated. These devices include polarizers, frequency filters, reflectors and phased-array antennas. It has been shown that these active devices can be controlled by light injection. The simpler control mechanism of the active devices will be especially useful for antenna arrays. Since there is no need for additional transmission lines or waveguides in the control unit of the active antenna, the active array offers a much simpler configuration and easier control than the passive array.

A self-oscillating and radiating device consisting of an active periodic structure is called a quasi-optical power combiner. It was first developed to replace electron tube oscillators with solid-state devices for low and medium microwave power sources [1-3]. The active element used in this device can be a two-terminal diode or a three-terminal transistor. Because of the low d.c. to a.c. conversion efficiency of the two-terminal devices, field effect transistors (FETs) are often used as active elements. Besides its application as a power source, a quasi-optical power combiner can also be used as an active phased-array antenna. Since each radiating element in an active phased array is fed by its own power sources, the need for a

complex, often lossy power distribution network and an expensive waveguide transition in the passive array can be eliminated.

Among all the quasi-optical power combiners, the planar grid structure has the simplest configuration. Integrating solid-state devices directly into a periodic grid was first developed by Rutledge and Schwarz [4]. This structure continues to be used in Rutledge's research group at the California Institute of Technology. Two years after the first grid phase shifter was demonstrated by Lam *et al.* [5], Popovic *et al.* developed the first transistor grid oscillator in 1988 [6]. The active grid structure has two distinguishing features: First, there is no conventional ground plane in the back of the substrate. Second, the active elements in the same row of the grid can be biased by the same bias line. Therefore, only two d.c. power supplies are needed for the entire array. Since it is possible to control an oscillator by injecting light into a gate region of a transistor[7-8], the simple grid type oscillator is gaining favor as a potential optically controlled active phased array antenna.

The lack of a conventional ground plane in the grid type active antenna raised difficulties in the theoretical analysis. Weikle and Pance *et al.* analyzed a planar grid oscillator assuming an infinite array with identical a.c. current sources [9-10]. Due to the symmetry configuration of the array, the electric and magnetic wall boundary conditions are established to reduce the array to a unit cell, in which the bias lines of the antenna array can be ignored. The induced EMF method is then applied to analyze the radiating structure with the assumed current distribution. The theory has had some success in designing oscillation frequency of grids with large numbers of

elements. Practically speaking, the conditions of the array are not as ideal as the theoretical assumptions. First, the size of the array is far from infinite; the largest array dimension built so far is only 2.6 wavelengths long [11]. Second, the transistors are not all identical. Hence, the symmetry condition of the radiation field may not cancel exactly to form a magnetic wall. Therefore, when the theory failed to predict the instability of the device, it was thought that the size of the antenna was not large enough. In addition, the EMF method cannot provide guidance to optimize the device. The optimization of an array with a large number of active elements becomes a more laborious and uncertain process. Because of the above limitations, our research is motivated to answer the following questions:

- 1) What is the working mechanism of the device?
- 2) How important is the edge effect in the operation of these devices?
- 3) What determines the oscillation frequency of a finite array?
- 4) How and to what degree will the non-identical transistors degrade the performance of the array?
- 5) What kind of interaction occurs between the neighboring active devices?
- 6) Can we ignore the bias lines in the analysis?

To address the above problems, we have to understand the essential physics of this device. Previous experimental investigations of this device centered on the spectrum, power, and radiation pattern measurements of the antenna array, and the reflection coefficient measurements of the passive structure. These experiments describe some of the effects of the bias, external mirror, and geometry on the device

as an entire array. However, the published data cannot fully explain the behavior of the active array nor answer the above questions. To investigate an active radiative structure, alternative measurement techniques that explore the real-time physical properties of the antenna are needed.

The objective of this thesis is to increase our understanding of the behavior of the active antenna and to provide design guidance for such devices. In our investigation, the non-invasive *in-situ* optical sampling technique is employed as the major method for characterization of the device. Several sizes of active antenna arrays are fabricated on a GaAs substrate for the optical sampling measurements. Results of the sampling data are analyzed by a Greens function especially developed for this radiative structure. The goal of optical sampling experiments is to map out the real time potential distributions and to identify the mode of operation of the active radiative structure. The performances of antenna arrays are also examined by conventional microwave measurements for further justification. By means of the new measurement technique, we can gain more insight into the operational principles of the device. The results of this work will be used as the basis for optimal design of such a device.

The rest of the sections in this chapter will review some of the concepts and techniques used in development of the active antenna. The analog between the active antenna and laser oscillators is also given. The last section of this chapter will present the organization of the rest of this thesis.

1.2 History of Active Antennas

The term active antenna refers to the use of an active element or gain producing device in the radiating structure. Over the last three decades, researchers have become increasingly concerned with the analysis and design of antennas that involve active elements. The earliest application of the active antenna was as a receiving antenna for radio broadcasting. Hence, the implementation of such antennas is not a recent development. The active antenna had already appeared in the literature by 1928. The schematic diagram of this active antenna built in 1928 is shown in Figure 1.1 [12-13]. In this circuit, the active element was a vacuum tube, and played the role of a head amplifier for the received signal. The output signal from the tube will certainly be stronger than the received signal, but thermal noise will also be introduced to the output by the amplifier.

Spurred by the development of high frequency transistors and the need for small, highly efficient, broadband antennas (especially in mobile communication systems), a flurry of activity occurred in the active antenna field. In 1966, Meinke first proposed using a transistor to obtain a resonant match with the receiving antenna to reduce its dimensions [14]. In the early 70's, the height reducing factor was reported to reach 1500 for high-efficiency antennas [15]. At the same time, the possibility of building a transmitting antenna was proposed by Tuner [16]. Later, actual configurations for the active transmitting antennas were studied by MaClean *et al.* and Anderson *et al.* [17-18]. Configurations of these active transmitting antennas are shown in Fig 1.2. Calculations of input impedances for these transmitting active antennas indicates that the FEBL has lower input resistance than the FBEL

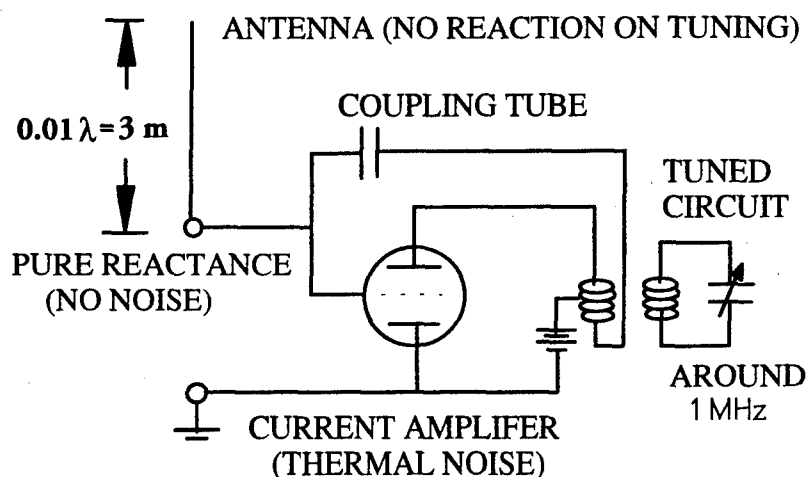


Figure 1.1. Small antenna with wideband coupling tube, used in a broadcast receiver (1928)

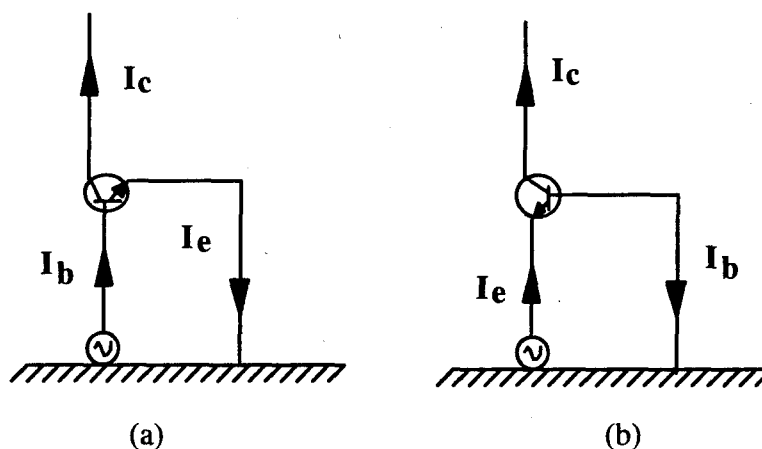


Fig. 1.2. The active transmitting antenna. (a) Fed-base emitter loop (FBEL), the short length radiating element appeared to be inductive and has high input resistance at resonance. (b) Fed-emitter base loop (FEBL), the short length radiating element appeared to be capacitive and has low input resistance at resonance (Ref. 17).

configuration. Since a suitable match is necessary to feed the antenna, type (b) is generally recommended for the transmitting antenna. The distinguishing feature of active antenna configurations in the 70's is that one port of the transistor is directly connected to the radiating structure and the other port is connected to the transmission line for either the input or output signal. The transistor is designed to operate in the stable region for both receiving and transmitting modes. Because of the non-reciprocity of the transistor, the detailed configuration of the active antenna is different for transmitting and receiving mode operations. In general, for the transmitting antenna, the microwave signal is fed into the radiating element through the transistor. In the receiving mode, the microwave signal is received by the radiating element, and passes through the transistor and is sent to the transmission line. The transistor in both configurations functions as active inductance. Compared to the passive inductance, the active inductance theoretically has an infinite Q factor [19, 20]. Therefore, the transistor active antenna is much less sensitive to frequency variation and consequently has wider matched bandwidth than passive matched inductance [21]. Because of these characteristics, active antennas have a lower resonant frequency, smaller size and higher radiation resistance [22-24]. The array performances of active antennas have also been studied [25, 26]. Due to the presence of a transistor, a sufficiently high impedance is found at the input terminals of each array element. Therefore, the effect of mutual coupling is suppressed, so that the bandwidth of the array increases. This yields a less frequency sensitive radiation pattern than those produced by a passive array. In summary, the main arguments

behind studying such active antennas at that stage were to increase bandwidth, make short antennas effectively longer, and to decrease mutual coupling between array elements.

In dealing with active antennas, stability is always a question. Active antennas are frequently observed to be unstable. Fanson and Chen first attempted to analyze the resonant condition of an active antenna with the assumption that the current distribution is the same as for the passive [27]. This is one of the few theoretical analysis in the literature.

The idea of building an oscillating active antenna array and placing it in an open cavity was introduced by Mink in the 1980's [3]. The research effort of self-oscillating active antennas was mainly aimed at the power combining of the solid-state devices. This approach is referred to as the "quasi-optical" or "spatial" power combining technique. In this period, FETs were often used as the active element. In a broader sense, the concept of integrating an oscillator with a radiating element can also reduce the complicated feed network of the transmitting antenna. To reach the goal of having a simple, compact and higher power antenna array, different methods are used for designing a self-oscillating antenna and array. These methods can be divided into two large general categories: the first is the guided wave design method for both an oscillator and radiator; the second is the non-conventional design method for a structure such as a grid type self-radiating antenna array.

In the first approach, a standard microstrip oscillator was built. Each oscillator was then connected or coupled to a radiator (in most cases a patch antenna)

to form an active antenna. The characteristics of this type of active antenna are: first, the oscillator is built in the guided-wave structure; second, the radiator resonates at half the wavelength; and third, a strong interaction between the active device and the radiative patch was avoided by a well-matched load. The one- or two-dimensional array can be formed by placing these active antennas in an appropriate geometry. Power can be added coherently by mutual coupling between the antennas or by external injection locking [29-31]. The advantage of this approach is that design procedures for the guided-wave oscillator and the radiator are commercially available. Hence, the oscillation frequency and the power of each antenna can be predicted once the geometry of the circuitry is defined. One disadvantage of this approach is that the patch antenna has inherently a narrow impedance matching bandwidth. Leverich *et al.* have offered an alternative by replacing a patch antenna with a notch antenna [32]. Other disadvantages of this configuration of the antenna are that the ground plane is on the other side of the substrate, and a via is necessary. Additionally, each active device needs separate d.c. bias lines and power supplies.

In the grid type of self-radiating antenna array, active elements are directly embedded in the periodic passive structure (such as a grid) lying on a dielectric substrate [11]. There is no ground on the other side of the substrate. To increase the coherent power output of the array, a mirror (a metal layer) is needed in front of the array to form an open cavity. A characteristic of this active antenna array is that the period of the grid need be much smaller than the resonant wavelength of the structure, which is surprising for a self-oscillating antenna. The advantages of the grid type

active antenna are that the structure is simple and compact, and all active elements can share a common d.c. power supply. The disadvantage of this approach is that the principle of operation and field distributions of a finite array are not totally understood. We cannot yet explain why in some situations the array oscillates at several frequencies instead of one. The object of our investigation is to obtain more knowledge of these devices.

1.3 Self-resonant Active Antennas with Periodic Structures

From now on the terminology of periodical active antennas in this thesis refers to the grid type active antenna with a thin substrate. In this geometry, there is no surface wave inside the substrate. As we know, the active antenna array is formed by embedding active elements in the periodic structure shown in Fig. 1.3. From the geometry of the structure, it is not immediately clear what the a.c. potential distribution is in this structure, how the voltage or current wave propagates, and what mode governs the operation of the active device.

Passive periodic structures have been analyzed previously as passive microwave components [33-34] to select the frequency and polarization. To date, few analyses have considered the behavior of active periodic structures in microwave frequency regions [35]. In contrast, evaluations of active periodic structure are quite common for lasers. Both distributed Bragg reflector (DBR) and distributed feedback (DFB) configurations were used in lasers for selecting and stabilizing the wavelength. Among all the corrugated waveguide structure lasers, the surface emitting laser (SEL)

most resembles the self-resonant active antenna array. From their physical configurations, both SEL and active antenna arrays are oscillators in different frequency regions. They both consist of periodic structures and an active medium. Both the SEL and the active antenna array have a surface radiation field in resonance. There are two typical SEL configurations: Figure 1.4a is the surface distributed feedback laser (SEDFBL) [36-37], and Figure 1.4b is the grating surface emitting laser (GSEL) [38-39]. Because of the differences in their structure, the operation principles of these SEL lasers are somewhat different.

In the SEDFB laser, the gain medium is uniformly distributed throughout the entire periodic structure. Due to the distributed perturbation of the grating, many modes arise from the interference of the forward scattering, back scattering and the surface diffracted output waves. However, large amounts of gain discrimination exist among the waveguide modes. Only the mode with the lowest threshold will lase. Theoretical calculations indicate that the lasing mode in the SEDFB laser is always an antisymmetric one [36]. That is, the laser operates in a single antisymmetric longitudinal mode. The characteristic of the far-field intensity of the SEDFB laser is a double-lobed profile. This has been consistently observed from the experiments[40].

Previous studies has shown that the active array with a thin substrate has only a single main lobe in the center of the far-field pattern. Therefore, the operational principle of the active antenna could be different from the SEDFB laser.

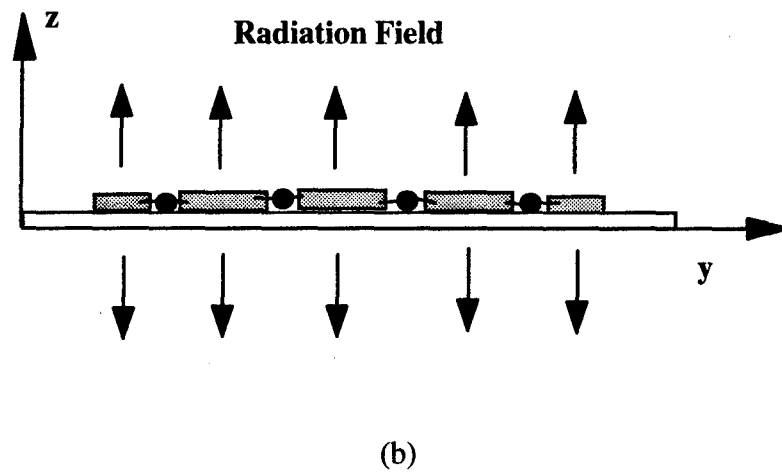
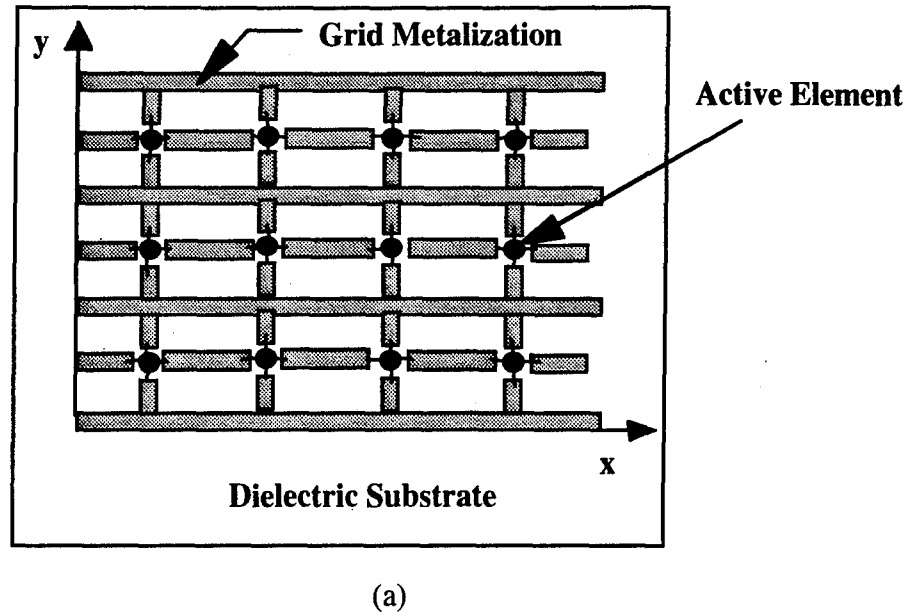
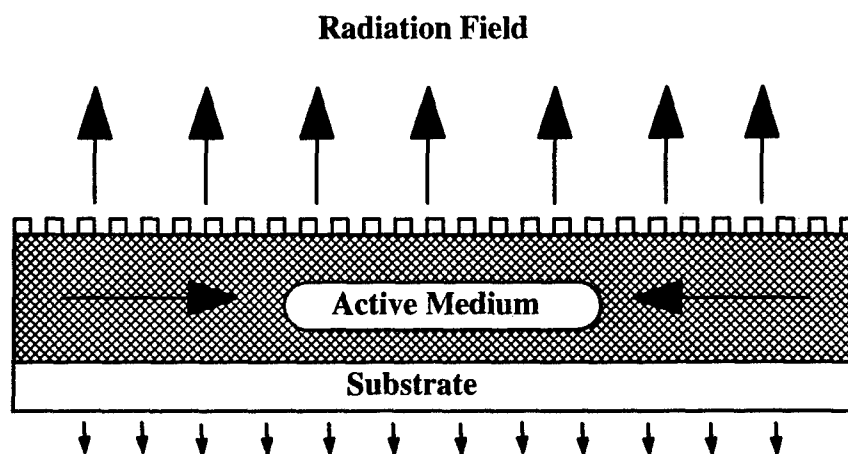


Fig. 1.3. Schematic illustration of a two-dimensional active array antenna (a), and side view of the array (b). The x oriented lines are the bias lines of the active elements. The main polarization of the radiation field is along the y direction. The energy of the radiation field propagates in both z directions [Ref .6].

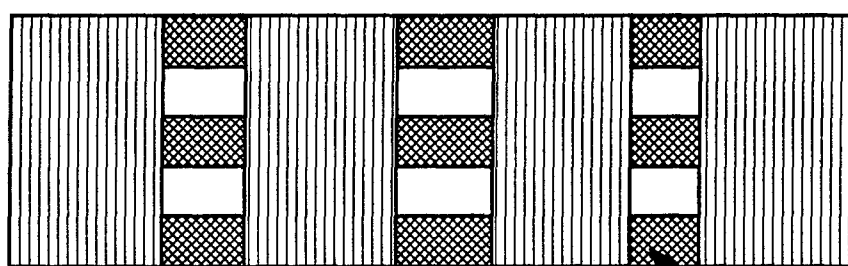
Figure 1.4b illustrates the configuration of a GSE laser. In this configuration, several gain sections are separated by grating sections. The grating in each waveguide section provides reflection radiation, and transmission to another element. In such a geometry, each gain section and two surrounding gain sections can be viewed as individual radiative oscillators. As light is transmitted from one gain section through the grating to the next gain section, the radiation power achieves coherent addition by mutual injection locking. The far-field pattern of the GSE laser has single lobes in the center.

Judging from the radiation pattern as well as the physical structure, there are common characteristics between the active antenna and the GSEL. It can be seen that each active element in the active antenna is analogous to a gain section of the GSEL. The period of each grating section is analogous to the period of the grid in the antenna. Each section of the grating is analogous to the non-uniform transmission line in each period of the grid. The role of the non-uniform transmission line in an antenna array provides reflection and radiation for each unit. In the GSE laser, the injection locking of each gain section is achieved by the transmitting wave in the waveguide channel. In the microwave antenna each active element is most likely mutually coupled by the injection of the radiation field.

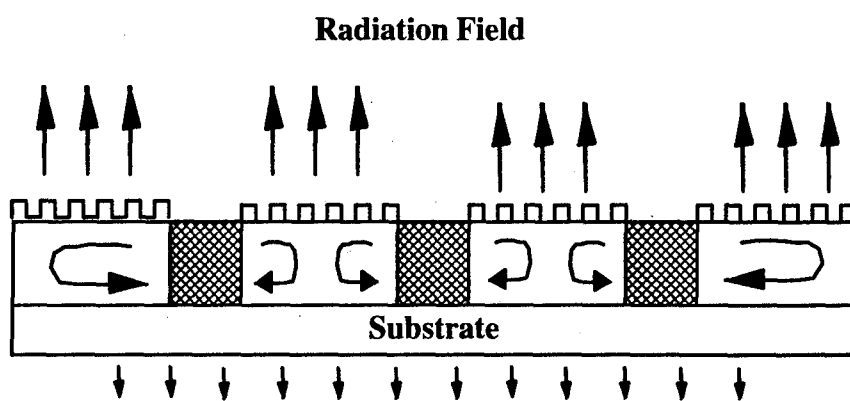
Since many theories have already been developed to analyze the GSE laser, comparing the active antenna array with the GSE laser means the knowledge gained from the study of the laser can be applied to active arrays. This gives us more insight into the fundamental physics of the device. This approach will be helpful as we proceed.



(a)



Active Medium



Substrate

(b)

Fig. 1.4. Sketch of surface emitting lasers. (a), the surface distributed feedback (SEDFB). (b), the grating surface emitting laser (GSEL) in top and side view.

The analogy between the GSE laser and the active antenna array needs to be further examined through our experiments. In cases where the simple model is not exact, the discrepancies can then be pointed out.

1.4 Organization of the Thesis

The remainder of the thesis consists of five chapters. I concentrate on two main research subjects. The first is investigating the nature of active antennas and arrays. Experimental results are presented in Chapters 3 and 4. The second is modeling the self-resonant antenna as a self-sustained oscillator and obtaining the corresponding parameters experimentally.

Chapter 2 gives a brief description of how to use active antennas to implement the optical control beam steering system. I will then show how this study links with other projects in the microwave optics group.

Chapter 3 contains comprehensive details of the characteristics of active antenna arrays. The derivation of Greens function for an antenna with a thin dielectric substrate is given. The first results of optical sampling measurements on the active radiative structures are presented. Fabrication and microwave characterization of the devices are also included in this chapter. Unique characteristics of the active array observed from these experiments are described.

Chapter 4 compares numerical simulations with measurements. To accurately interpret the data measured on the active structure, the possible modes of an active

antenna are numerically simulated to identify the operation mode of an active array. The accuracy of optical sampling of a non-guided wave structure is also addressed.

In chapter 5, a Van der Pol oscillator model is further justified and adopted for using in transistor oscillators. Experimental procedures to determine the Van der Pol parameters are further developed. This technique is also theoretically analyzed and experimentally examined.

Chapter 6 is a summary of the work in the preceding chapters. Major questions posed in Chapter 1 are answered.

References:

1. K. Kurokawa, "The Single -Cavity Multiple-Device Oscillator," *IEEE Trans. Microwave Theory Tech.*, vol. 19, pp.793-801, Oct., 1971.
2. K. Chang, and C. Sun, "Millimeter-Wave Power Combining Techniques," *IEEE Trans. Microwave Theory Tech.*, vol. 31, pp. 91-107, Feb. 1983.
3. J. W. Mink, "Quasi-Optics Power Combining of Solid-State Millimeter-Wave Sources," *IEEE Trans. Microwave Theory Tech.*, vol. 34, pp. 273-279, Feb., 1986.
4. D. B. Rutledge, S. E. Schwarz, "Planar-Multimode Detector Array for Infrared and Millimeter-Wave Applications," *IEEE J. of Quantum Electronics* vol. 17, pp. 407-414, March, 1981.
5. W. W. Lam, C. F. Jou, N. C. Luhmann, Jr., and D. B. Rutledge, "Diode Grids for Electronic Beam Steering and Frequency Multiplication, " *Int. J. Infrared and Millimeter Waves*, vol. 7, no. 1, pp. 27-41, 1986.
6. Z. B. Popovic, M. Kim, D. B. Rutledge, "Grid Oscillator," *Int. J. Infrared and Millimeter Waves*, vol. 9, no. 7, pp. 647-654, 1988.
7. A. A. De Salles and J. Forrest, "Initial Observation of Optical Injection Locking of GaAs Metal Semiconductor Field Effect Transistor Oscillators, " *Appl. Phys., lett.*, vol. 38, pp. 392-3944, 1981.
8. S. Tiwari, "Compound Semiconductor Device Physics," Library of Congress cataloging-In-Publication Data, 1992.
9. R. M. Weikle, "Quasi-Optical Planar Grids for Microwave and Millimeter-wave Power-Combining," Ph. D. dissertation, CALTE, Pasadena, 1991.
10. A. Pance, M. J. Wengler, "Microwave Modeling of 2-D Active Grid Antenna Arrays," *IEEE Trans. Microwave Theory Tech.*, vol. 41, Jan. 1993.
11. Z. B. Popovic, R. M. Weikle, II, M. Kim, and D. B. Rutledge, "A 100-MESFET Planar Grid Oscillator, " *IEEE Trans. Microwave Theory Tech.*, vol. 39, pp. 1930-200. Feb., 1991.
12. H. A. Wheeler, "Small Antenna," *IEEE Trans. on Antenna and Propagat.*, vol. 23, pp. 462-469, (1975).
13. This 1928 work is referenced in J. H. Dunlavy and B. C. Reynolds, "Electrically Small Antennas," in 23rd Ann. USAF Antenna Symp., (Oct., 1972).

14. H. H. Meinke, "Active Antennas," *Nachrichtentech. Z.*, vol. 19, pp. 697-705, Dec. 1966.
15. A. P. Anderson, W. S. Davies, M. M. Dawond and P. E. Galanakis, "Note on Transistor-Fed Active-Array Antennas," *IEEE Trans. on Antennas Propagat.*, vol. 19, pp. 537-539, July, 1971.
16. E. M. Turner, "Subminiature Integrated Antenna," *Proc. 18th Ann. Conf. IEEE Veh. Group*, Dec. 1967.
17. T. S. M. Maclean and P. A. Ransdale, "Short Active Aerials for Transmission," *Int. J. Electron.*, vol. 36, pp. 261-269, Feb., 1974.
18. A. P. Anderson and M. M. Dawond, "The Performance of Transistor Fed Monopoles in Active Antennas," *IEEE Trans. on Antennas Propagat.*, vol. 21, pp. 371-374, May, 1973.
19. J. E. Raue, "Power Amplification at 55-65 GHZ with 18 GHZ Gain-bandwidth Product," *Proceedings of IEEE G-MTT International Microwave Sym.* pp. 60-62, 1973.
20. P. S. Sarma, and S. Venkateswaran, "Simulated Inductance with A Transistor and R. C. Elements," *Electronics letters*, vol. 5 No. 26, Dec. 1969.
21. P. K. Rangole and S. S. Midha, "Short Antenna with Active Inductance," *Elec. Lett.*, vol. 10, pp. 462-463, Oct., 1974.
22. M. Dawond and A. P. Anderson, "Calculations Showing the Reduction in the Frequency Dependence of a Two-Element Array Antenna Fed by Microwave Transistors," *IEEE Trans. Antennas Propagat.*, vol. 20, pp. 497-499, (1972).
23. I. Kontorovich and N. M. Lyapunova, "Active Antennas," *Radio Eng. Electron. Phys.*, vol. 19, pp. 126-127, 1974.
24. W. C. Wong, "Single and Noise Analysis of a Loop-Monopole Active Antenna," *IEEE Trans. on Antennas Propagat.*, pp. 574-632, July, 1974
25. J. P. Daniel, "Mutual Coupling Between Antennas for Emission or Reception--Application to Passive and Active Dipoles," *IEEE Trans. on Antennas Propagat.*, vol. 22, pp. 347-349, March, 1974.
26. J. P. Daniel and C. Terret, "Mutual Coupling between Antennas--Optimization of Transistor Parameters in Active Antenna Design," *IEEE Trans. on Antennas Propagat.*, vol. 23, pp. 513-516, July, 1975.

27. P. L. Fanson and Ku-Mu Chen, "Instabilities and Resonances of Actively and Passively Loaded Antennas," *IEEE Trans. on Antennas Propagat.*, vol. {22}, pp. 342-347, March, 1974.
28. K. Chang and K. Hummer, J. L. Klein, "Experiments on Injection Locking of Active Antenna Elements for Active Phased Arrays and Spatial Power Combiners," *IEEE Trans. on Microwave Theory Tech.*, vol. 37, pp. 1078-1084, July, 1989.
29. R. A. York and R .C. Compton, "Quasi-Optical Power Combining Using Mutually Synchronized Oscillator Arrays," *IEEE Trans. Microwave Theory Tech.*, vol. 39, pp.1000-1009, June, 1991.
30. J. Birkelland and T. Itoh, "A 16 Element Quasi-Optical FET Oscillator Power Combining Array with External Injection Locking," *IEEE Trans. Microwave Theory Tech.*, vol. 40, pp. 475-481, March, 1992.
31. W. K. Leverich, X. Wu, and K. Chang, "FET Active Slotline Notch Antenna for Quasi-Optical Power Combining," *IEEE Trans. on Microwave Theory Tech.* vol. 41, Sept. 1993.
32. J. A. Arnaud, and F. A. Pelow, "Resonant-Gird Quasi-Optical Diplexers," *The Bell Sys. Tech. J.* pp. 263-283, Feb., 1975.
33. R. C. Hall, R. Mittra, and K. M. Mitzner, "Analysis of Mutilayered Periodic Structures Using Generalized Scattering Matrix Theory," *IEEE Trans. Microwave Theory Tech.*, vol. 36, no. 4, pp. 511-517, April, 1988.
34. H. Shigesawa, and M. Tsuji, "A Completely Theoretical Design Method of Dielectric Image Guide Grating in the Bragg Reflection Region," *IEEE Trans. Microwave Theory Tech.*, vol. 34, pp. 420-426, April, 1986.
35. S. W. Lee, and T. T. Fong, "Electromagnetic Wave Scattering from an Active Corrugated Structure," *J.Appl. Phys.*, Vol. 43, pp. 388-396. Fed., 1972.
36. R. J. Noll, and S. H. Macomber, "Analysis of Grating Surface Emitting lasers," *IEEE J. Quantum Electron.*, vol. 26, pp. 456-466, 1990.
37. R. F. Kazarinov, and C. H. Henry, "Second-order Distributed Feedback Lasers with Modes Section Provided by First-Order Radiation Loss," *IEEE J. Quantum Electron.*, vol. 21, pp. 144-151, 1985.
38. W. Streifer, R. D. Burnham, and D. R. Scifres, "Analysis of Grating Coupled Radiation on GaAs:GaAlAs Lasers and Waveguides," *IEEE J. Quantum Electron.*, vol. 12, pp. 422-428, 1976.

39. W. Streifer, D. R. Scifres, and R. D. Burnham, "Analysis of Grating Coupled Radiation on GaAs:GaAlAs Lasers and Waveguides-Part II," *IEEE J. Quantum Electron.*, vol. 12, pp. 494-499, 1976.
40. C. H. Henry, R. F. Kazarinov, and R. A. Logan, "Observation of Destructive Interference in the Radiation Loss of the Second-order Distributed Feedback Lasers," *IEEE J. Quantum Electron.*, vol. 21, pp. 151-154, 1985.
41. N. Camilleri, and B. Bayraktaroglu, "Monolithic Millimeter-Wave IMPATT Oscillator and Active Antenna," *IEEE Trans. Microwave Theory Tech.*, vol 36, no12, pp. 1670-1676, Dec., 1988.

CHAPTER 2

APPLICATION OF ACTIVE PHASED ARRAYS

2.1. Introduction

Active elements (such as MESFETs and HEMTs) have inherent optical controllability. Use of an active array antenna as a phased array offers a direct means for optically controlled beam steering. In this chapter, we will briefly review the methods for beam steering and explain why the optically-controlled method is desirable. How this project relates to this application is also addressed.

2.2. Beam Steering for Passive Arrays

One of the applications of a phased array is to direct the major radiation of the array to any direction (scanning) by controlling the phase excitation between the elements. In practice, continuous scanning is accomplished by using phase shifters to provide linear phase variations of the AC signal across the array. To realize a progressive phase change between the elements, electronic phase shifters are commonly used in phased-array antennas. One of the early analog phase shifters is the ferrite phase shifter [1-2]. The amount of phase shifting produced by this ferrite device is directly related to the amount of current flowing through the wire. With requirements for the implementation of scanning arrays, the digital phase shifter was developed for reducing the size, increasing the speed and offering easier computer control. However, each array element needs an individual electronic phase shifter, so

that the scanning system of a phased-array becomes complex, heavy and expensive. To eliminate the number of passive phased shifters in the large-aperture array, Mailoux *et al.* proposed a control method in 1968 [3]. In their proposed system, harmonic frequencies were used to provide a phase increment for an array, and the scanning was realized by using only one phase shifter. Despite the processes involved in electronic beam steering, the complexity, transition loss and the cost of control systems are still problems that need to be solved. The approach of using a coherent optical technique for passive phased-array antennas was therefore developed to replace microwave phased shifters and feedlines with free space optic components and optical fibers [4]. A good review of these methods has been given by Charczenko [5].

2.3. Optical Control Beam Steering for Active Arrays

There are many control methods for active phased arrays. All these methods are aimed at the advantages of the tuning ability of active elements. A summary of these methods is presented in Figure 2.1. The first technique for beam steering in active antenna arrays was developed by Al-Ani *et al.* [6]. This approach can be classified as electronic beam steering. In this approach, active elements were used to perform dual functions of locking and phase shifting, thereby, eliminating the passive phase shifters. Beam steering of the active array was achieved by locking the oscillator to the n th harmonic of the external electric injection signal. A block diagram of the beam steering system is shown in Figure 2.2. R. F. sources in the active antenna array are solid state oscillators. Isolators are used to reduce the mutual

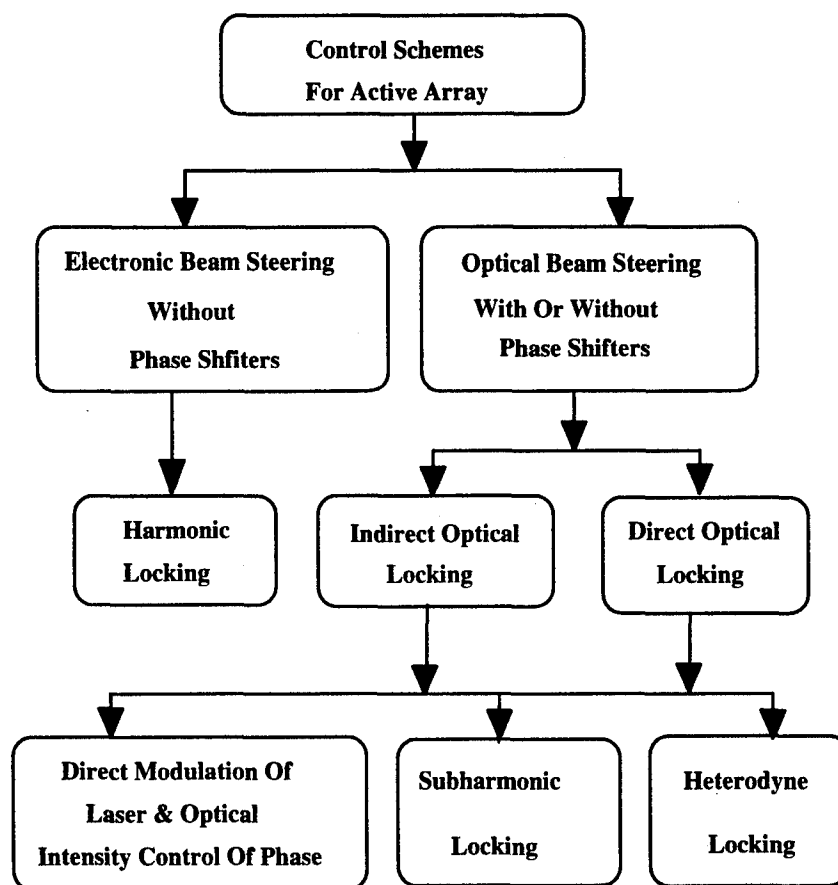


Figure 2.1. Block diagrams of control schemes for the active phased array

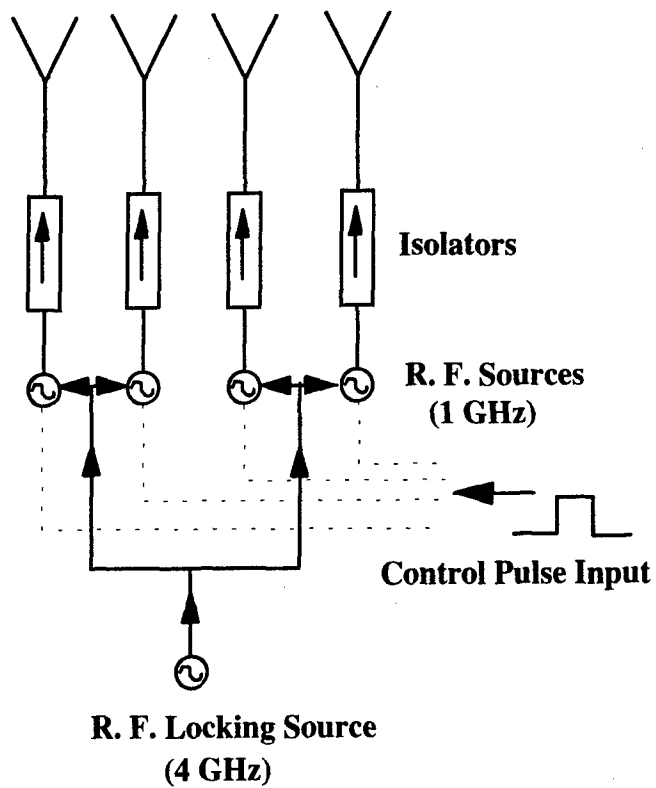


Figure 2.2 Diagram of complete electronic beam steering of active array antennas.

coupling between antennas at the fundamental frequency. Beam steering by using an active antenna has provided a simpler control circuit and there are no passive shifters involved. The disadvantage of the method comes from the harmonic locking scheme. As the frequency of the oscillator increases, the locking power for the higher harmonic is also dramatically increased.

In recent years, the control of microwave devices and circuits by optical illumination has become a subject of great interest [7-9]. Indirect and direct injection locking are two main approaches for optically controlled oscillators. In the former approach, a photodiode is used to connect to an oscillator circuit and to convert an optical signal to an electrical signal. The latter approach directly illuminates the optical signal into the gate region of a FET [10, 11]. Many researchers claim that wider locking bandwidth and over 180° phase shifts can be achieved by using indirect optical injection [12-14]. Despite better performance of the indirect injection locking over the direct one, the indirect control approach has the disadvantage of the additional photodiodes required for the system. To investigate the possibilities of active arrays with the periodic structure, the direct injection method is more suitable. The reasons are as follows: first, the circuit structure is much simpler than the indirect method, which is important for the system still in the research stage, and second there is no guided wave structure in this active antenna, so the indirect method is difficult to apply to this device.

A schematic diagram of the preliminary active scanning array is shown in Figure 2.3. An optical heterodyne technique and optical phase shifters were also used

in this proposed system. In the system configuration, optical beams with an optical frequency ω_o from the laser array are coupled into fibers which guide the beams to the input of the single side band modulators (except the reference beam). Then a microwave signal ω_m is applied to the electrodes of the modulators. The frequencies of optical control beams shift to $\omega_o + \omega_m$ at outputs of the modulators. After the optical control beams pass through the optical phase shifters, each optical beam carries a different phase. A reference beam is introduced to heterodyne the optical control beams, and each control beam will carry a signal with the same microwave frequency ω_m but with a different microwave phase. These control beams will illuminate the gate region of the active elements for injection locking. If the microwave frequency ω_m falls within the frequency locking range of a phased array, the active phased array will be synchronized to the injection frequency and phase. Therefore, the necessary phase progression for beam steering can be achieved optically.

One of the challenges of implementation that we want to achieve in this proposed system is to use fewer control beams to control a larger array through mutual coupling of the active elements. To reach this goal, knowledge of the dynamic behavior of the active arrays and models for the coupled oscillator are necessary. This project is a preliminary research investigation into an optically controlled beam steering active antenna array.

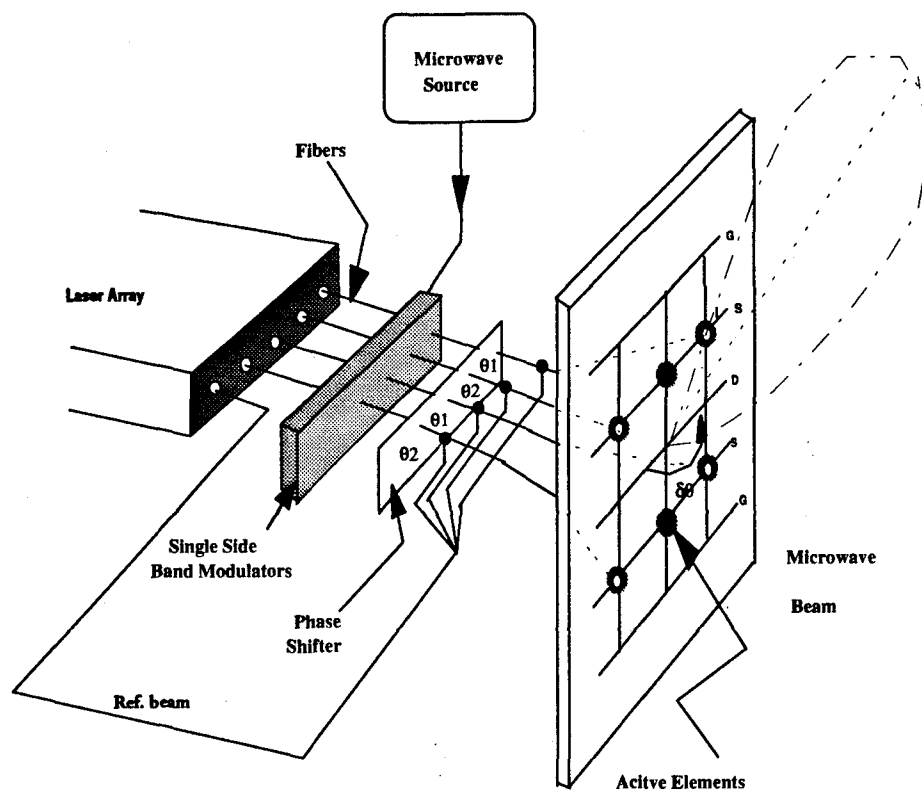


Figure 2.3. The schematic diagram of optical beam steering for an active phased array.

References

1. J. D. Kraus, "Antennas," McGraw-Hill Book Company, Second edition, 1988.
2. C. A. Balanis, "Antenna Theory-Analysis and Design," John Wiley & Sons, 1982.
3. R. J. Mailoux, P. R. Caron, and F. J. LaRussa, "An Array Phasing Device which Uses Only One Phase Shifter for Each Direction of Scan," IEEE Tans. on Antenna propagat. vol. 16, pp. 258-260., March, 1968.
4. G. Koepf, "Optical Processor for Phased-Array Antenna Beam Forming," SPIE, vol. 477, Opt. Tech. for Microwave Applications, pp. 75-81, May, 1984.
5. W. Charczenko, "Coupled Mode Analysis, Fabrication, and Characterization of Microwave Integrated Optical Device," Ph.D. Thesis, University of Colorado at Boulder, see also Guided Wave Optics Lab., report #27, 1990.
6. A. H. Al-Ani, A. L. Cullen and J. R. Forrest, " A Phase-Locking Method for Beam Steering in Active Array Antenna," IEEE Trans. Microwave Theory Tech., vol. 22, pp. 698-703, June, 1974.
7. A. De Salles, and J. R. Forrest, "Initial Observations of Injection Locking of Ga As Metal Semiconductor Field Effect Transistor Oscillators," Appl. Phys. Lett., vol. 38, no.5, pp. 392-394, March, 1981.
8. H. J. Sun, R. J. Gutmann, and J. M. Borrego, "Optical Tuning in GaAS MESFET Oscillators," MTT-S Int. Microwave Sym. Dig., PP. 40-42, 1981.
9. L. Goldberg, C. Rauscher, J. F. Weller, and H. F. Taylor, "Optical Injection Locking of X-Band FET Oscillator Using Coherent Mixing of GaAS Lasers," Electron. Lett., vol. 19, no.20, pp. 848-850, Sept., 1983.
10. A. Madjar, A. Paolletta, P. R. Herczfeld, " Light Interaction With GaAS-MESFET and Its Applications-A Review," Microwave and Optical Lett., vol. 6, pp. 22-27, Jan., 1993.
11. A. Bangert, and M. Ludwig, "A Direct Optical Injection Locked 8-GHz MMIC Oscillator," IEEE MTT-S Int. Microwave Sym. Dig., pp. 499-502, 1992
12. A. Bangert, J. Rosenzweig, A. Hulsmann, G. Kaufel, K. Kohler, and J. Schneider, "Optical Control of Pseudomorphic HEMT-Based MMIC Oscillators," Microwave and Optical Lett., vol. 6, pp. 36-38, Jan., 1993.

13. D. J. Sturzebecher, X. Zhou, X. S. Zhang, and A. S. Daryoush, "Optically Controlled Oscillators for Millimeter-Wave Phased-Array Antennas." *IEEE Trans. Microwave Theory Tech.*, vol. 41, pp. 998-1003, June/July, 1993.
14. R. D. Esman, and L. Goldberg, and, J. F. Weller, "Optical Phased Control of an Optically Injection-Locked FET Microwave Oscillator," *IEEE Trans. Microwave Theory Tech.*, vol. 37, pp. 1312-1518, Oct., 1989.
15. R. Fralich and J. Litva, "Beam-Steerable Active Array Antenna," *Electron. Lett.*, vol. 28, no.2, pp. 184-185, Jan., 1992

CHAPTER 3

INVESTIGATIONS OF ACTIVE ANTENNAS AND ACTIVE PHASED ARRAYS

3.1 Introduction

The most ubiquitous microwave circuit diagnostic technique, that of network analysis, measures only terminal characteristics. In a frequency limit where elements can be considered as lumped, this information is enough for full circuit characterization. However, with increasing frequency, circuits become increasingly distributed and the detailed placement of elements can determine terminal performance. Electromagnetic solvers can be used to try to predict terminal characteristics in such cases. These simulations predict much more than just the terminal characteristics. They also predict details of internal charge distributions on the lines. There is unfortunately, no commonly used technique to verify these theoretical predictions.

Various forms of electrooptical sampling have been developed for on-chip metrology. During the past several years, our group here in Colorado has concentrated on the direct electrooptic sampling technique, its calibration [1], its use to verify electromagnetic models of both passive microstrip circuits [2] and coplanar waveguide (CPW) circuits [3]. The results have been quite encouraging to present.

The basic idea behind optical sampling is that a field in an electrooptic crystal will cause a change in the index of refraction of the crystal. Depending on crystal type and orientation, the integrated change in index in traveling through the substrate

can be read out by placing the substrate either in an arm of an interferometer or in a polarimeter. This integrated change of index must then be proportional to the voltage difference along that path, as the local index change is linearly proportional to the local field. In general, in a microwave circuit, the only charge density is the surface charge density on the electrodes. Clearly, one can relate the potential difference in the circuit to the surface charge density through the Green's function. In this manner, a two-dimensional optical sampling map can yield both the potential distribution and the surface charge distribution within a microwave circuit. Such mappings yield a wealth of information about the electromagnetic operation of such a circuit. The measurement data can serve as a stringent test of any electromagnetic simulation of such a circuit. In references [2] and [3], such comparisons are performed and shown to be in agreement with the simple passive guided wave structures considered.

The potential distribution on an antenna can be measured by the conventional microwave measurement technique such as an electric probe. However, the probe will load the antenna and active devices. Because of the radiative and active nature of the active antenna, potential measurements on the active antenna can only be accessible by using the non-invasive *insitu* optical sampling.

This chapter is organized as follows: in Section 2, optical sampling and what it measures will be discussed in detail. In Section 3, the requisite mathematical relations between these quantities will be derived. In Section 4, test structures used in this work will be described, device fabrication is described, and electrical characterization of devices are presented. In Section 5, the results of the sampling

measurements will be presented. Section 6 is devoted to a discussion of the sampling results and what they seem to tell us about the operation of the test structure.

3.2. Optical Sampling and What It Measures

As has recently been shown, the direct optical sampling technique can be used in concert with a calibration algorithm [1] for two-dimensional mapping of charge and potential distributions in both microstrip [2] and coplanar waveguide circuits [3]. This technique has good spatial resolution ($<10 \mu\text{m}$) and with proper calibration can exhibit a 50 dB dynamic range. Now the usual microwave characterization technique of network analysis can achieve such dynamic range, but only at terminals. In this sense, optical sampling can provide one with a wealth of spatial information not amenable to "standard" characterization techniques. Further, the optical sampling technique is truly noninvasive, as neither charge nor microwave energy need be extracted from the circuit under test, whereas probing techniques must by nature, move charges.

An optical sampling head is discussed in much more detail in [2]. The basic idea is that the incident beam is polarized in an elliptical state that is maximally sensitive to the effect of the electrooptic coefficient of the GaAs substrate. The microwave electric field in the substrate, through the electrooptic coefficient, induces a rotation in the polarization state, which is then read out by an analyzer placed in front of a slow detector. The magnitude and phase of the signal received by the detector will then be proportional to a voltage defined by:

$$V_{eo} = \text{const.} \int E_{\mu}(x, y, z) d\ell, \quad (2.1)$$

where V_{eo} is the electrooptic voltage, E_{μ} is the microwave field and x, y, z and ℓ are defined in Figure 3.1. From Figure 3.1, it is quite evident that the measured signal will be a function of the thickness t of the sample. However, there are two limits in which the measured quantity becomes directly proportional to physical quantities. Clearly, for a sufficiently thick sample, the voltage $V_3(x)$ of Figure 3.2, will approach the reference potential at infinity (ground) and the measured $V_{eo}(x, z)$ will become identical with the potential $V_1(x)$ of the top surface. Additionally, in the limit where the sample thickness becomes small, the optical wave will see only the normal component of E_{μ} evaluated at $E_{\mu}(x, y=0, z)$, which will then be directly proportional to σ , the surface charge density on the upper surface electrodes. In the next section, we will see that measurements for microwave circuits with arbitrary substrate thickness t are sufficient to determine both σ and V_1 .

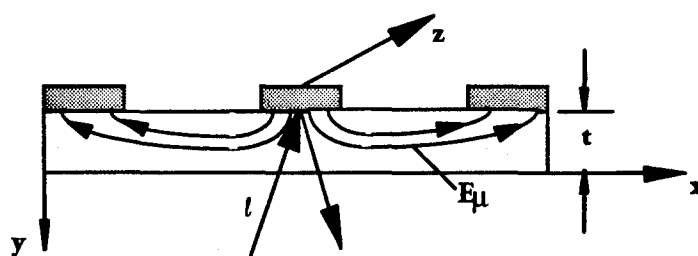


Figure 3.1. Schematic depiction of the device under test defining the coordinate system and sampling geometry.

3.3. Mathematical Relations between the Potential and Charge Distributions

As is well known, Maxwell's equations,

$$\nabla \times \mathbf{E}(\mathbf{r}, t) = -\frac{\partial \mathbf{B}(\mathbf{r}, t)}{\partial t}, \quad (3.3.1a)$$

$$\nabla \times \mathbf{H}(\mathbf{r}, t) = \mathbf{J}(\mathbf{r}, t) + \frac{\partial \mathbf{D}(\mathbf{r}, t)}{\partial t}, \quad (3.3.1b)$$

$$\nabla \cdot \mathbf{B}(\mathbf{r}, t) = 0, \quad (3.3.1c)$$

$$\nabla \cdot \mathbf{D}(\mathbf{r}, t) = \sigma(\mathbf{r}, t), \quad (3.3.1d)$$

can be rewritten in the form of:

$$\nabla^2 V(\mathbf{r}, t) + \frac{1}{c^2} \frac{\partial V(\mathbf{r}, t)}{\partial t} = -\frac{\sigma(\mathbf{r}, t)}{\epsilon}, \quad (3.3.2a)$$

$$\nabla^2 \mathbf{A}(\mathbf{r}, t) + \frac{1}{c^2} \frac{\partial \mathbf{A}(\mathbf{r}, t)}{\partial t} = \mu \mathbf{J}, \quad (3.3.2b)$$

$$\nabla \cdot \mathbf{A}(\mathbf{r}, t) + \frac{\partial V}{\partial t} = 0. \quad (3.3.2c)$$

Where $\mathbf{A}(\mathbf{r}, t)$ and $V(\mathbf{r}, t)$ are defined by:

$$\mathbf{E} = -\nabla V - \frac{\partial \mathbf{A}}{\partial t},$$

$$\mathbf{B} = \nabla \times \mathbf{A},$$

and it has been tacitly assumed that the μ and ϵ may be inhomogeneous, but must be nondispersive over the frequency bandwidth of interest. Equation (3.3.2a) admits a formal solution in the form as:

$$V(\mathbf{r}, t) = \int G(\mathbf{r}, \mathbf{r}', t, t') \sigma(\mathbf{r}', t') d\mathbf{r}' dt', \quad (3.3.3)$$

where many books have been written on techniques for finding the Green's function G [4]. Equation (3.3.3) provides us with the needed relationship between $V(r,t)$ and $\sigma(r,t)$ which will allow us to determine $V(r,t)$ and $\sigma(r,t)$ uniquely from optical sampling data taken on a sample with finite thickness t .

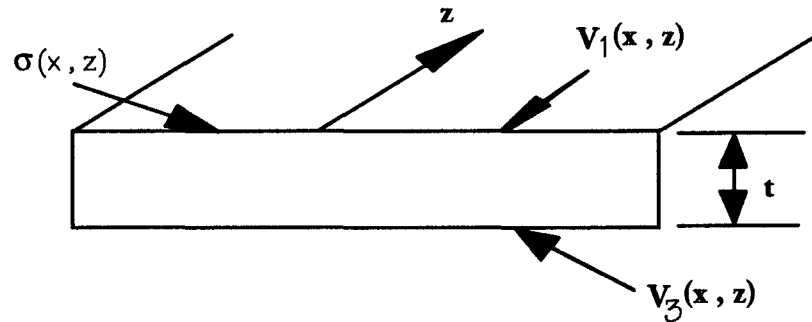


Figure 3.2. Schematic depiction of the device under test of Figure 3.1, with the surfaces upon which $\sigma(x)$ and $V_1(x)$ (top surface) and $V_3(x)$ are labeled.

Now, when the dimensions of the circuit are small compared to a microwave wavelength, a useful approximation can be the quasi-static one which dates back to Pocklington [5]. As has been recently demonstrated, this approximation works quite well as far as predicting the characteristics of coplanar waveguide structures [3]. In the quasi-static approximation, one assumes that for the purposes of calculating the charge distribution from a known potential, one can ignore the time dependence of Equation (3.3.3) and write it in the form of:

$$V_{qs}(x, z) = \int G(x, z; x', z') \sigma(x', z') dx' dz'$$

where $G(x, z; x', z')$ is now the static Green's function, and σ the surface charge density. The approximation is equivalent to ignoring small phase shifts between the

current and the charge. For the guided wave case, to recover the dynamics of the circuit, one then assumes that:

$$V(x, z, t) = (a_f(z)e^{i\beta z} + a_b(z)e^{-i\beta z}) V_{QS}(x, z)e^{-i\omega t}, \quad (3.3.4a)$$

$$\sigma(x, z, t) = (a_f(z)e^{i\beta z} + a_b(z)e^{-i\beta z}) \sigma_{QS}(x, z)e^{-i\omega t}, \quad (3.3.4b)$$

where the a_f and a_b can be found from a knowledge of the impedance $Z(z)$ along the equivalent transmission line. In the case where the wave distributions were purely forward propagating, i.e., the ideal matched microwave transmission line, one would simply write that as:

$$V(x, z, t) = a V_{QS}(x, z)e^{-i\beta z}e^{-i\omega t}, \quad (3.3.5a)$$

$$\sigma(x, z, t) = a \sigma_{QS}(x, z)e^{-i\beta z}e^{-i\omega t}. \quad (3.3.5b)$$

Now, if one considers the specific case as illustrated in Figure 2, in the quasi-static limit one can write that:

$$\begin{aligned} V_{eo}(x, z) &= V_1(x, z) - V_3(x, z) \\ &= \int G(x, x', z, z') \sigma(x', z') dx' dz' \end{aligned} \quad (3.3.6)$$

where $V_1(x, z)$ is the potential on the top surface of the sample, $V_3(x, z)$ is the potential on the bottom surface of the sample and the Green's function can be deduced from the expressions for the potentials. The $V_1(x, z)$ and $V_3(x, z)$ are then given by[6]

$$V_1(x, z) = \frac{\sigma}{4\pi\epsilon_0} \int_0^\infty J_0(kr)e^{-k|z|} dk + \int_0^\infty \phi(k) J_0(kr)e^{kz} dk, \quad (3.3.7)$$

where,

$$\phi(k) = \frac{\beta (e^{-2kr} - 1)}{1 - \beta^2 e^{-2kr}}, \quad (3.3.8)$$

$$r = \sqrt{(x - x')^2 + (z - z')^2}, \quad (3.3.9)$$

and:

$$\beta = \frac{\epsilon_r - 1}{\epsilon_r + 1}, \quad (3.3.10)$$

with ϵ_r being the relative substrate permittivity, and

$$V_3(x, z) = \frac{(1 - \beta^2)\sigma}{4\pi\epsilon} \int_0^\infty \frac{J_0(kr)e^{-kt}}{1 - \beta e^{-kt}} dk, \quad (3.3.11)$$

with β as in (3.3.10). With expressions of the potential distributions on the front and back side of the substrate given, the Green's function in Eq. (3.3.6) can be easily obtained:

$$G(x, z) = \frac{1}{4\pi\epsilon} \left\{ \frac{1}{r} + \sum_{n=0}^{\infty} \frac{\beta^{2n+1}}{\sqrt{r^2 + (2t(n+1))^2}} - \sum_{n=0}^{\infty} \frac{\beta^{2n+1}}{\sqrt{r^2 + (2tn)^2}} - \sum_{n=0}^{\infty} \frac{\beta^{2n}(1 - \beta^2)}{\sqrt{r^2 + (t(2n+1))^2}} \right\} \quad (3.3.12)$$

After obtaining calibrated measurement data for $V_{eo}(x, z)$, one can use standard numerical techniques to invert equation (3.3.6) and obtain $\sigma(x, z)$, the charge distribution. One can then use relations in equations (3.3.7) and (3.3.11) to determine the front and backside potentials. Results of this procedure will be presented in Sections 4 and 5 of this chapter. First however, some discussion will be given to the test structure.

3.4. Device Fabrication and Electrical Characteristics

For the purpose of optical sampling experiments, single active antenna and active antennas in an array structure were constructed on a semi-insulating undoped

GaAs. The thickness of the GaAs ($\epsilon_r = 12.5$) wafer is 500 μm . Figures 3.3 and 3.4 show the structures of a single active antenna and an archetypal active antenna array. The metallization on the GaAs was performed using a standard photolithography technique. First, a 100 \AA layer of titanium was evaporated on the substrate as an adhesion layer. This was followed by 100 \AA layer of gold evaporated onto the titanium and then plating the gold to a thickness of 1.5 μm . Finally, HEMTs and MESFETs in chip form (Fujitsu FHX35X, and FHX02x) were epoxied onto the metallized substrate using opo-tk70 epoxy (chosen for its high thermal conductivity). These chips were used as the active elements because of their gain at high frequencies. The gate, drain and source pads on the chip were bonded to plated leads using thermal compression.

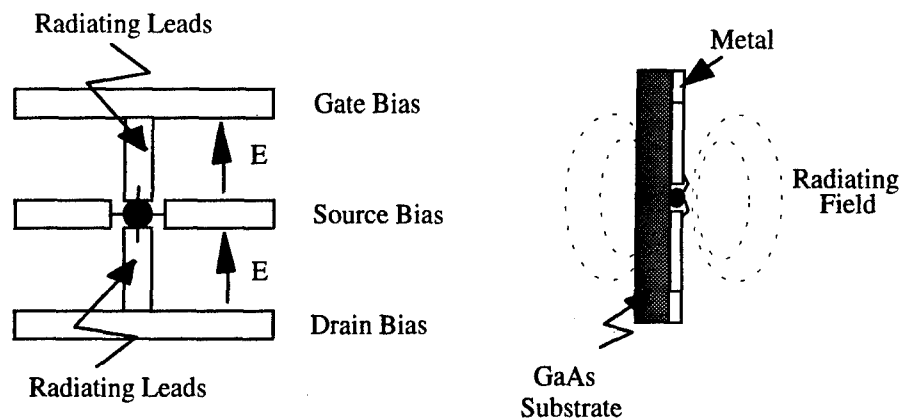
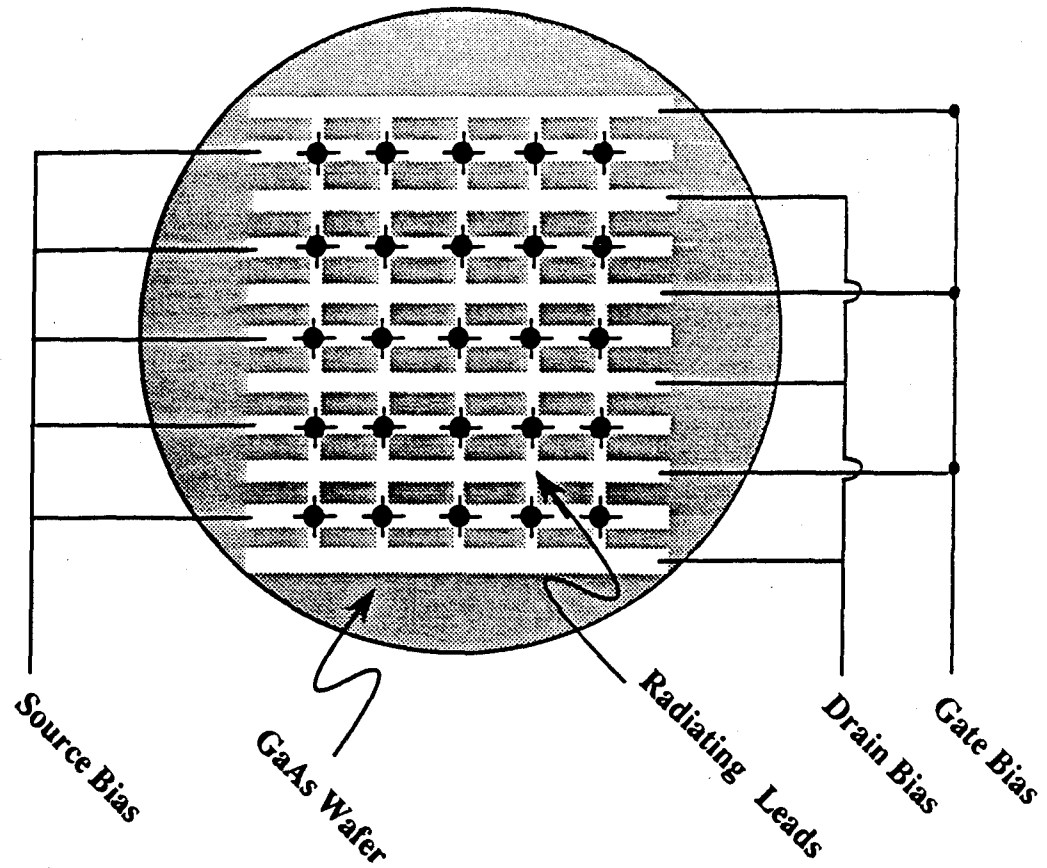


Figure 3.3. The structure of single active antenna.



Grid period	: 5 mm
Width of the radiating leads	: 0.6 mm
Width of the bias lines	: 0.8 mm
Thickness of GaAs substrate	: 0.5 mm

Figure 3.4. The structure of an archetypal active antenna array

Various sizes (5x5 to 1x1) of active antenna arrays were built by the fabrication procedure described above. The microwave characteristics of these active antennas were tested before optical sampling was performed. The illustration of the experimental set up is shown in the Figure 3.5. In the experiment, a horn antenna and a spectrum analyzer were used for spectral and power measurement of antennas. The 25 HEMT array oscillated at 5.89 GHz with mirror feedback and bias voltages of $V_{gs} = -0.6$ Volt and $V_{ds} = 0.6$ Volts, respectively. Polarization of the radiation field is mainly along the gate and drain leads. Radiation fields in the cross polarization state along the bias lines are about 20 dB less. The oscillation frequency of the grid is strongly related to the drain and source bias d.c. current I_{ds} . When the total I_{ds} was smaller than 12.8 mA, the grid oscillated at 5.27 GHz. When the total current I_{ds} was larger than 12.8 mA, the oscillation frequency stabilized at 5.9 GHz. Increasing the current I_{ds} to approximately 15.7 mA caused the oscillation frequency to increase to 7.0 GHz with other lower unsurpressed frequencies also present. Changes in either the bias voltages or the mirror position changed the current I_{ds} , which in turn affected the oscillation frequency of the oscillator. The injection locking range of the 25 HEMT array is about 2 MHz around the center frequency. The 1x1 single active HEMT antenna has very similar microwave characteristics $V_3(x,z)$ to the 5x5 HEMT antenna array. It oscillated around 5.8 GHz when it was biased at the same bias conditions as the 25 element array. Figure 3.6a shows the radiated power of the single active antenna versus bias voltages and the effect of the bias voltages on the oscillation frequency of the active antenna which is shown in Figure 3.6b. Figure

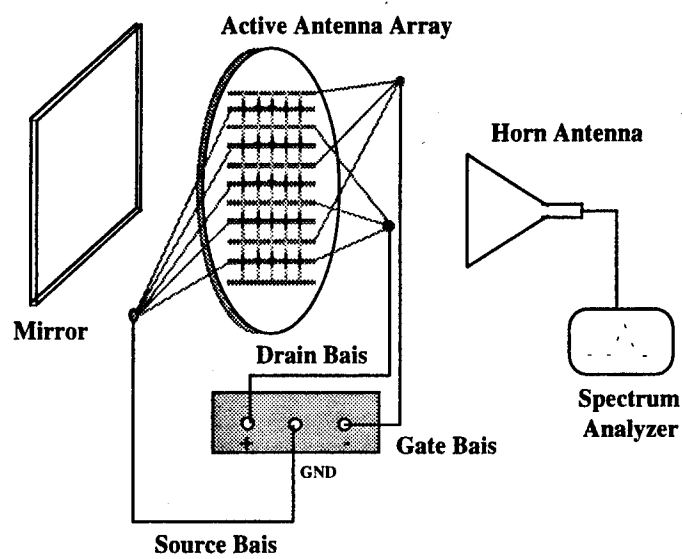


Figure 3.5. Illustration of a experimental set up for measuring the microwave characteristics of active antennas.

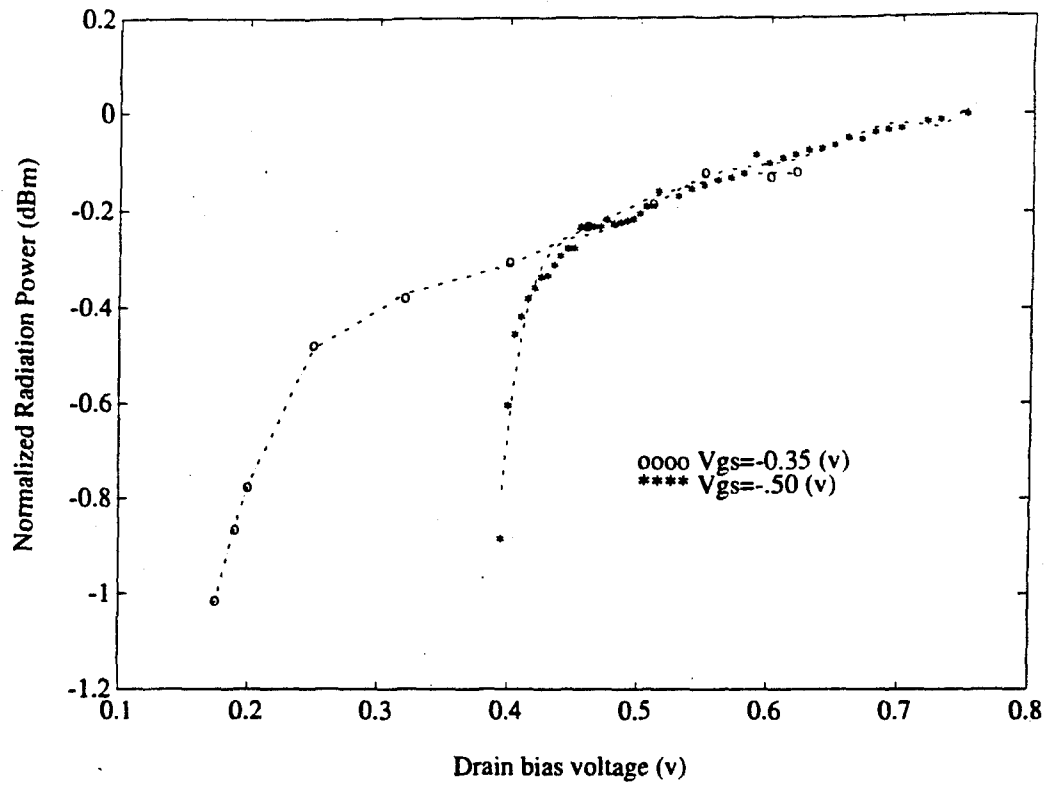


Figure 3.6a. The radiated power of the single active antenna versus bias voltages.

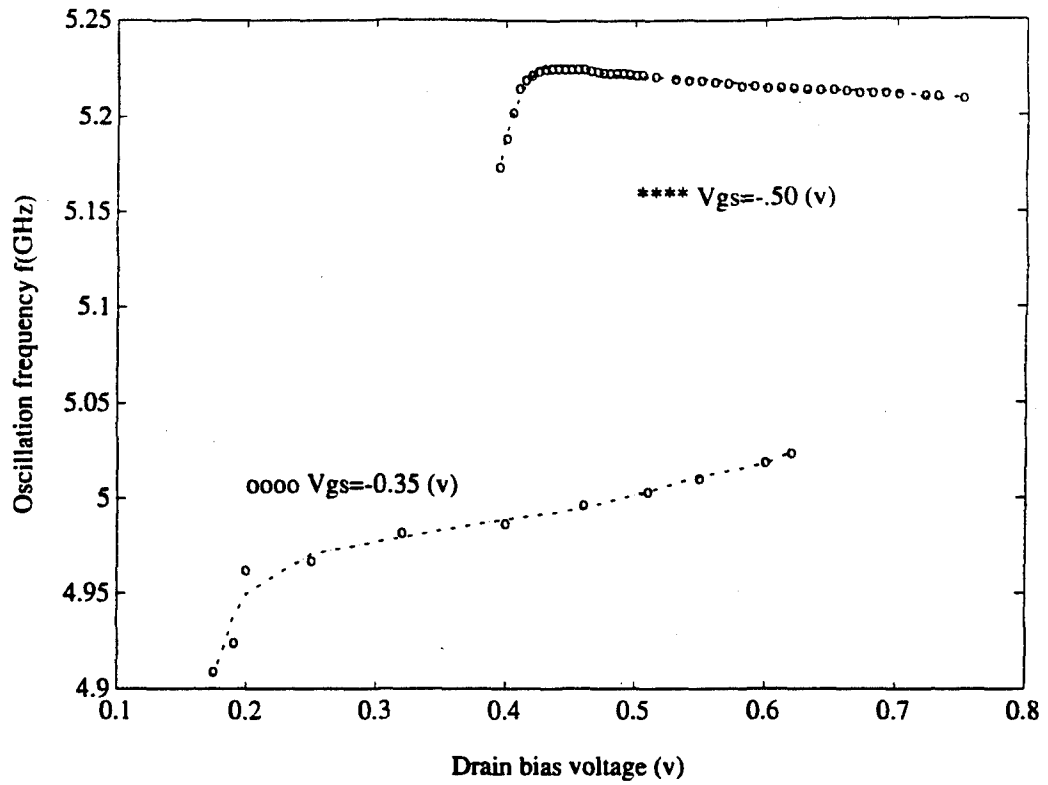


Figure 3.6b. The effect of the bias voltages to the oscillation frequency of the active antenna.

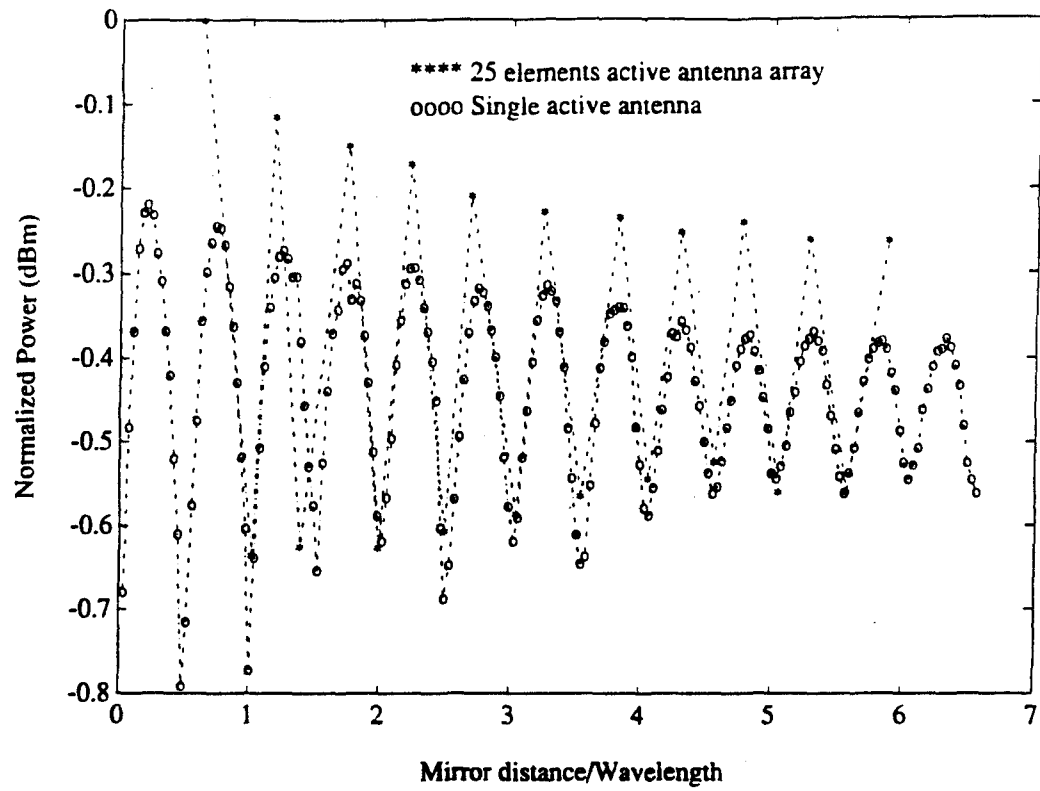


Figure 3.6c. The comparison of the radiated power between the 25 HEMT element array and a single active HEMT antenna as it changes with the mirror distance.

3.6c shows the comparison of the radiated power between the 25 HEMT element array and a single active HEMT antenna as it changes with the mirror distance. We can see that the mirror feedback mainly provides injection locking in the larger array, therefore the power in the larger array can add coherently, and the power level of the array is higher than the single antenna.

Another single active antenna was built on the same passive circuit structure but using a Fujitsu MESFETs FHX02x. This active antenna oscillated at 6.78 GHz at the bias condition of $V_{gs} = -0.5(V)$, $V_{ds} = 0.4(V)$. The effect of different active elements in the same passive structure not only changed the radiation frequency, but also changed the radiated power of the active antenna. The comparison of radiated powers of these two single active antennas are shown in Figure 3.7(a). Even though these two antennas radiate at different power levels and different frequencies, the effect of the mirror feedback to the power level of the antennas is the same. Figure 3.7(b) shows the oscillation frequencies of the active antennas versus the mirror distance. We observed that the oscillation frequencies are almost constant as we move the mirror beyond the distance of half of the wavelength away from the device. This means that the effect of the mirror on the oscillation frequency is minor if the mirror is more than one wavelength away from the device. These results show that the self-oscillating conditions are mainly determined by the near field radiation effects on the antenna structure, not by the mirror feedback. The effect of near field radiation to the charge distribution of the active antenna can only be obtained from non invasive electro-optical sampling measurements.

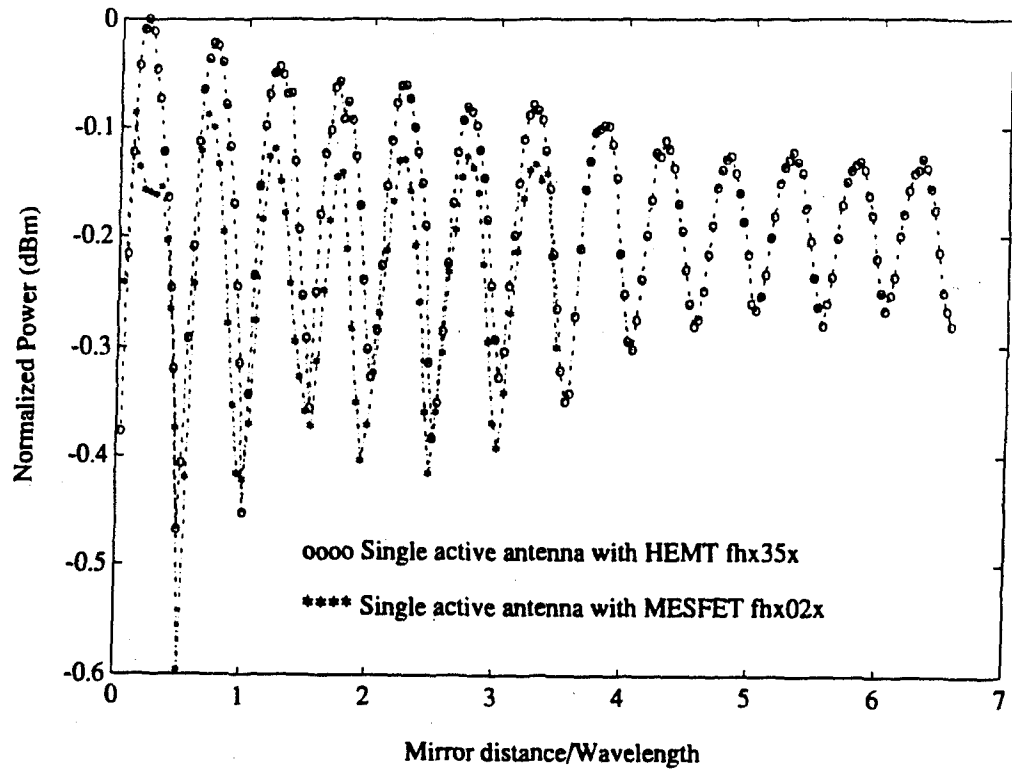


Figure 3.7a. The comparison of the radiated power of two active antennas with different active elements.

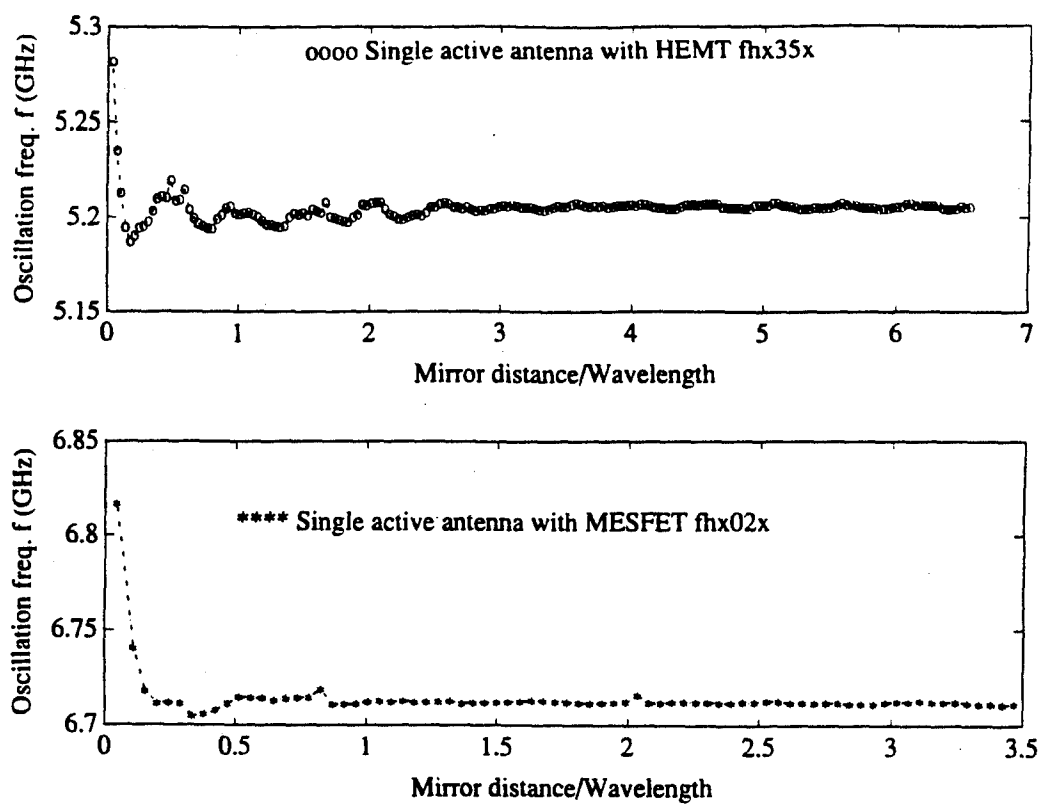


Figure 3.7b. The oscillation frequencies of single active antenna versus mirror distance.

3.5. Optical Sampling Measurements

A radiating microwave oscillator can have its oscillation frequency affected by disturbances from nearby surroundings. Slight drifts in frequency away from the harmonic of the laser pulse in a sampling measurement will produce inaccurate results due to the narrow bandwidth (1 MHz) used in the detector/amplifier. Therefore, microwave injection locking to the laser mode locker is necessary. The optical sampling arrangement for measuring the amplitude of the potential is shown in Figure 3.8a. A 10 dB microwave directional coupler was used to separate the injected signal and the detected signal of the active array structure. A spectrum analyzer is used to monitor the injection process while conducting optical sampling and is also used to record the output signals of the probe beam collected by a detector/amplifier while sending this data to a computer. During real time measurements, the probe beam scans the active structure. Polarization of the probe beam will change its direction due to the local potential difference of both sides of the substrate, which modulates the intensity of the optical beam. The relative phase in the potential distribution can also be measured by feeding the laser reference and reflected beam to a lock-in amplifier that heterodynes the two signals. The modified optical sampling analyzer is shown in Figure 3.8b. Calibration of the electrooptic signal, due to small thickness variations across the wafer, is done by comparing the direct current optical power to the reflected beam as the scanning is performed. In general, calibrations relevant to the measurements are made by making "known" test structures on the same substrate as the device under test and scanning these structures to determine the calibration parameters [1].

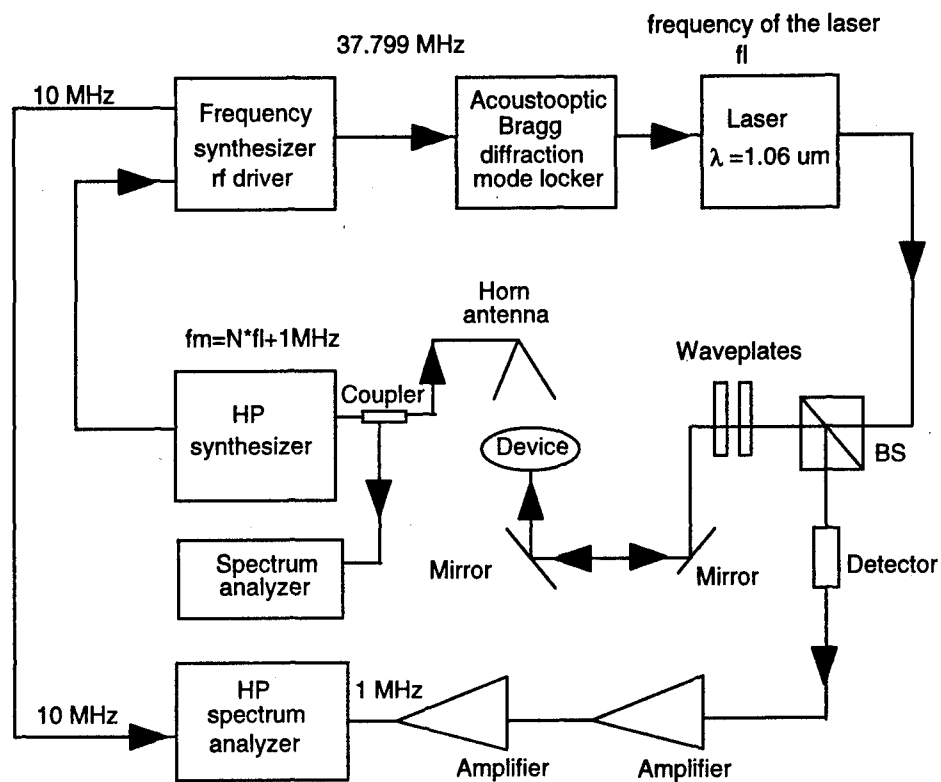


Figure 3.8a. The optical sampling arrangement for measuring the amplitude of potential distribution.

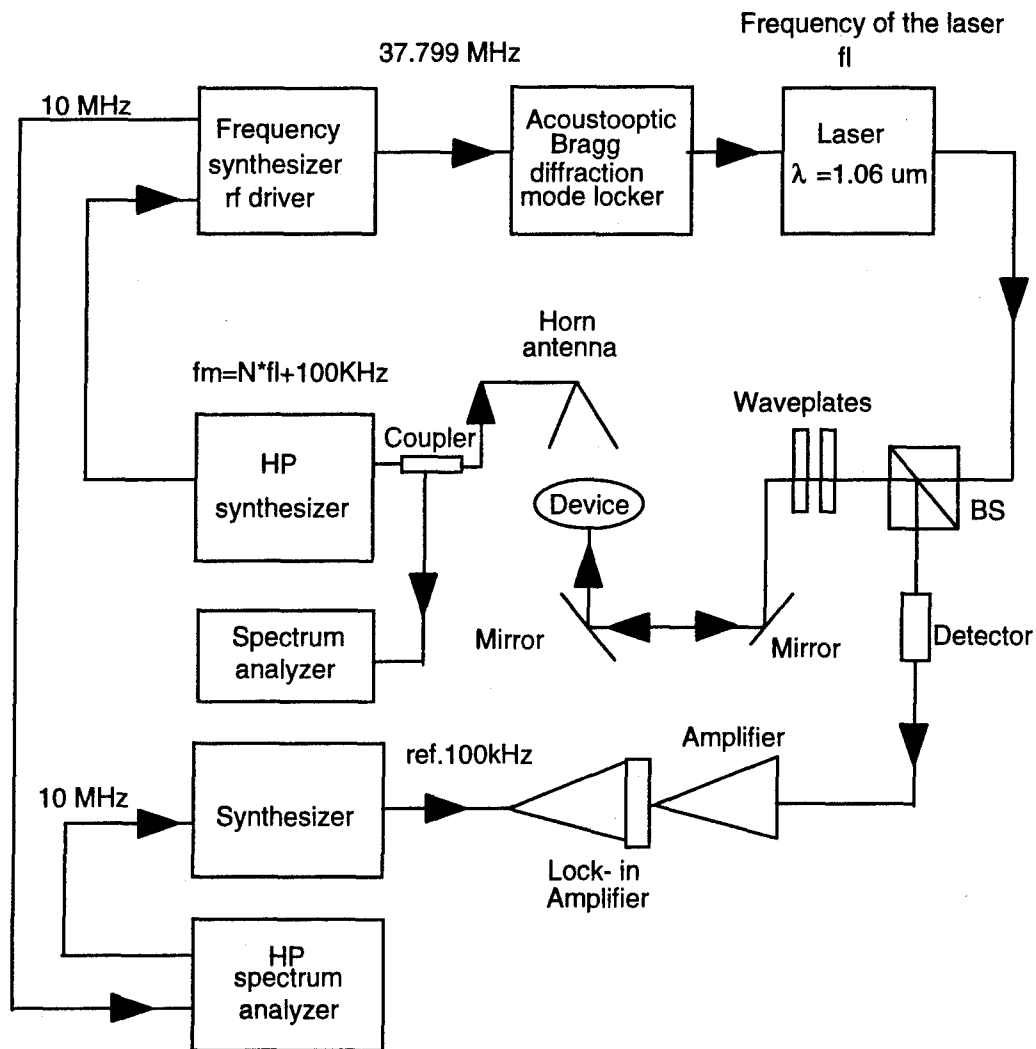


Figure 3.8b. The optical sampling arrangement for measuring the phase of potential distribution.

A schematic diagram of the two-dimensional optical sampling for measuring the amplitude potential distribution is shown in Figure 3.9. The entire arrangement is located on an optical table and controlled by a computer. In this experiment, light from a ND^{+3} :YAG mode-locked laser ($\lambda = 1.06 \mu\text{m}$, 70 ps pulse width) is guided to the bottom side of the GaAs wafer and serves as the probe beam. As was earlier discussed, the polarization of the probe beam is rotated in proportion to the complex value of the relative potential on the structure due to the electrooptic coefficient of GaAs. Therefore, measurements of the potential distribution while the active antenna array is oscillating can be made. The in-situ measurement is realized by injection locking the oscillation frequency of the active antenna array to one of the components of the mode locked laser pulse. In order to stabilize the oscillation frequency of the active antenna array, the frequency of the array was adjusted to be around 5.89 GHz. A broadband horn antenna was placed approximately 30 cm away from the active antenna structure. Thus, the horn antenna was able to injection lock the structure at 5.8967 GHz. This frequency was then synchronized with the 78th harmonic of the laser pulse to within a receiver bandwidth of 1 MHz.

Figures 3.10(a-d) show some of the measured potential distributions along a column of the active HEMT array obtained from the non-invasive optical sampling apparatus. The data was taken in real time with the array oscillating at 5.8967 GHz and represents the potential difference between front and back sides of the GaAs wafer. A higher potential is measured where the drain and gate leads are close to the active devices. A π phase shift was measured across the active devices. The maximum value of the potential in the drain is slightly higher than the one in the gate,

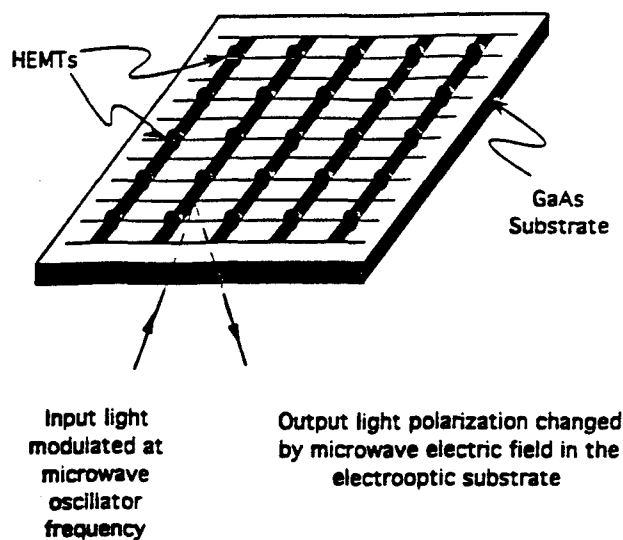


Figure 3.9. A schematic diagram of two-dimensional optical sampling for measuring the amplitude potential distribution.

displaying much lower potential values in the source leads even at points close to the HEMT. The measured potential values on the source leads close to the active element are non-zero, but their maximum is significantly lower than those of the gate or drain leads shown in Figure 3.10e. Optical sampling results reveal a zero relative potential difference between the gate and drain bias lines (shown in Fig. 3.10f). Figure 3.10g shows the two-dimensional distribution of the potential in a cell of the 25 HEMT element arrays. These results depict some unusual features of active antenna structures when they are under a large signal operation. Of particular interest is the complete absence of boundary effects near the center bias lines.

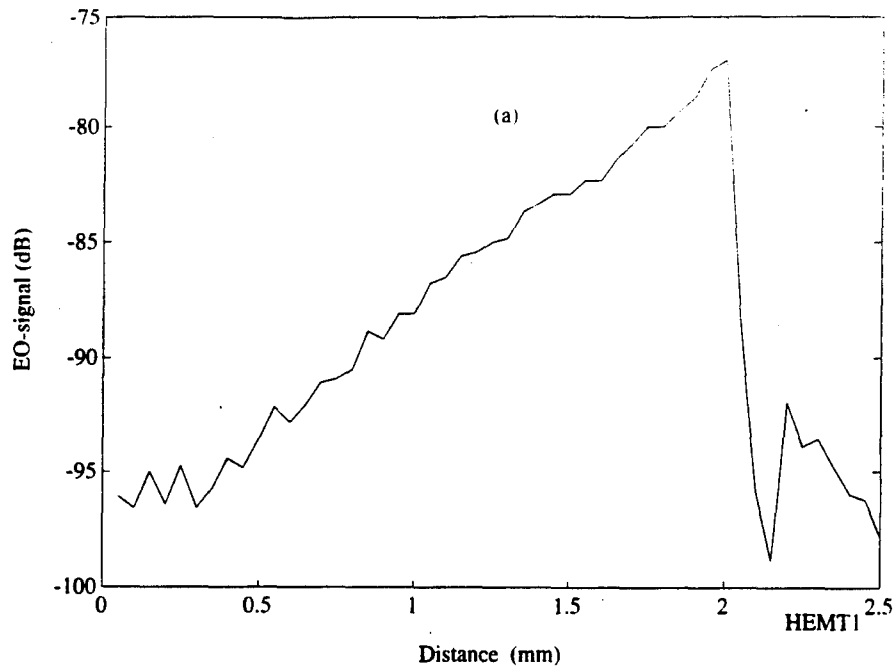


Figure 3.10(a-f). Some of the measured potential distributions along a column of the active HEMT array are obtained from the non-invasive optical sampling. (a), a potential distribution along gate radiating lead.

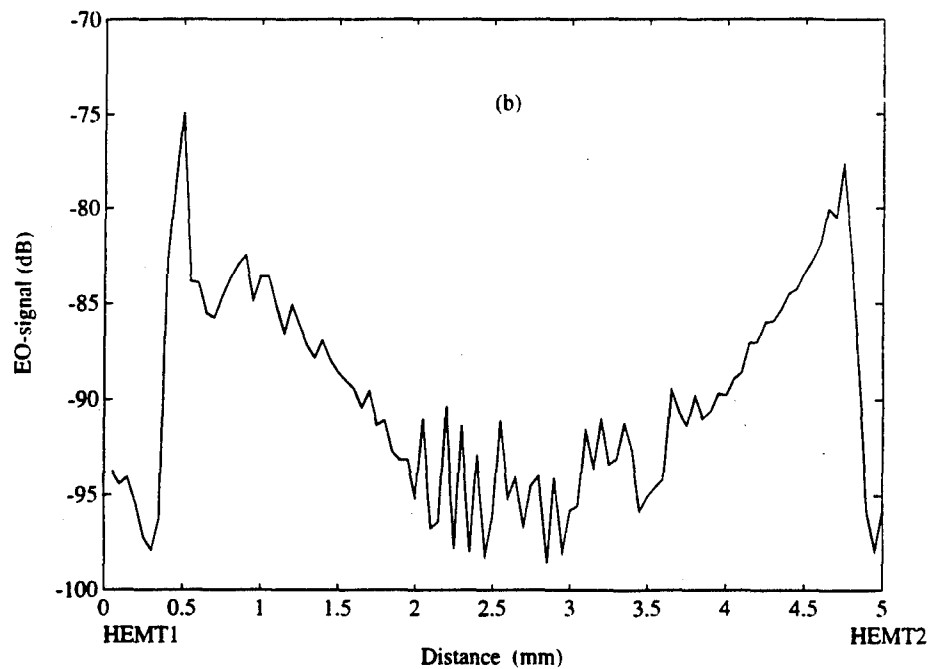


Figure 3.10b. A potential distribution along drain radiating lead between two active elements.

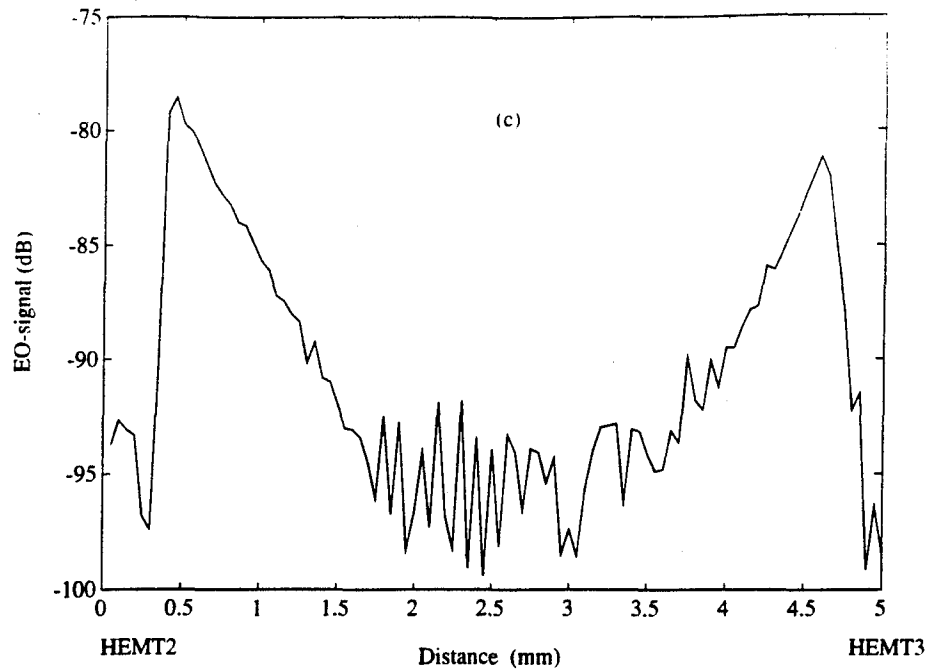


Figure 3.10c. A potential distribution along gate radiating lead between two active elements.

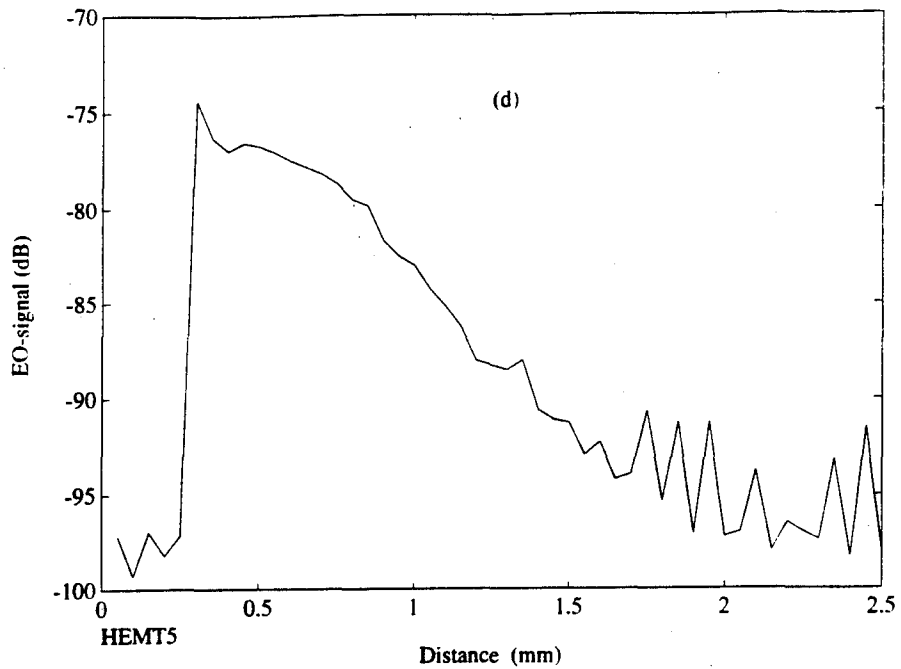


Figure 3.10d. A potential distribution along drain radiating lead.

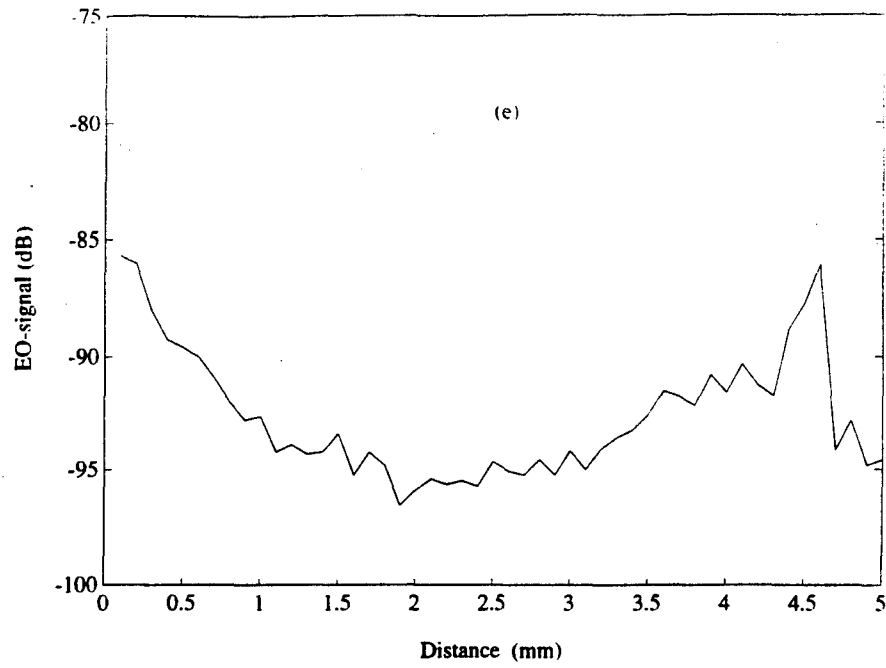


Figure 3.10e. A potential along a source bias line of two active elements.

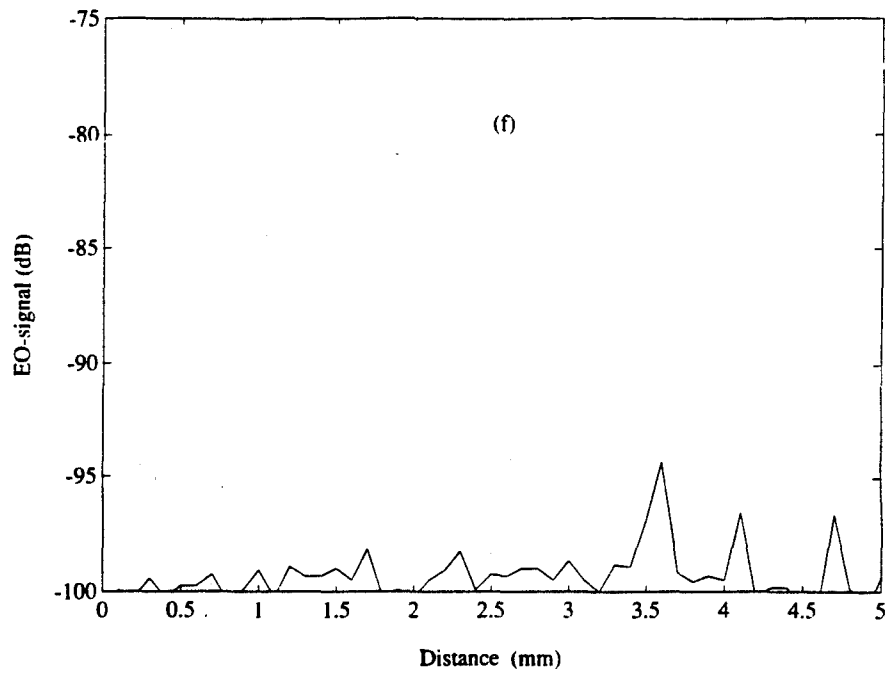


Figure 3.10f. A potential along a gate bias line of two active elements

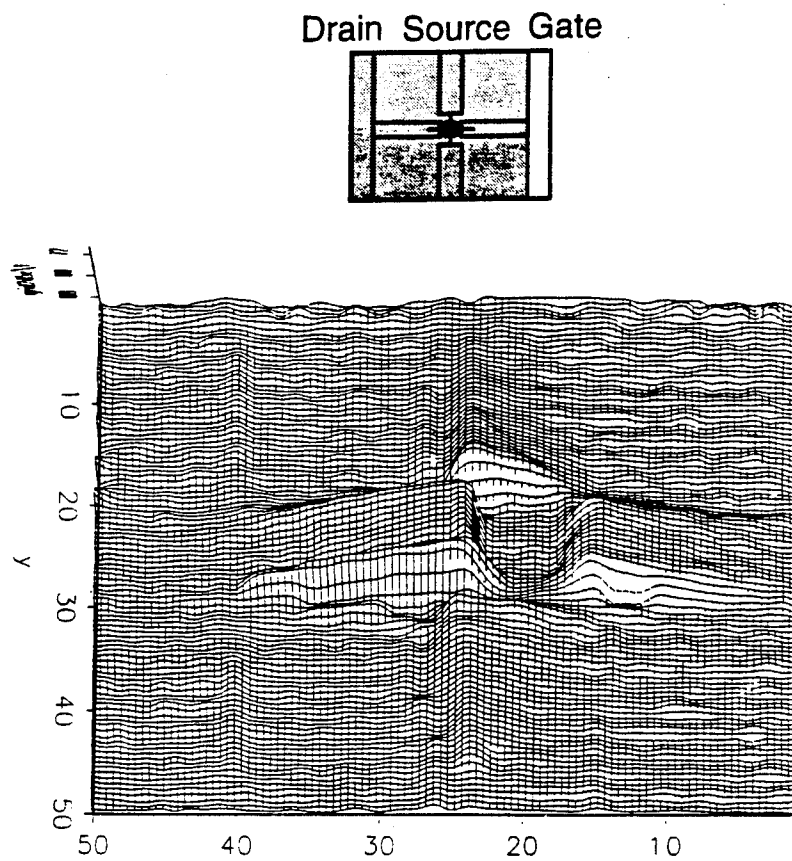


Figure 3.10g. A two-dimensional distribution of the potential in an element cell of the 25-HEMTs arrays.

The measured potential distributions of all cells in the active structure were found to exhibit remarkably similar forms. Only the magnitudes of the potential distributions vary slightly from one transistor to the next, possibly due to non-identical transistors. Removing a HEMT from the array did not affect the potential distribution in an adjacent cell. Further evidence of the independence of these structures manifests itself in the measurements across a single active antenna (1x1). In this case, the distribution is similar to that of a single unit cell placed in an entire active antenna array. Measurements of the potential distribution of a single cell are illustrated in Figure 3.11(a-c). It is interesting to note, that the potential appears qualitatively quite similar to any of the cells that were connected together in the array structure except that the edge effect appears on the source bias line. In the array structure the measured potential at the edge of the source bias line of each elementary cell are relatively lower than the one with the single active antenna. It is almost as if the elements of the array structure act independently of one another.

To examine the function of the bias lines, the planar drain and gate bias lines are removed from the single active antenna and replaced by two shield wires. Even though the rest of the structure remains the same, it is found that without the drain and gate bias lines, neither the a.c. field can be measured from optical sampling nor can oscillation be detected from a spectrum analyzer. In other words, the transistor is stable. The results of these experiments suggest that the presence of the bias lines is critical to the oscillation condition of an active antenna. They should not be ignored in the circuit calculations.

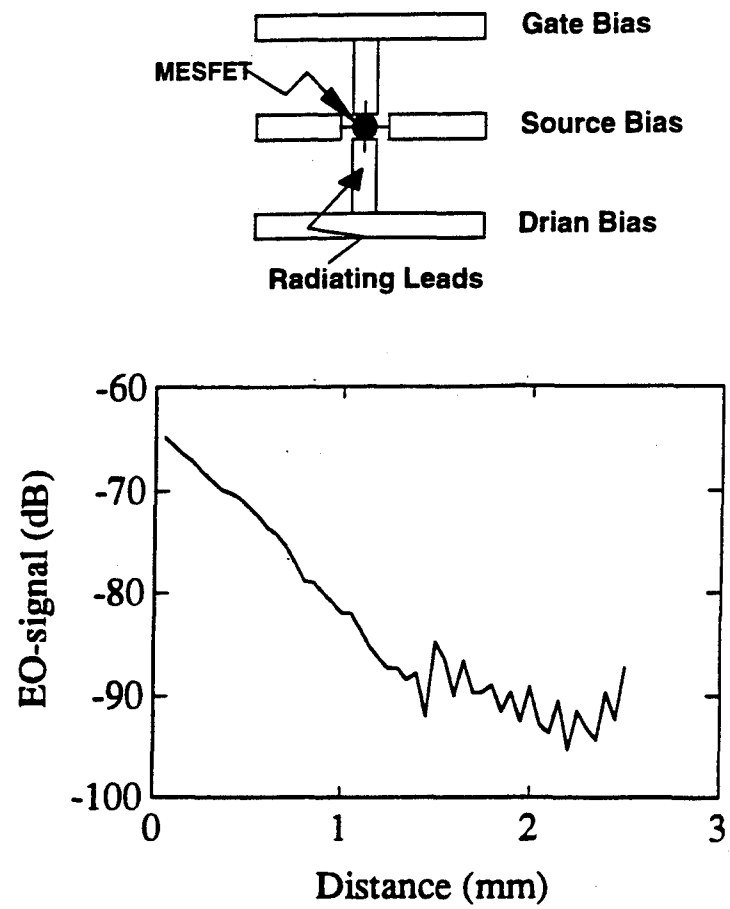


Figure 3.11a. Measurements of the potential distribution of a single MESFET active antenna. (a), potential distribution along the drain radiating lead.

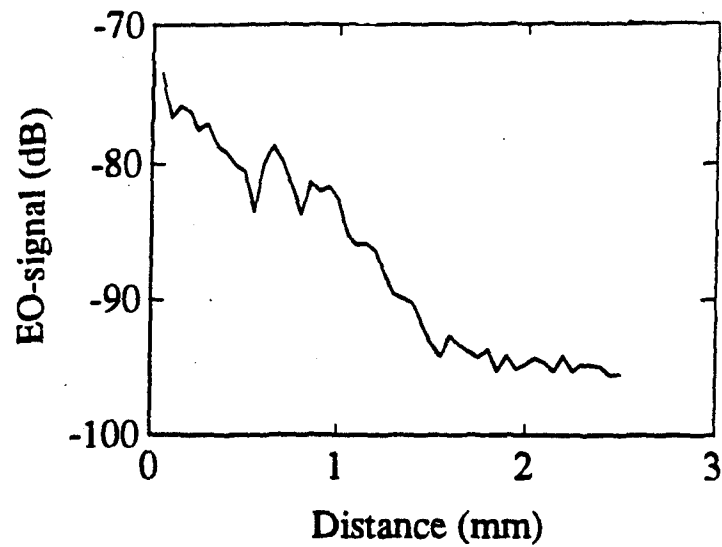


Figure 3.11b. A potential distribution along the gate radiating lead of a single active antenna.

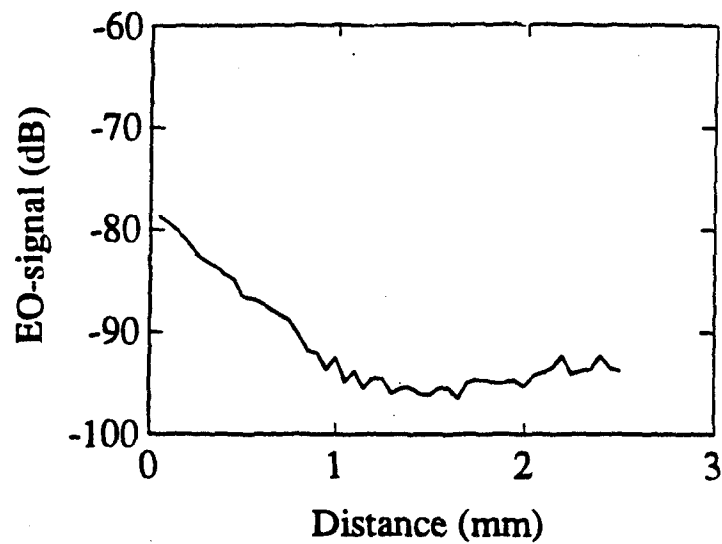


Figure 3.11c. A potential distribution along the source bias line of a single active antenna.

3.6. Summary

Different active antennas are fabricated on GaAs substrates especially for optical sampling measurements. HEMTs and MESFETs are used as active elements in antenna arrays for their higher frequency performance and power conversion efficiency. Extensive measurements on these active antennas are performed by optical sampling and conventional microwave measurement techniques. Significant experimental results are observed. This is proof that the optical sampling technique provides a wealth of real time information on the potential distributions of active antennas. As we know, the mode of a resonant active antenna can be identified if the potential distributions on the structure are recognized. The phase of potential across the transistor is also measured. The relative phase difference in the potential on the drain and gate terminals of the transistor is approximately 180 degrees (the phase distribution along the radiating leads cannot be measured due to the low signal to noise ratio). Sampling experiments also show that the potential distribution on each period of the grid are not critically perturbed by the presence of its neighbor. Stability conditions of the active element are determined by the geometry of the structure inside each grid period. Therefore, the oscillation condition of the active array is not influenced by its size. These are unique characteristics of an active array which are discovered for the first time. To further prove the optical sampling results, a single active antenna was also built. The geometry of the signal active antenna is the same as in each elementary cell of the array. It was demonstrated that the single active antenna is indeed unstable. The oscillation frequency of the single active antenna is

close to the active array antenna (within injection locking range of an electric signal). It is suggested that the coherent operation of the array is achieved from the mutual coupling of the active elements. To justify the observation from optical sampling measurements, spectra measurements on a 5x5-HEMTs element array were performed. Results show that without the feedback from a mirror, six spectra are measured, which indicates loose mutual coupling between active elements. With a mirror feedback, the antenna array oscillates at one frequency and the radiation power of the array is increased. Broadly speaking, the operational principles of the active antenna array are analogous to the grating surface emitting laser (GSEL) as we suggested in Section 1.3. That is, when each active element formed an individual oscillator in each elementary cell of the grid, the coherent operation of the device is achieved by the mutual coupling between the active elements. In general, the input impedance of a passive antenna is effected by the mutual coupling between the elements. Results of these experiments have also shown that the change of the impedance is suppressed by the presence of the transistor (this phenomenon is also observed from non-resonant active antennas [7-9]). Therefore, coupled oscillator array theory can be used to predict the performance of active arrays.

The optical sampling has revealed some new characteristics of an active antenna array. Based on our new understanding, the optimization design of the active array can proceed in two steps: first is that we can optimize the power or locking bandwidth of a single active antenna; and second, by obtaining coupled parameters of a single antenna, the optimization of the array can be calculated from theories of coupled oscillators.

References

1. D. R. Hjelme and A. R. Mickelson, "Voltage Calibration of the Direct Electrooptic Sampling Technique," *IEEE Trans. on Microwave Theory and Tech.*, vol. 40, pp. 1941-1950, Oct., 1992.
2. D. R. Hjelme, M. J. Yadlowsky, and A. R. Mickelson, "Two-Dimensional Mapping of Microwave Potential on MMIC's Using Electrooptic Sampling," *IEEE Trans. on Microwave Theory and Tech.*, vol. 41, pp. 1149-1158, June/July, 1993.
3. V. Radisic, D. R. Hjelme, A. Horrigan, Z. B. Popovic and A. R. Mickelson, "Experimentally Verifiable Modeling of Coplanar Waveguide Discontinuities," *IEEE Trans. on Microwave Theory and Tech.*, vol. 41, pp. 1524-1533, Sept., 1993.
4. I. Stakgold, "Boundary Value Problems of Mathematical Physics," vol. 1 and 2, The Macmillan Company, London, 1972.
5. Pocklington, "Electrical Oscillation in Wires," *Proceeding of the Cambridge Philosophical Society*, pp. 324-333, 1897.
6. R. Smyth, "Static and Dynamic Electricity," Hemisphere Publishing, New York 1989.
7. M. Dawond and A. P. Anderson, "Calculations Showing the reduction in the Frequency Dependence of a Two-Element Array Antenna Fed by Microwave Transistors," *IEEE Trans. Antennas Propagat.*, vol. 20, pp. 497-499, 1972.
8. J. P. Daniel, "Mutual Coupling Between Antennas for Emission or Reception--Application to Passive and Active Dipoles," *IEEE Trans. on Antennas Propagat.*, vol. 22, pp. 347-349, March, 1974.
9. J. P. Daniel and C. Terret, "Mutual Coupling between Antennas--Optimization of Transistor Parameters in Active Antenna Design," *IEEE Trans. on Antennas Propagat.*, vol. 23, pp. 513-516, July, 1975.
10. M. G. Li, and C. H. Lee, "Intermixing Optical and Microwave Signal in GaAs Microstrip Circuit and Its Applications," *Microwave and Optical Tech. Lett.* vol.6, pp. 27-32, Jan. 1993.

CHAPTER 4

ANALYSIS OF OPTICAL SAMPLING DATA ON RADIATIVE STRUCTURES

1. Introduction

In a high frequency microwave active device, the circuit parameters which will determine the working conditions of the active element are distributed. Knowing the field distribution on a structure will enable us to identify the operation mode and the components that play role in the circuit. Understanding the intrinsic field configuration of the device will provide the means for us to use more efficient analysis methods for designs. One of the purposes of our investigation of the active antenna by using optical sampling is to identify the operation mode of the active device. At the same time, through the analysis of field distribution on the structure, we can ascertain the identity of the grid structure in the active device operation. Therefore, it is important to interpret the sampling results correctly from the measurement data.

As we described in Chapter 3, the actual quantity measured by optical sampling, dV , is the potential difference between the front and back of the substrate. Knowing the Green's function for the particular geometry of the test circuit, the charge distribution can be calculated from the experiment using the measured quantity. As a result, the potential structure on either side of the substrate can be recovered. Previous studies of the potential field on passive coplanar waveguide

structures have shown that the corrections to the electric field on a conductor are small [1-3]. In other words, the value of the measured potential distributions are close to the actual one on the conductors. The reason for the small correction found in the coplanar waveguide is that the fields are often strongly confined in the guided wave structure. Also, in the case of the coplanar guide, the thickness of the dielectric substrate is much larger than the dimension of the gap between the conductors. Consequently, the potential on the back of the substrate can be considered zero. Subsequently, the measured potential distribution is the same as the potential on the conductor. In the case of the guided-wave structure, the circuit characteristics can be interpreted directly from the measurement data

As in the present case, the structures we measured are operating in a radiating mode. The dimension of a single active antenna or an elementary cell is $5 \times 5 \text{ mm}^2$, the width of the electrodes are about 0.8 mm and the thickness of the sample is only 0.5 mm . One would assume that there would be a significant potential on the back surface of the substrate. Accordingly, the potential distribution on the electrode V_1 , will be different from the measured potential dV .

4.2. Potential Distribution of a Single Active Antenna

Since our measurement data has shown such remarkable similarity between the elementary cell of an array and a single active antenna, the single antenna can be used as an example for finding the actual potential from the optical sampling measurement. It is noticed that the normalized value of measured potential

distributions dV have noise floor at 0.1 V, which means that any value of dV on the antenna lower than roughly 0.1 V will be detected as noise. To calculate the potential distribution of V_1 on the electrode, the Green's function derived in Section 3 was first used for that analysis. From the calculation of the charge distribution, we found that the calculated charge distribution is sensitive to the exact potential value on the noise floor. As a result, the actual distribution of V_1 on the electrodes are also sensitive to the value of the noise floor. Therefore, the direct inversion method of Eq. [3.3] in Chapter 3 will not be especially accurate in this case. To restore the information lost in the noise, and to recover the actual potential distribution from the measurement as accurately as possible, an expression of the distribution V_1 has to be estimated first. We will presently develop a procedure to evaluate the possible distributions of V_1 . The structure of the active antenna consists of three bias lines (shown in Figure 3.3) which form three coplanar lines. These lines can support two fundamental modes, one an even mode $[0 \ 1 \ 0]$, the other an odd mode $[-1 \ 0 \ 1]$. Any operation mode of this structure must be a combination of these two modes. Knowing that the antenna is a radiating structure, the dominant mode of the structure must be an odd mode. Due to the π phase shift crossing the active element, opposite charges on both sides of the active device will tend to cancel out their effect on the potential on the back of the substrate V_3 . This results in V_3 having minimum magnitude near the active device, and increased magnitude as one moves away from the active device. Hence, the correction in V_1 from the measured value dV is smaller near the active device. Away from the active device region, the difference between V_1 and dV could be large. This

depends on the charge distribution. In light of experimental results, various 2D-potential distributions of V_1 under odd dominant mode operations are assumed. The 2D-distributions of dV in these cases are calculated from the distributions of V_1 using the Green's function derived in Chapter 3 and the method of moments. The calculated 2D-distributions of dV will then be compared with the measurements. Since the experimental value has a noise floor value at 0.1 V, the calculated distributions will also use 0.1 V as noise floor value.

We will presently illustrate five possible cases. Figure 4.1 shows the 2D-potential distribution of V_1 in cases 1 and 2. The distributions of V_1 are assumed as follows: the potential V_1 is constant through the gate region (including radiating lead and bias line), where $V_1 = V_g$. The same assumption is made for the drain region. Where $V_1 = V_d$ and the potential V_1 in the source bias line is set to $V_1 = V_s$. In summary, in case 1, potentials are set to $[V_g, V_d, V_s] = [0.5V, 0V, -1.0V]$ and in case 2, potentials are set to $[V_g, V_d, V_s] = [0.525V, 0.25V, -1.25V]$. Figure 4.2 shows the potential distribution of V_1 in cases 3 and 4. In these cases, the potential distribution V_1 is assumed to be linearly decaying along the gate and drain radiating lead as V_1 is moved away from the active device. Near the active device, $V_g = 0.525V$ and $V_d = -1.25V$, and the potentials on all the bias lines are assumed to be uniform. In case 3, the potentials on the bias lines are set as $[V_{gb}, V_{sb}, V_{db}] = [0V, 0.25V, 0V]$. In case 4, the potentials on the bias lines are set to $[V_{gb}, V_{sb}, V_{db}] = [0.25V, 0.15V, -0.1V]$ respectively. Figure 4.3 shows the potential distributions of V_1 in case 5. In this case, the potential distributions of V_1 are assumed to be linearly decaying along the radiating leads and the source bias line as V_1 is moved away from

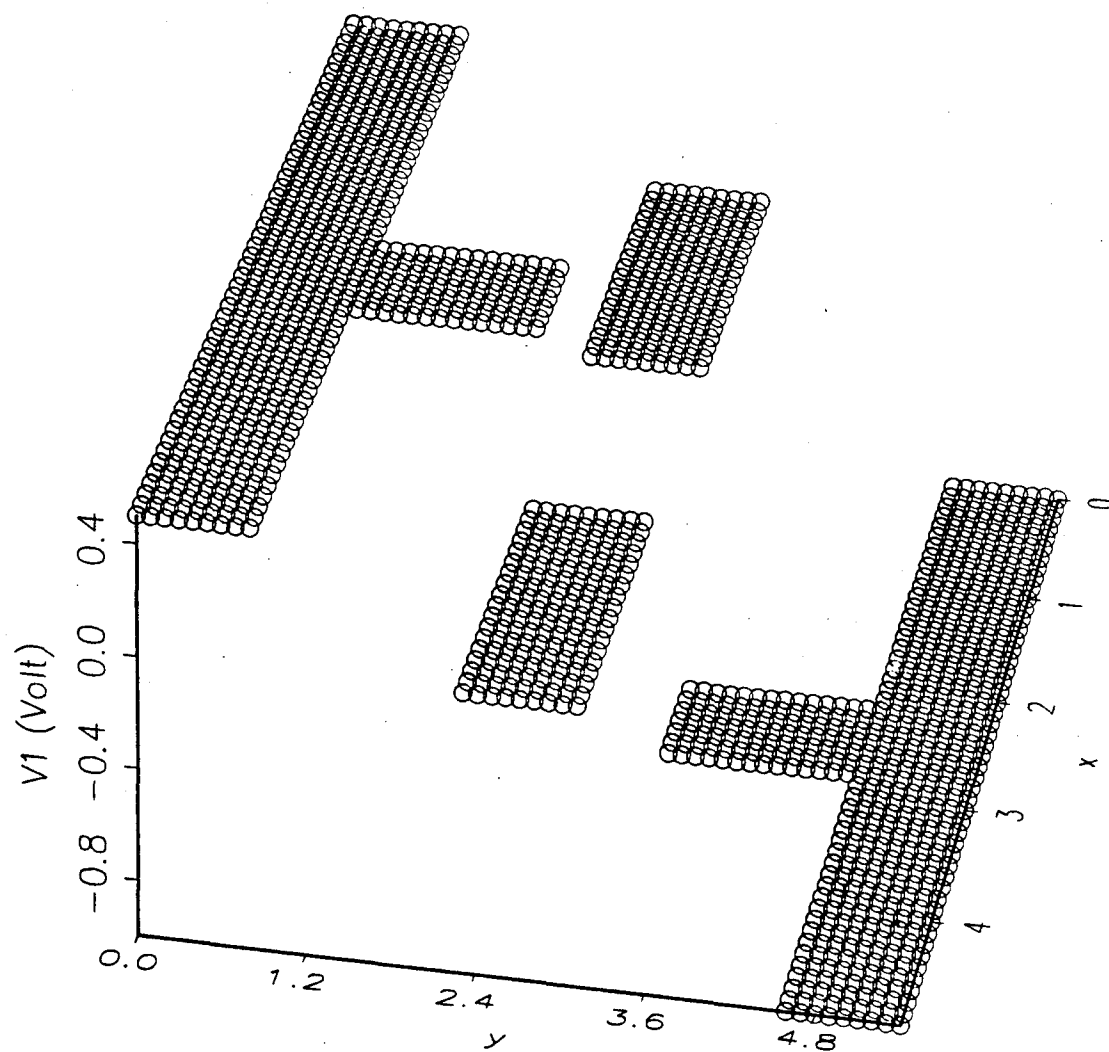


Figure 4.1. Assumed potential distribution of V_1 in case 1. Case 2 has the same distribution profile except the value on the source bias lines are set to equal to $-1.25V$.

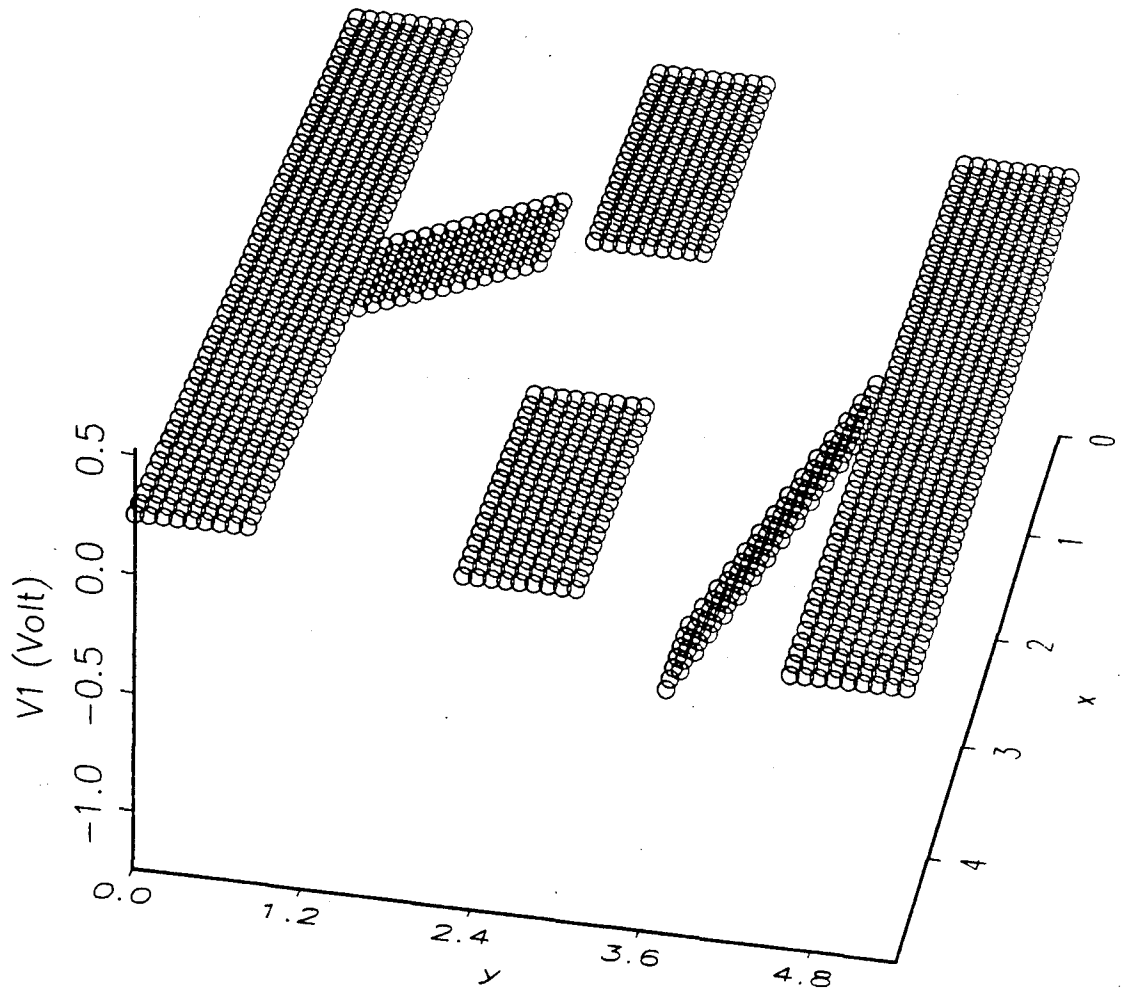


Figure 4.2. Assumed potential distribution of V_1 in case 4. Case 3 has a similar distribution profile except the value on the gate, drain and source bias lines are set to equal to 0 V.

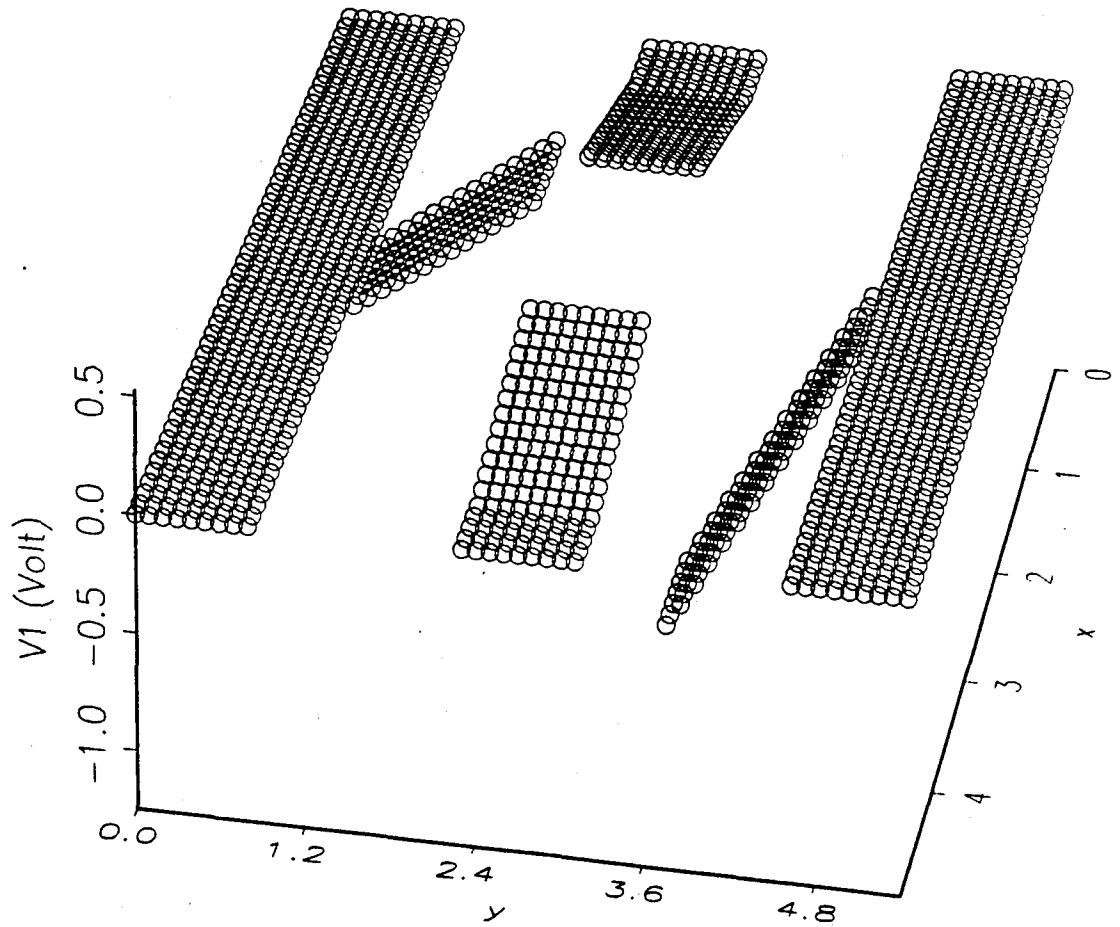


Figure 4.3. Assumed potential distribution of V_1 in case 5.

the active device. Near the active device, the potentials are set to $[V_g, V_s, V_d] = [0.525V, 0.25V, -1.25V]$. The calculated dV distributions from these five cases are compared with the measured 2D dV distribution. From the experiment, the total numbers of sample points, $nq = 1420$, are taken from the electrodes of the antenna and each sampling increment step is $100 \mu m$. Therefore, the calculated dV is also arranged in the same manner, that is, there are a total of 1420 calculated points and each incremental step is $100 \mu m$. The standard deviation σ_{sd} of the calculated dV_c from the measured dV_m is defined as:

$$\sigma_{sd}^2 = \frac{1}{nq} \sum_{i=1}^{i=nq} \sigma_{sdi}^2 = \frac{1}{nq} \sum_{i=1}^{i=nq} (dV_{ci} - dV_{mi})^2, \quad (4.1)$$

where, dV_{ci} is the calculated potential of dV, dV_{mi} is the measured potential of dV and $\max(\sigma_{sdi})$ is the maximum value among the σ_{sdi} . The results of these comparisons are shown in Table 4.1.

Table. 4.1

Comparison of Calculated Potential Distribution from the Measured Distribution.

case Number	Standard Deviation σ_{sd}	Maximum Deviation $\max(\sigma_{sdi})$
case 1	0.0858	0.4840
case 2	0.1034	0.4128
case 3	0.0368	0.2234
case 4	0.0418	0.2780
case 5	0.0358	0.1940

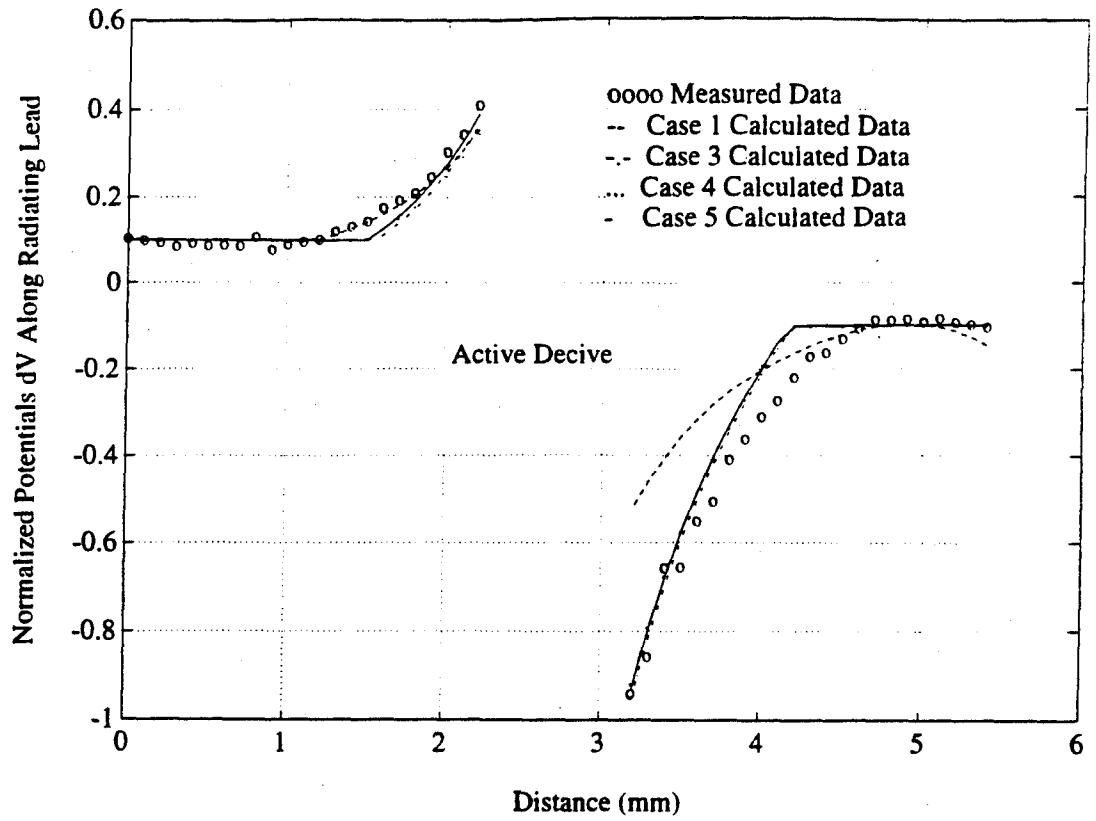


Figure 4.4a. Comparison of measured potential dV with calculated potentials dV on radiating leads at both sides of the active device.

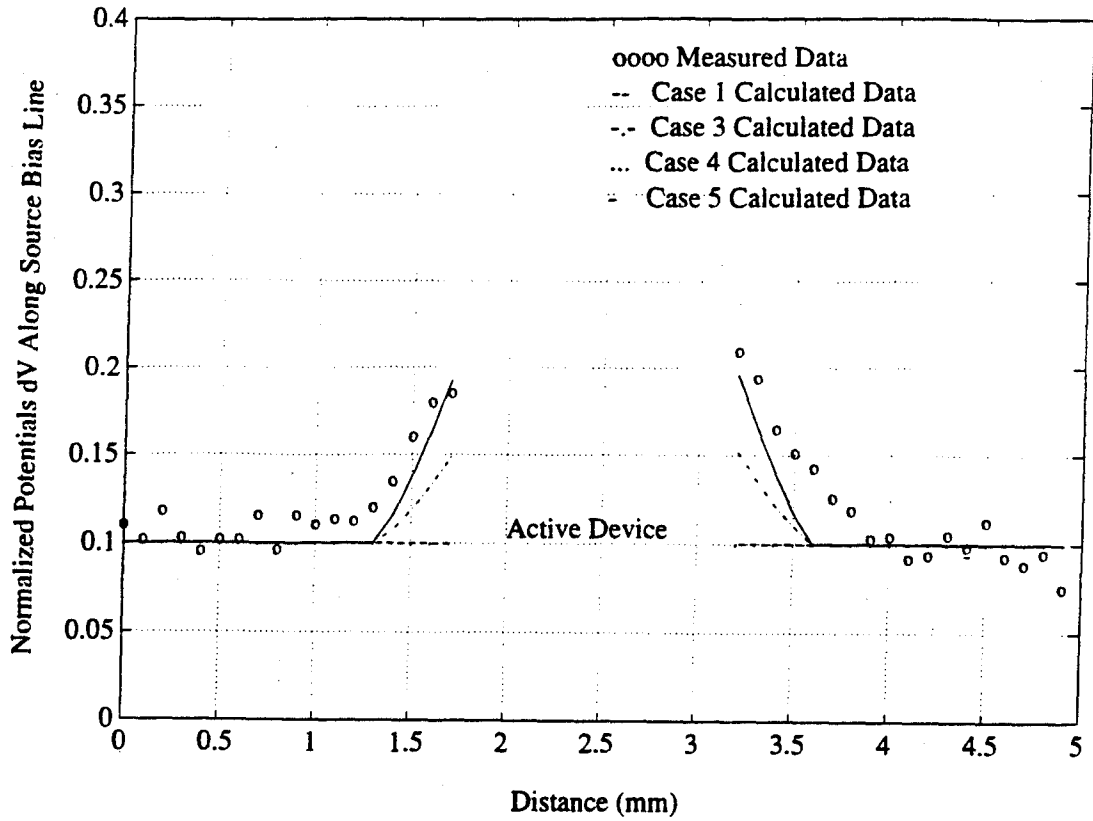


Figure 4.4b. Comparison of measured potential dV with calculated potentials dV on a source bias line.

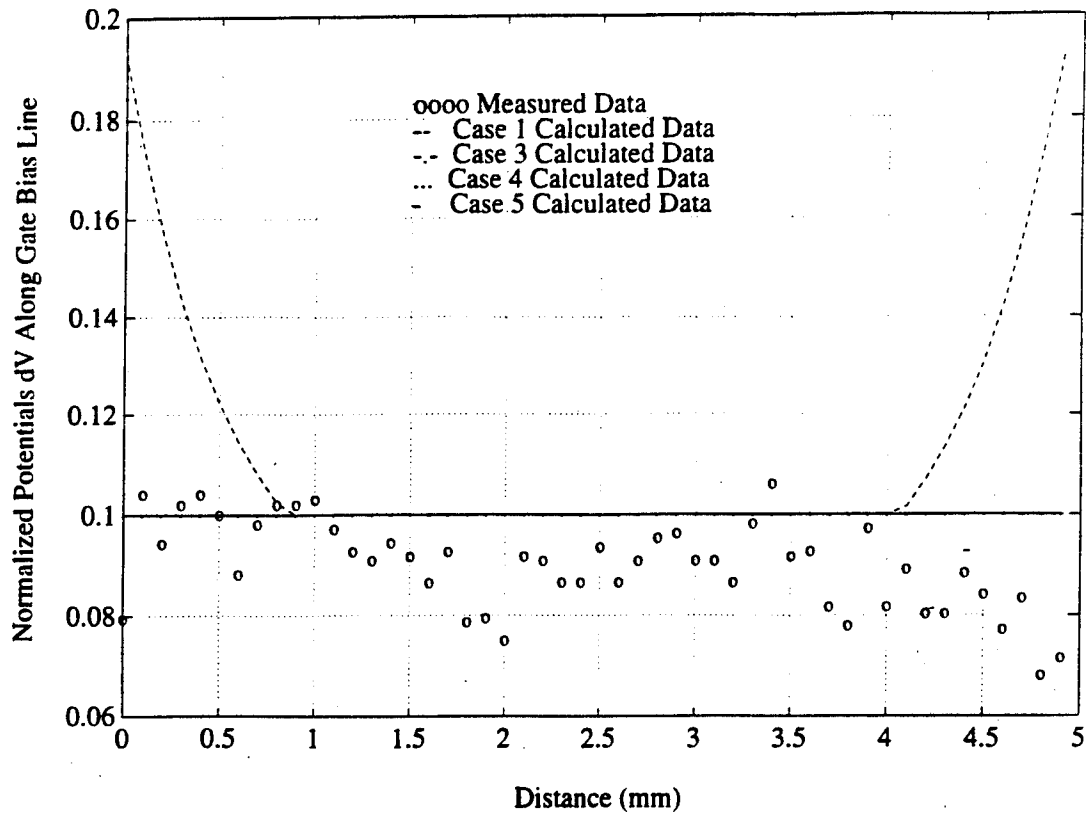


Figure 4.4c. Comparison of measured potential dV with calculated potentials dV on a gate bias line.

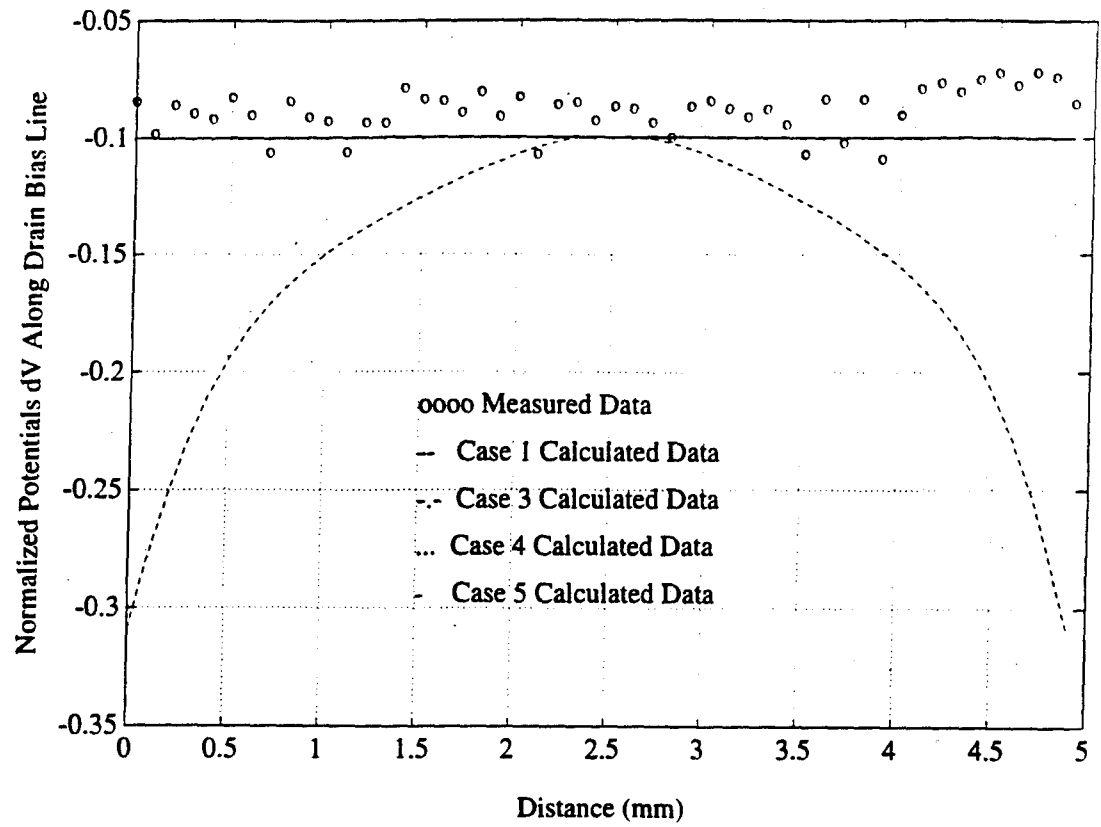


Figure 4.4d. Comparison of measured potential dV with calculated potentials dV on a drain bias line.

Note that cases 1 and 2 have assumed a uniform distribution of V_1 , in the gate, drain, and source regions. The assumption for this type of distribution fits poorly to the experimental results (measurement error from the experiment due to the noise is lower than 4.3%). Both the standard deviation and maximum deviation are nearly twice as large as other cases. The difference between these two cases is indistinguishable. The best fit potential distribution is the one in case 5. In this particular case, the potential distribution is assumed as linearly decaying throughout the radiating lead and the source lead. The second best fit is followed by case 3, then case 4. Figures 4.4(a-d), show the comparison of the calculated potential and the measured potential. These one-dimensional plots have presented the same results as shown in Table 1. Figures 4.5a-b show the comparison of 2D-calculated potential and the measured potential. As is seen, there is a definite correction of V_1 from dV . In case 5, the correction for V_1 is not more than 20% of the $dV = V_1 - V_3$ curve, but the correction for V_1 is more than 400% in case 1. These results are shown in Figure 4.6 (a-b). In the remainder section, discussion will be given as to possible explanations for these distributions.

In Sections 3.5 of this chapter we have presented the results of the measurements and these results are analyzed using numerical simulations. Because of the radiating nature of the structure, the electric fields are not strongly confined in the sample. Further, the substrate is thin in comparison to the linewidth, sample measurements are therefore more sensitive to the charge distribution than the potential distribution as was discussed in Section 3.2. The change in the measured distribution of dV is therefore not as sensitive to variations as the converse in V_1 .

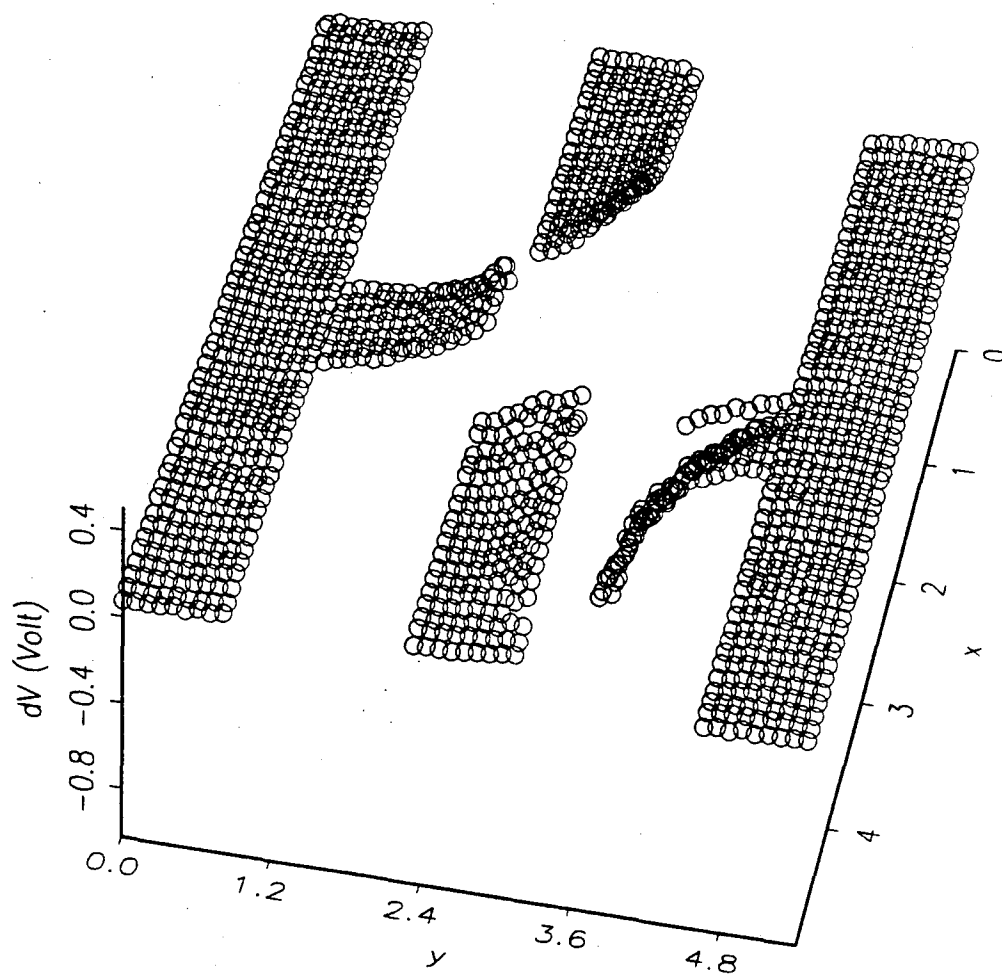


Figure 4.5a Measured potential dV obtained from optical sampling.

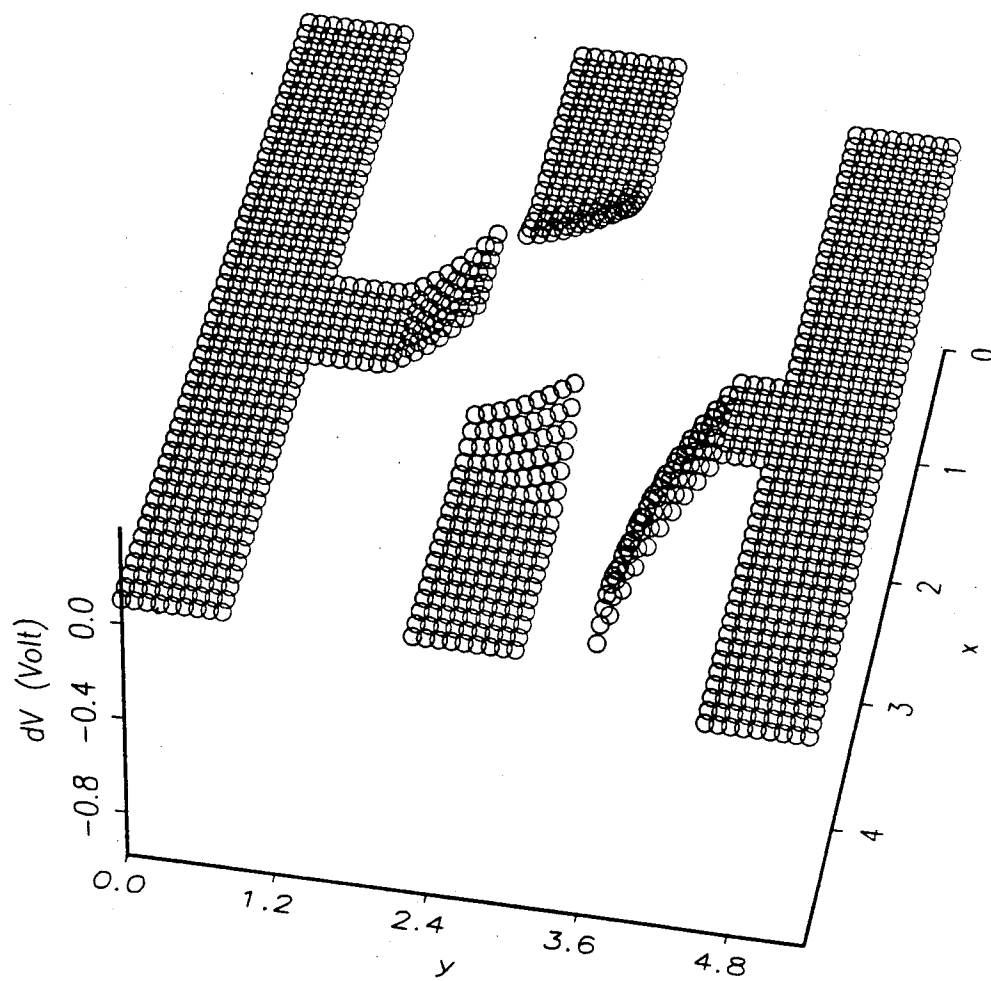


Figure 4.5b The calculated potential dV from case 5.

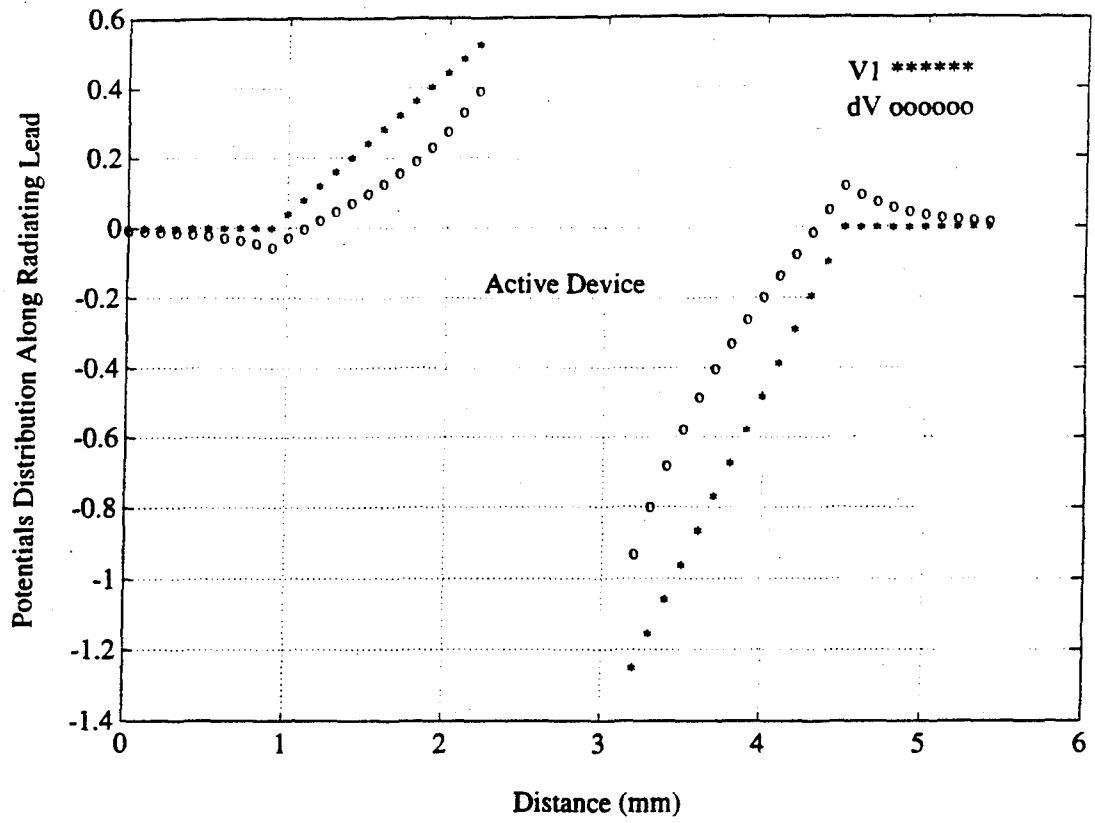


Figure 4.6a. The comparison of the potential V_1 and potential $dV = V_1 - V_3$ in a radiative structure in case 5.

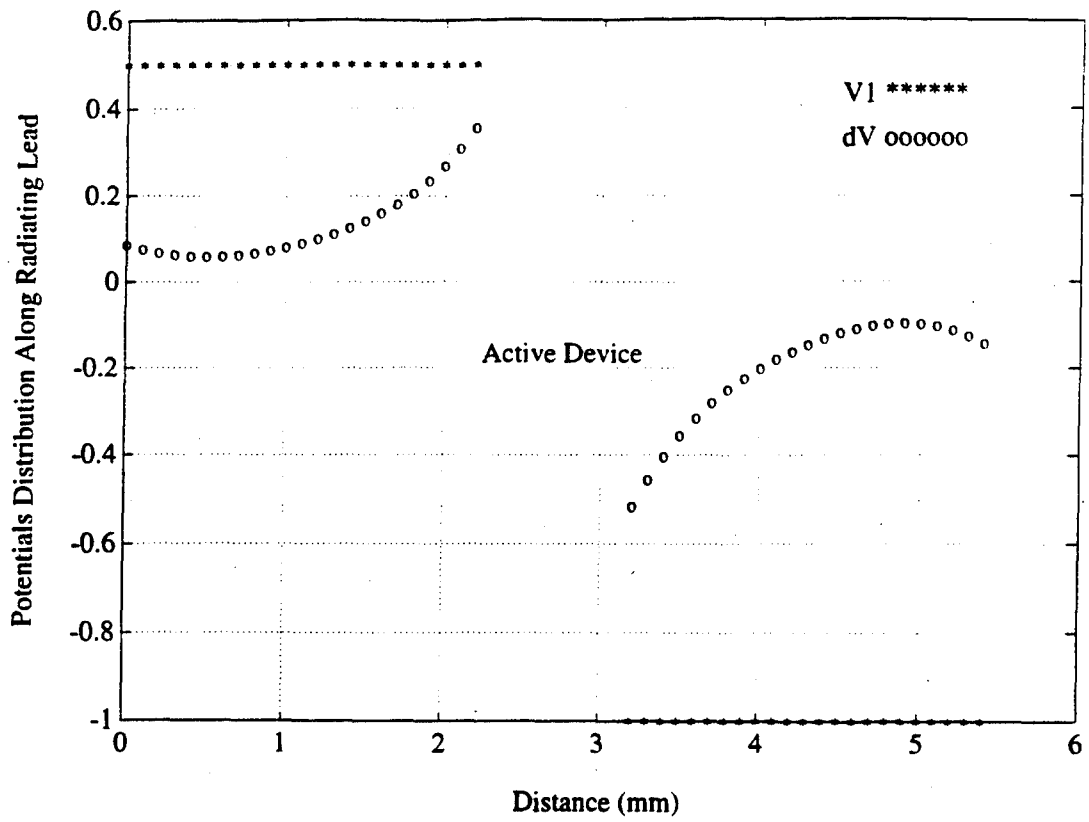


Figure 4.6b. The comparison of the potential V_1 and potential $dV = V_1 - V_3$ in a radiative structure in case 1.

Reasonable fit of the distribution of V_1 from the measured data will not be unique. Therefore, caution must be employed in interpreting the measurement results. The purpose of the following discussion is to obtain a self-consistent modeling that can explain the measured data we obtained from both the single element and the array antenna.

Comparisons of the calculated distributions of dV from all five cases of measured data show that uniform potential models of V_1 (the classic distribution for capacitive loaded dipole) have the largest standard deviation. The values of 8.58-10.34% are well above the measurement error (which is $< 4.3\%$). This means that the uniform potential distribution approximation for the active antenna does not fit well with our experimental results. In contrast, the linearly decaying models suggested in cases 3-5, have the average standard deviation below the measurement error. Among them, the model in case 5 has the lowest value for the maximum deviation of the measurement value. The plot in Figure 4.4 shows that the model of case 5 agrees well with the experimental measurement. The model of case 3 also shows agreement with the measured data in the radiating leads and the bias line. However, the fitting in the source bias line is not as good as the one from case 5. The same conclusion can also apply to case 4. As we recall, along the radiating lead of the antenna, the distribution of V_1 is assumed to be linearly decaying from the active device in these three cases. In cases 3 and 5, the potential is made to decay to zero on the gate and drain bias line, but in case 4 some residual value of the potential is set on both of the bias lines. For the distribution of V_1 on the source bias line, constant distributions are considered in cases 3 and 4, and the linearly decaying potential from

the active device is assumed in case 5. In case 5, the value of V_1 on the source line will reach zero at the place where the distance from the active device is larger than the length of the radiating leads. Even though the potential distributions in cases 3-5 are similar, they represent different modes of operation. Figures 4.7a-c, show the schematic diagrams of the potential distributions and the main field lines in cases 3-5. As we can see, the antenna is dominated by the odd mode in the region near the active device in all cases, therefore, the radiating fields of the antenna are polarized along radiating leads. However, away from the active device, the field lines are different for different cases. Figure 4.7a shows that an even (guided) mode is formed in the bias lines, hence some energy will guide along the bias lines in this particular case. Figure 4.7b shows that the odd mode continues to dominate in case 4. Some energy will also be guided on the bias lines, but radiation losses will be larger than the ones in case 3. Figure 4.7c shows there will be no energy guided along the bias lines, and all the energy will radiate into free space in case 5. The approximated potential distributions from these three cases have common characteristics, that is, most of the field strength is clustered around the region near the active device. At a place further away from the active device, the field strength is weaker. This indicates that the near fields have the strongest influence on the circuit parameters as well as the oscillation condition of the antenna. That explains why the microwave characteristics of the single active antenna are similar to the ones in the array. It is also noticed that the magnitude of excitation voltage in the gate terminal of the active device is smaller than the drain, here the

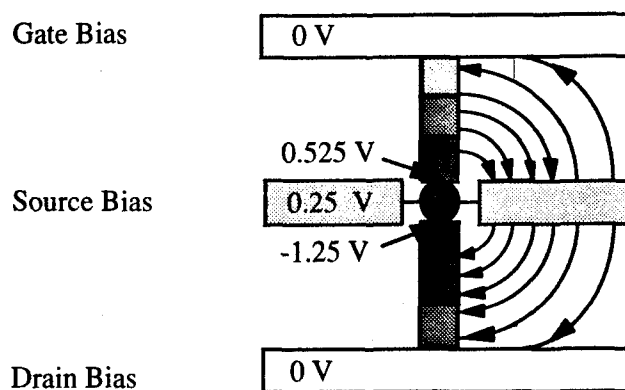


Figure 4.7a. The schematic diagrams of the potential distributions and the main field lines presented in case 3.

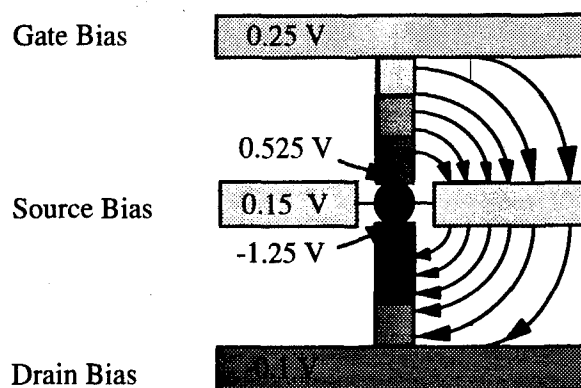


Figure 4.7b. The schematic diagrams of the potential distributions and the main field lines presented in case 4.

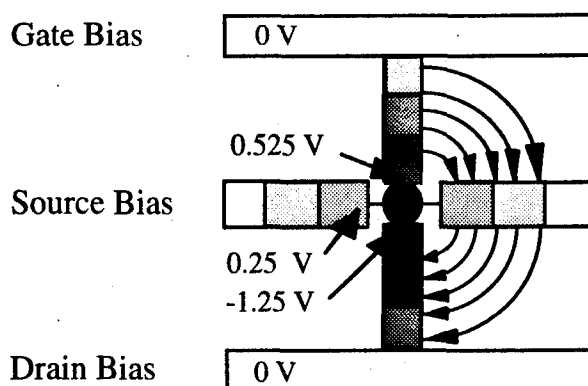


Figure 4.7c. The schematic diagrams of the potential distributions and the main field lines presented in case 5.

active antenna is always somewhat asymmetrically excited.

The decaying potential on the radiating lead can be explained as follows. The three bias lines for the active device terminals can be viewed as coplanar lines. In order for the antenna to radiate energy into space, the odd mode (radiated mode) must be the dominant mode for these coplanar lines. The radiating leads are in a position perpendicular to the bias lines but parallel to the polarized direction of the radiated field, therefore, the radiating leads appear to be inductive to the a.c. current of the active device. This distributed inductance is the main reason for the a.c. potential decay along the radiated leads. Even though the cross polarized field is 20 dB lower than the main one, the field has polarization along the bias lines. This has the same effect for the a.c. potential along the source line, and the potential on the source bias line could have linearly decaying behavior. Furthermore, as the transistor resonates, a large amount of phase shift takes place inside the active device. This may explain

why the active antenna will resonate at a length much smaller than half of the oscillation wavelength.

Now, a remaining question might be: will the potential distribution on the radiative lead decay to zero as it reaches to the bias line as suggested in the models in cases 3 and 5? or, will it decay to some non zero value as in case 4? Since we have progressively lower signal to noise ratios as we sample farther away from the active device. Noise peaks cause about 4.3% measurement uncertainty in our measurement. The 4.3% measurement uncertainty in the noise floor will not allow enough sensitivity for us to distinguish between these three possible distributions. Further examination of cases 3-5 has to come from the information of the phase measurement of an array.

4.3 Models of Operation Mode of an Antenna array

If a single active antenna has potential distributions as those presented in cases 3 and 5, that is the potential will decay along the radiating lead to zero on the gate and drain bias lines, a schematic depiction of the global potential distribution of a column of an active antenna array will be as shown in Figure 4.8a (the un-shaded bias lines are the gate and drain bias line). Potential distribution shown in Figure 4.8a has two distinguishing features. First, the amplitude of the sampling quality, dV , will have the same form of distribution in each elementary cell. The relative phase measurement across each active device will be about 180 degrees. These characteristics agree with the results of the sampling measurement on active antenna arrays. The global

potential distributions of a column of active antenna arrays for distributions suggested in case 4, is shown in Figure 4.8b. In this diagram, the possibility of floating potentials on each bias line of the active device are assumed. Although actual potential of an electrode V_j in Figure 4.8b are dramatically different from the one in Figure 4.8a, the optical sampling for the amplitude measurement of dV , will not be that different in these two cases. One of the reasons is that, the GaAs substrate we used is quite thin compared to the size of the active antenna. The probe beam can only be sensitive to the difference in the local field (generally within the elementary cell). However, the difference in the above two cases can be easily distinguished by the phase measurement of the potential. As we can see, π phase shifts can be easily detected as the probe beam scans, crossing each active device in the column in Figure 4.8a, while there will be no phase shift for each active device in the distribution shown in Figure 4.8b. Hence, the model in case 4 can be eliminated.

Combined with all the information obtained from the experiments, the results suggest that the potential distribution presented in cases 3 and 5 for a single active antenna and the global potential distribution of an array antenna shown in Figure 4.8a are the most suitable approximation solutions compared with the other cases. So far, our experiment is not accurate enough to distinguish cases 3 from 5.

4.4. Summary

Based on our experimental results and numerical simulations, the potential distribution models were developed in this chapter. Information of exact potential

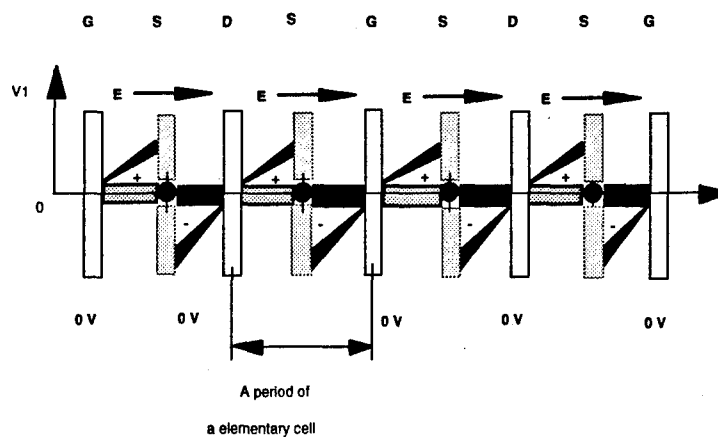


Figure 4.8a. Schematic depiction of the global potential distribution on a column of active antenna array in cases 3 and 5.

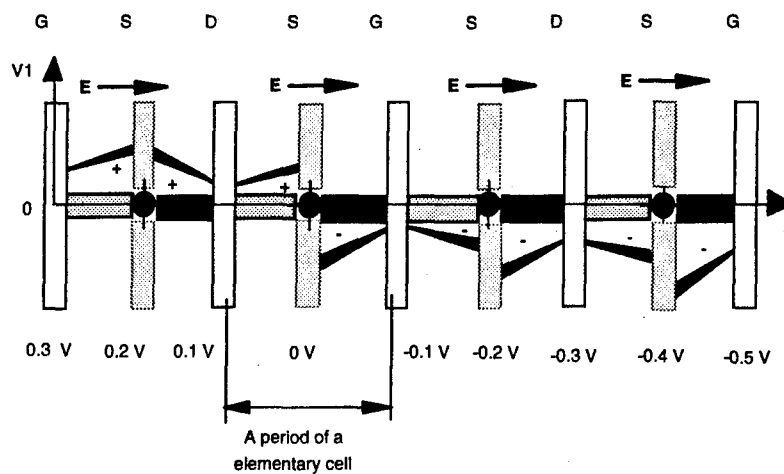


Figure 4.8b. Schematic depiction of the global potential distribution on a column of active antenna array in case 4.

distribution on the electrode that was lost in the noise level of the measurement is recovered by the numerical simulations and experimental comparisons. It is also found that the phase information which can be detected from the sampling measurement is very informative in the study of an active device. Experimentally observed phenomena on active antennas are explained well by the potential distribution models. From the study of these active antennas, we have uncovered some unique characteristics which relate to the working mechanism of active devices. More specifically, we have observed that the uniform potential distribution assumed for an "ideal" small dipole may not always be the case for a small active antenna. The linear decaying distribution is found on a small active antenna. Analyses of potential distributions indicate that bias lines have dual functions. Not only do they provide d.c. bias voltage to the active device, but also they provide a coplanar structure that supports radiation mode (odd mode). Therefore, we cannot ignore the function of the bias line in the design consideration. Since higher potential value around an active device is discovered from the calculation of the sampling measurement, oscillation conditions for such active antennas governed by their near field distributions is evident. This means that the stability of the active device is not determined by the field boundary conditions imposed by their neighbors. Instead, it is determined by excitation of the near field and the geometry within a period of an elementary cell.

References

1. D. R. Hjelme and A. R. Mickelson, "Voltage Calibration of the Direct Electrooptic Sampling Technique," *IEEE Trans. on Microwave Theory and Tech.*, vol. 40, pp. 1941-1950, Oct., 1992.
2. D. R. Hjelme, M. J. Yadlowsky, and A. R. Mickelson, "Two-Dimensional Mapping of Microwave Potential on MMIC's Using Electrooptic Sampling," *IEEE Trans. on Microwave Theory and Tech.*, vol. 41, pp. 1149-1158, June/July, 1993.
3. V. Radisic, D. Hjelme, A. Horrigan, Z. Popovic and A. R. Mickelson, "Experimentally Verifiable Modeling of Coplanar Waveguide Discontinuities," *IEEE Trans. on Microwave Theory and Tech.*, vol. 41, pp. 1524-1533, Sept., 1993.
4. I. Stakgold, "Boundary Value Problems of Mathematical Physics," vol. 1 and 2, The Macmillan Company, London, 1972.
5. S. Liao, "Microwave Device & Circuits", third edition, Prentice Hall, 1990.

CHAPTER 5

AN EXPERIMENTAL TECHNIQUE FOR DETERMINATION OF VAN DER POL PARAMETERS OF A TRANSISTOR OSCILLATOR

5.1. Introduction.

It has been shown from the previous chapters that an active antenna has similar behavior to coupled oscillators. To optimize the array performance of the active antenna array, the values of the coupling parameters which determine the size of array, and degree of coherence of the radiating power of an array must be defined. These parameters can be calculated from the circuit parameters of the oscillator. In the following sections, a brief review of conventional methods will be given. Reasons for using the Van der Pol oscillator model for a transistor oscillator are explained, and a new experimental technique to determine the Van der Pol parameters of a transistor are discussed.

In the conventional approach in determining circuit parameters of a transistor oscillator, transistors are investigated by using large signal models of MESFETs or HEMTs. The harmonic balance technique is often used in these large signal transistor models for nonlinear microwave circuit designs [1-8]. These models have shown advantages for power MMIC amplifiers and oscillator designs [9]. However, using CAD tool packages to analyze a coupled oscillator array, we are faced with a problem that is not easily solved with current software. That is, the large signal models of the transistor have many variables. As the number of oscillators in the array increase, the

array performance becomes more difficult to analyze. Consequently, the computer time and the probability of errors introduced for the large signal model will also increase. Since the Van der Pol (VDP) coupled oscillator theory has been recognized as an effective way to describe the performance of a coupled oscillator array, a VDP equation for a single transistor oscillator is used in our modeling. The purpose of this chapter is to develop a simple experimental technique to determine the VDP parameters for transistor oscillators.

In 1927, Van der Pol investigated the self-sustained triode oscillator. He observed that the saturation term in a triode equation is the one that is proportional to the cube of the oscillation intensity [10]. Later the formula, $\ddot{x} - (\epsilon - \eta x^2)\dot{x} + \omega_0^2 x = 0$, to describe this type of self-sustained nonlinear oscillation was named as the Van der Pol (VDP) oscillator equation. Since 1927, extensive work in the field of self-sustained oscillators has been carried out by many researchers. Examples include laser, mechanical, and electrical oscillators [11-14]. Previous studies have shown that even though different mechanisms govern the self sustained oscillator, they can still be described by the VDP equation. In this equation, the parameters are related to the individual physics of the oscillator. Describing an oscillator with the VDP equation is convenient for the researcher, because it provides the advantage of analyzing a nonlinear coupled oscillator array in a more sophisticated and less complex way [15]. A quasi-optical oscillator array using the VDP coupled oscillator theory has been analyzed by York [16]. In general, there are two approaches to obtain VDP parameters: numerical or experimental. The numerical

approach yields low accuracy because it is based on the circuit parameters of the oscillator which shows uncertainty in the large signal limit. Therefore, the experimental approach was used in our research. The steady state solution of the VDP equation contains only information for one parameter. It seemed difficult to determine both parameters in a steady state using an experimental approach. This chapter provides a method to determine the VDP parameters of the transistor oscillator by applying a periodic perturbation to the bias voltage of the transistor oscillator. The analysis of the slightly perturbed oscillator was carried out by using the multiple scale expansion method. We discovered that when a transistor is modulated, several sidebands are generated in the power spectrum of the oscillator. These sidebands contain information on the parameters which are not easily detected from a steady state measurement. The proposed approach is then experimentally verified and the results agree with the theoretical prediction. This technique provides an avenue to measure parameters of transistor oscillators in real time. The experimental set-up is simple, risk free and easy to perform. With the advantage of only two defined parameters in the transistor modeling, the requirements of computer time and memory are reduced and the analysis of the array performances will be more efficient.

The remainder of this chapter is organized as follows: in Section 2, we will give an example of, what is perhaps the simplest case, to show that the behavior of the transistor oscillator can be described by the VDP equation. In this example, we will demonstrate that the VDP parameters are directly related to the circuit parameters of

the oscillator in a large signal limit. In Section 3, a method for experimentally determining the VDP parameters is derived. From the theoretical derivation and numerical calculations, we show that the VDP parameter which cannot be measured from a steady state oscillator can be evaluated by the proposed technique. In Section 4, the experimental implementation and results for verifying the theory are discussed. Summary of the chapter is in Section 5.

5.2. VDP Equation for a Self-Sustained Transistor Oscillator

A) Instability of a Radiating Oscillator

The feedback mechanisms of transistor oscillators can take many different forms. They can have common source, common gate and common drain configurations, or they can have additional capacitance, inductance or resistance as feedback elements. As we mentioned in the previous section, even though the physical feedback mechanisms are different, a self-sustained oscillation can be described by the VDP equation. To demonstrate that the VDP parameters are a function of the circuit parameters of an oscillator, we will use a radiating oscillator built with a Fujusui HEMT (fhx35x) as a specific example. An equivalent circuit model of the oscillator is shown in Figure 5.1. Without lost generality, a conventional circuit model of an intrinsic MESFET or HEMT [17] is adopted in our modeling. The circuit parameters of the transistor are extracted from the data sheet [18]. The impedance of source-drain load is represented by the symbol Z_l , and the impedance of gate-source terminal load is represented by the symbol Z_g . Both impedances can

be calculated from the passive circuit geometry once the main operation mode in the structure is defined. Starting with small signal equivalent circuit of Figure 5.1, letting A_o be the ratio of the alternating voltage drop v_1 in the gate-source capacitor C_{gs} to the gate-source voltage v_{gs} , then:

$$A_o = \frac{v_1}{v_{gs}} = \frac{1}{j\omega \tau_1 + 1}, \quad (1)$$

where, $\tau_1 = C_{gs} * R_{gs}$, typically, the value of τ_1 is in the order of 10^{-12} , with a design frequency in GHz range, we can consider that $A_o \cong 1$.

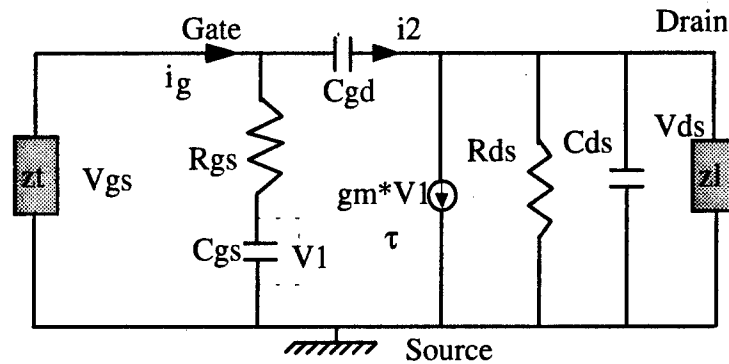


Figure 5.1. Equivalent circuit model of a common source transistor oscillator.

We define $A_1 = v_{ds} / v_{gs}$, as the voltage amplification factor. By applying the approximation of $A_o \cong 1$, we get:

$$A_1 = -\frac{g_m R_{ds} Z_l}{j\omega(C_{ds} + C_{gd})R_{ds}Z_l + (R_{ds} + Z_l)}, \quad (2)$$

Therefore, the input admittance Y_{in} is:

$$Y_{in} = j\omega C_{gs} + j\omega C_{gd} \left(1 - \frac{g_m R_{ds} Z_l}{j\omega(C_{ds} + C_{gd})R_{ds}Z_l + (R_{ds} + Z_l)} \right). \quad (3)$$

Following a similar discussion made by Sevin [19], it can be seen from Eq. 3 that if Z_l is either pure resistive or capacitive, the input impedance $Z_{in} = 1/Y_{in}$ has a positive resistance and the transistor is stable. However, when Z_l is inductive, the input impedance has negative resistance and the transistor is unstable. Substituting $Z_l = i\omega L_l$ into (2), we also observe that when the transistor is unstable, $|A_1| \geq 1$, and the phase of A_1 is 180° , that is v_{gs} and v_{ds} were out of phase. The phase relationship of the transistor in the unstable region agrees with our optical sampling measurement on this radiating oscillator [20]. Oscillation initiates inside the transistor when the magnitude of the negative resistance is larger than the load impedance. As the intensity of the oscillation increases, the effect of nonlinear components in the circuit will govern the saturation characteristics of the transistor oscillation to reach the steady state.

B). Saturation of a Radiating Oscillator.

To reach steady state, the oscillator must have a nonlinear feedback element. In our case, this element is the transistor. The I-V curve of the fhx35x is shown in Figure 5.2. The HEMT advanced Curtice model[1-3] is used to fit the curves at different gate-source voltages. The Curtice model describes the drain current with respect to the drain-source and gate-source voltages as:

$$I_{ds}(V_{gs}, V_{ds}) = \beta(V_{gs} - V_{to})^\kappa (1 + \lambda V_{ds}) \tanh(\alpha V_{ds}) \quad (4)$$

$$g_m = \frac{dI_{ds}}{dV_{gs}} \quad (5)$$

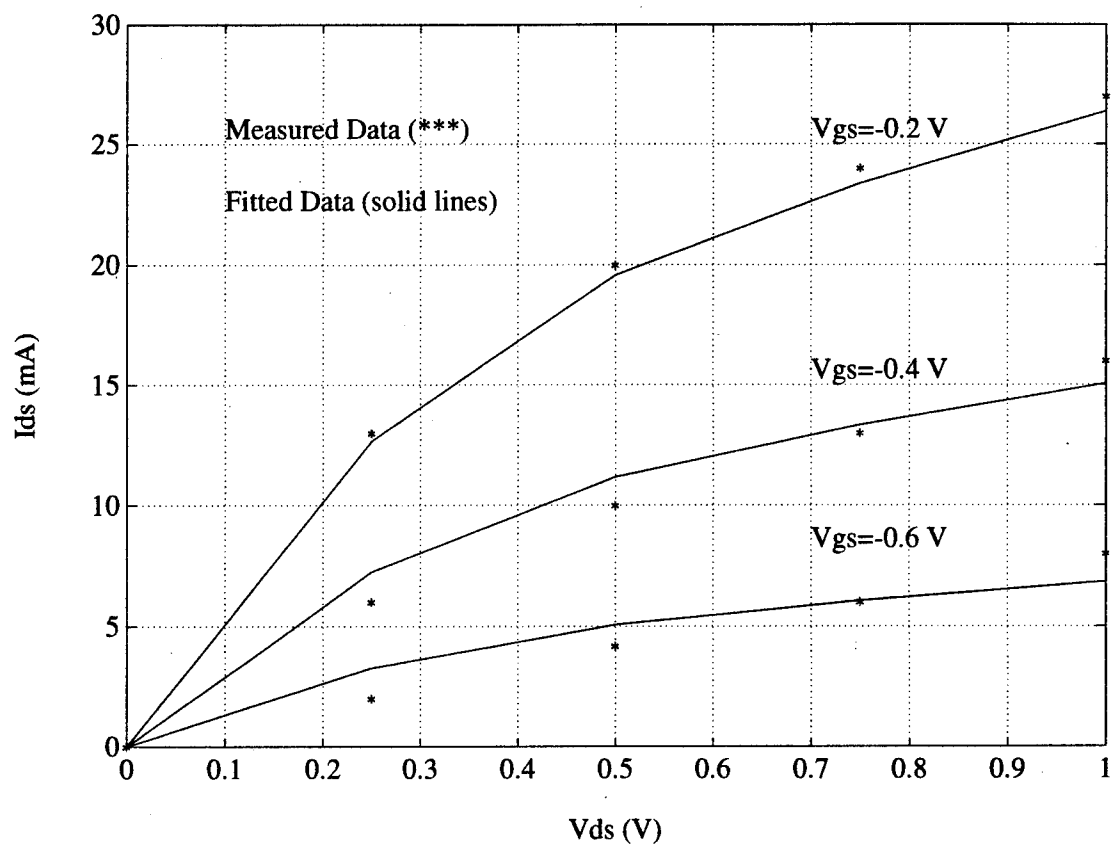


Figure 5.2. The I-V curves of the HEMT fhx35x.

Value of parameters β , κ , λ and α are obtained from nonlinear fitting of the I-V curves, and are bias independent. Voltage $V_{io}=1$ volt is defined from the measurement. The d.c. bias conditions of our oscillator are $V_{gsq}=-.06$ V, $V_{dsq}=0.6$ V. As the oscillator starts oscillation at ω with a.c. voltage amplitude v_{gs} and v_{ds} , the voltages V_{gs} and V_{ds} in equation (4) becomes:

$$V_{gs} = V_{gsq} + v_{gs} \cos(\omega t), \quad (6)$$

$$V_{ds} = V_{dsq} + v_{ds} \cos(\omega t + \phi). \quad (7)$$

By substituting equations (6) and (7) along with fitting parameters β , λ and α into equation (4), and equating the term with ω^0 , ω^1 , 2ω , the current in the channel I_{ds} becomes the superposition of the following terms:

$$I'_{ds} = I_{ds}(\omega^0) + I_{ds1}(\omega^1) + I_{ds2}(2\omega) + \dots \quad (8)$$

and I_{ds} is the component of the d.c. current in the channel. Figure 5.3 shows the relationship of the magnitude of the d.c. current I_{ds} versus the magnitude of the alternating voltage of v_{gs} . It can be seen that as v_{gs} increases, the I_{ds} increases. The drift of the d.c. bias voltage ΔV_{gs} due to the change of d.c. current can be calculated as follows:

$$\Delta V_{gs} = \frac{I_{ds} - I_{dsq}}{g_{mq}}, \quad (9)$$

Where g_{mq} is the transconductance in the original bias point. Notice that all the circuit components of the transistor are bias dependent. However, the sensitivity to

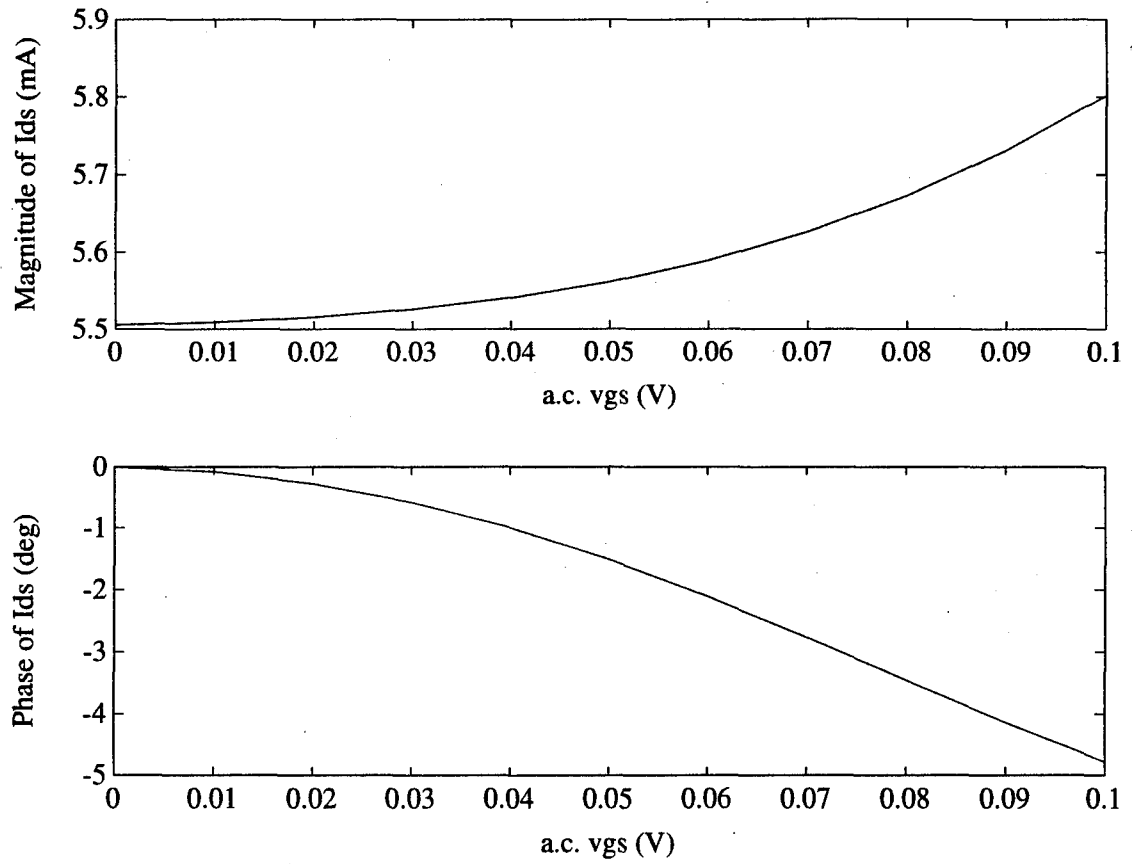


Figure 5.3. The effect of the amplitude of a.c. gate-source voltage to direct drain-source current in the channel.

the change of the voltages are different from component to component. It has been shown that transconductance is the main gain mechanism of the HEMT, and is also the most nonlinear component in the transistor [17,19]. The relationship of the transconductance g_m with respect to a.c. voltage amplitude v_{gs} can be computed directly from (5) and (9). Their relationship is shown in Figure 4.

The effect of the bias dependence of gate-source capacitance C_{gs} on oscillation has also been studied. The results of the calculation indicate that the capacitance C_{gs} plays the role of positive feedback and the transconductance g_m plays the role of negative feedback in our oscillator. Since the saturation effect is the main consideration in the investigation (that is, we only consider the case that the oscillator will reach the steady state), we conclude that the main effect of nonlinearity is from the transconductance. Figure 5.4 shows that the value of the transconductance is increased as the a.c. voltage increases. Letting $Z_{in} = 1/Y_{in} = R_{in} + iX_{in}$, be the input impedance of the transistor, the effect of the amplitude of a.c. voltage on the input resistance and the input reactance of the transistor is shown in Figures 5.5a and 5.5b. Their relationship can be fit into the simple form of:

$$R_{in} = -R_{in0} + m_{in} v_{gs}^2, \quad (10)$$

where R_{in0} is the initial input resistance of the transistor, and m_{in} is the fitting parameter. When the magnitude of R_{in0} is larger than the load resistance, the amplitude of the oscillation increases. As a result, the negative input resistance decreases (shown in Figure 5.5a). Eventually when the magnitude of the negative resistance equals the load resistance, the oscillation reaches a steady state.

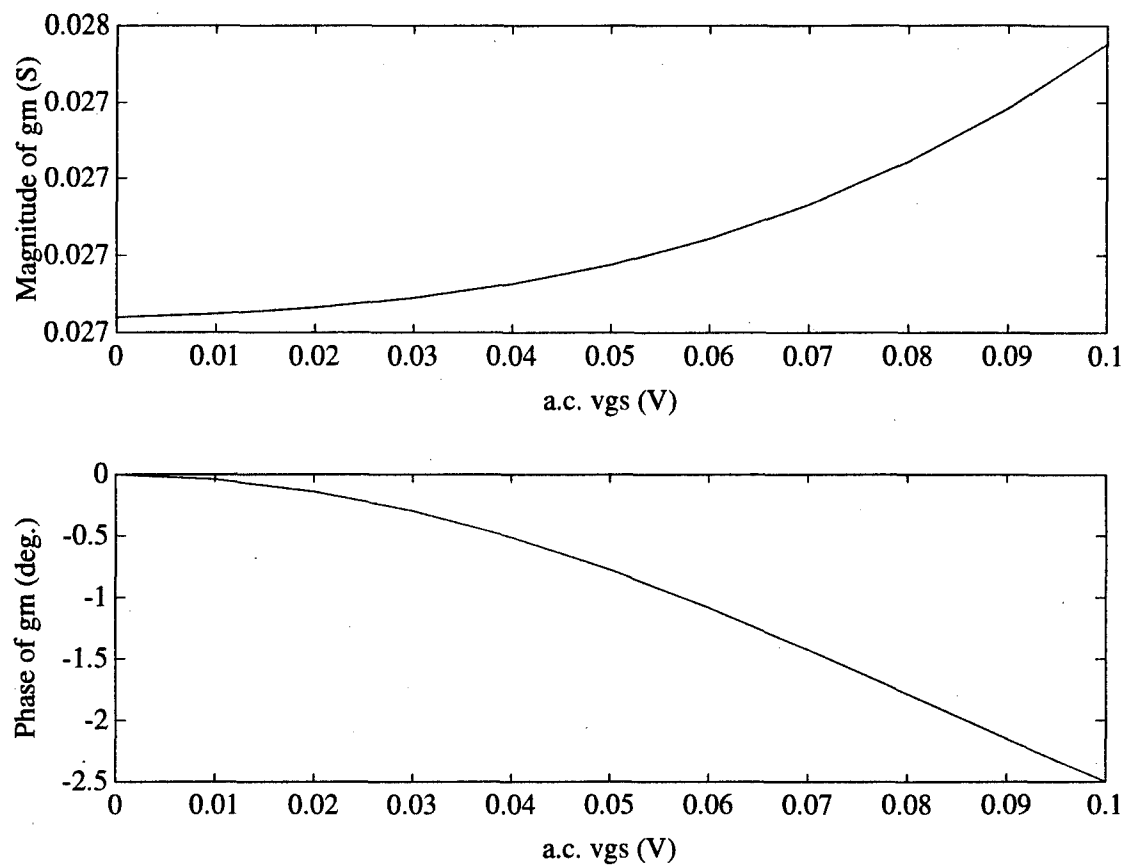


Figure 5.4. The effect of the amplitude of a.c. gate-source voltage to transconductance from the nonlinear computation.

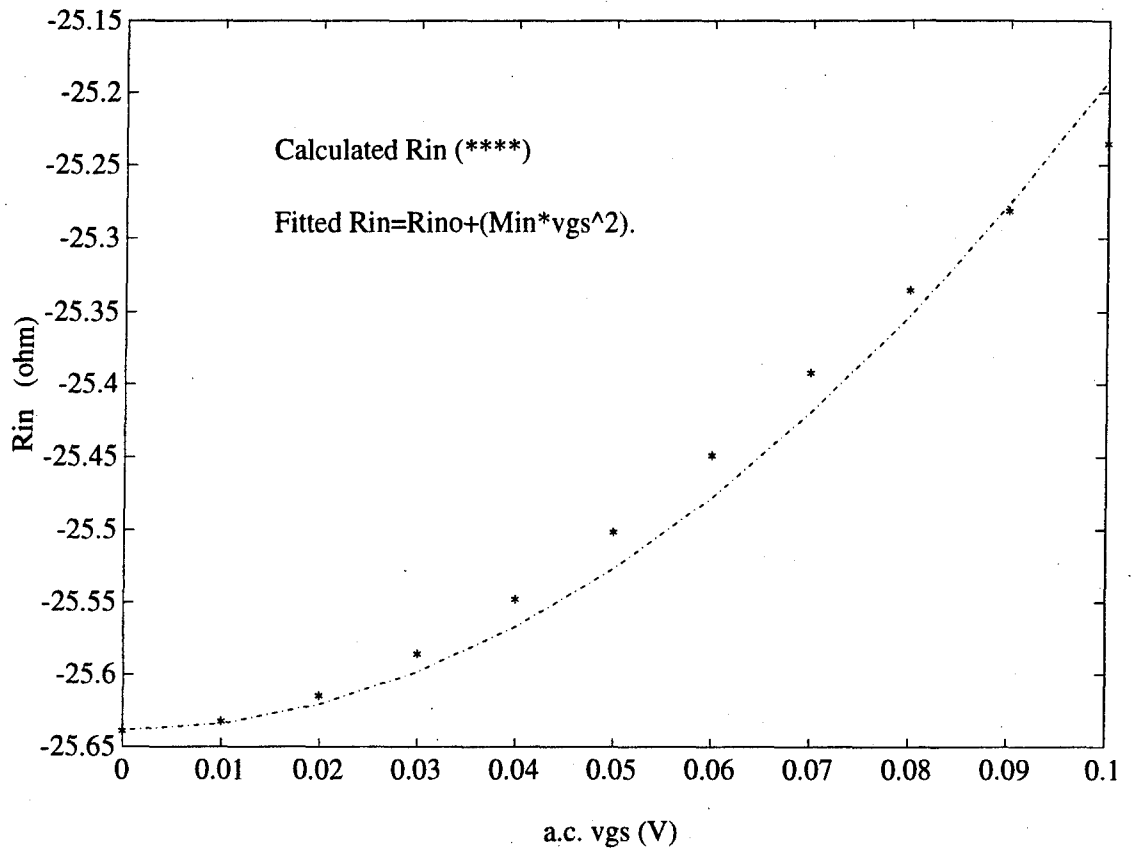


Figure 5.5a. The effect of the amplitude of a.c gate-source voltage to the input resistance of a transistor.

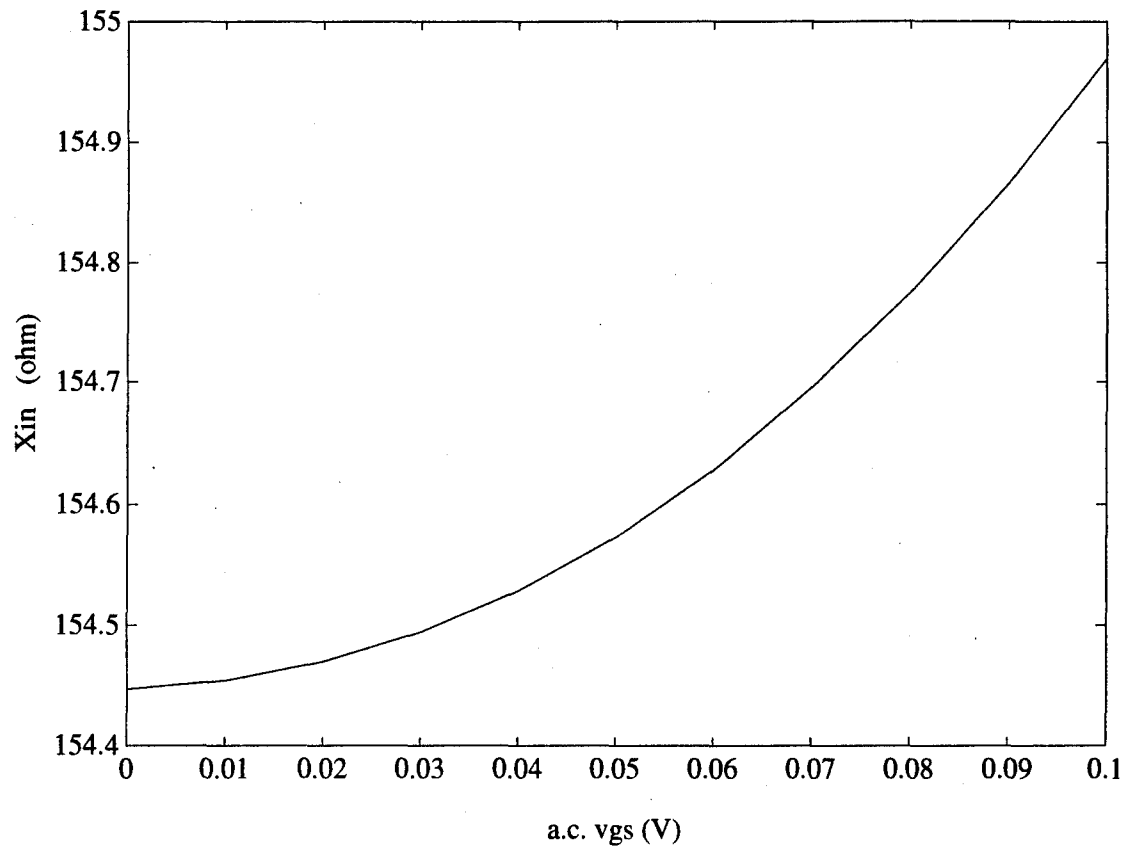


Figure 5.5b. The effect of the amplitude of a.c gate-source voltage to the input reactance of a transistor.

Figure 5.5b shows that the input reactance X_{in} is inductive in our oscillator. The value of the reactance also changes with the amplitude of the oscillation. Defining R_o and C_o as load resistance and capacitance of the passive circuit parameters, the equation of the oscillator circuit can be formed as follows:

$$\frac{d^2u}{dt^2} - \left(\frac{R_{in0} - R_o}{L_{in}}\right) \frac{du}{dt} + \left(\frac{m_{in}}{L_{in}} u^2\right) \frac{du}{dt} + \omega_0^2 u = 0. \quad (11)$$

Where,

$$\omega_0 = \frac{1}{\sqrt{L_{in} C_o}}.$$

Letting $\epsilon = (R_{in0} - R_o) / L_{in}$, $\eta = m_{in} / L_{in}$, $\gamma = \eta / \epsilon$, and $x = u$, then equation (11)

can be rewritten in the form of:

$$\frac{d^2x}{dt^2} - (\epsilon - \eta x^2) \frac{dx}{dt} + \omega_0^2 x = 0.$$

or:

$$\frac{d^2x}{dt^2} - \epsilon (1 - \gamma x^2) \frac{dx}{dt} + \omega_0^2 x = 0. \quad (12)$$

The derivation has qualitatively shown that the oscillation of a transistor oscillator is in the form of VDP equation. The nonlinear input resistance is the saturating factor of the oscillator in this case. When the configuration of the oscillator changes, the form of the equation should remain the same. However, the detailed relationship between the VDP parameters and the oscillator parameter can be dramatically different.

In Equation 12, parameter η is the saturation coefficient or damping constant, and ω_0 is the resonance frequency in the absence of dissipation or gain. The

parameter ϵ is the linear net gain [11]. The constant ϵ is proportional to ω_0 / Q , where Q is the quality factor of an oscillator. In the case of a high Q factor resonator where the frequency locking range of the oscillator $\Delta\omega \ll \omega_0$, the value of ϵ is much smaller than 1.

The direct relationship between the VDP parameters and the transistor parameters is shown in the previous derivation. It appears to be that the VDP parameters can be evaluated numerically. However, the direct calculation of the VDP parameters from the large signal transistor parameters has the following disadvantages. First, the calculated parameters are model dependent. Accurate models of the I-V curve, and the nonlinear components of a transistor are required. Any error in one of these models will result in a different value of ϵ and γ , which in turn will result in a false prediction of the coupled transistor performance. Second, the calculated VDP parameters are circuit dependent. Different configurations of the passive circuit structures will result in different types of relationships between them. Therefore, real time measurements on an oscillator to obtain VDP parameters are more realistic.

5.3. Theory for Determination of the VDP Parameters Experimentally

In Section 1 and 2, we have justified that a self-sustained oscillation of the transistor oscillator is governed by the VDP equation. It is known that there exists an analytical stationary solution of equation (12) under the condition of ϵ is small, which is given by [21, 22],

$$x = \frac{2}{\sqrt{\gamma}} \cos \tau + \varepsilon \left(\frac{3}{4\omega_0\gamma} \sin \tau - \frac{1}{4\omega_0\gamma} \sin 3\tau \right) + \dots,$$

where,

$$\tau = \omega_0 t \left(1 - \frac{\varepsilon^2}{16\omega_0^2} + \dots \right). \quad (13)$$

Since ε and γ are of the same order of magnitude, they are both much smaller than ω_0 , the higher order terms of the solution can be neglected. The approximated stationary solution of VDP force free oscillation is:

$$x = \frac{2}{\sqrt{\gamma}} \cos \omega_0 t. \quad (14)$$

With a high Q resonator, an oscillation frequency of the VDP oscillator is close to the resonant frequency ω_0 . The amplitude of the oscillation is inversely proportional to the parameter $\gamma = \eta / \varepsilon$. It is noticed that the larger the net gain, ε , or the smaller the damping coefficient, η , the larger the oscillation amplitude will be. The oscillation frequency and the magnitude of a VDP oscillator can be both obtained from the measurement by using a spectrum analyzer. Therefore, parameter γ can be determined experimentally. Figure 5.6, shows the spectrum of a self-oscillating active antenna. We can see that the second and higher order terms of the steady state solution in (13) are too small to be detected by the spectrum analyzer. This is further proof that the active antenna is a VDP oscillator and has small values of ε and γ .

Notice that the stationary solution of the VDP equation in (14) only reveals the information of the parameter γ , but has no information of the absolute values of both ε

and η . If one wants to determine all VDP parameters experimentally, one needs another experimental approach. Since the constant ϵ is proportional to ω_0 / Q , the

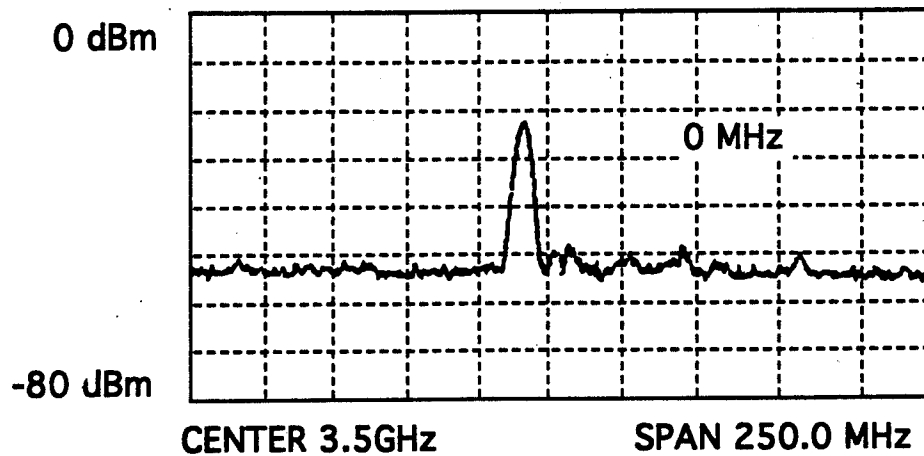


Figure 5.6. Power spectrum of the transistor oscillator.

relative value of ϵ can be estimated from measuring the locking bandwidth of the oscillator. However, the absolute value of ϵ must be determined by an additional measurement. The technique we propose in the following derivation can be used to complete the parameter measurement by using a spectrum analyzer. In this approach, we add an external sinusoidal signal with frequency ω_f to the original bias voltages of a self-sustained transistor oscillator. Thus, the formulation which corresponds to the VDP equation can be described as follows:

$$\frac{d^2x}{dt^2} - \epsilon \cos\omega_f t \cdot (1 - \gamma x^2) \frac{dx}{dt} + \omega_0^2 x = 0. \quad (15)$$

Further, we will show theoretically, what the frequency response of a VDP oscillator is with a periodic coefficient. The VDP equation with constant coefficients has been

treated by many research workers [10, 11, 21, 22]. However, to our knowledge the solution of equation (15), is not available in any of the previous studies of the VDP equation. As we know, there is no simple closed form expression for such a nonlinear oscillation, but it is possible for one to try to obtain the approximate solution of the different equations under certain conditions. In this section, we will use a multiple scales expansion method to analyze the equation (15) and to predict what we will measure with a spectrum analyzer. Further, we will explain how to extract the parameters from the measurement. Again, this approach is under the assumption that ε is much smaller than 1. The comprehensive treatment of this type of stationary oscillation is shown as follows. Using the method of multiple scales [21], we introduce new independent variables according to:

$$T_n = \varepsilon^n t, n = 0, 1, 2, \dots$$

It follows that the derivatives with respect to t become partial derivatives with respect to T_n according to:

$$\frac{d}{dt} = \frac{\partial}{\partial T_0} \frac{dT_0}{dt} + \frac{\partial}{\partial T_1} \frac{dT_1}{dt} + \dots = D_0 + \varepsilon D_1 + \dots, \quad (16)$$

$$\frac{d^2}{dt^2} = D_0 + 2\varepsilon D_0 D_1 + \dots,$$

where,

$$D_n = \frac{\partial}{\partial T_n} \frac{dT_n}{dt}, n = 0, 1, 2, \dots$$

Taking the ε^0 , and ε^1 as the first order approximation, we seek an approximate solution of (15) in the form:

$$x(t, \varepsilon) = x_0(T_0, T_1) + \varepsilon x_1(T_0, T) + \dots \quad (17)$$

Substituting (17) into (15) and transforming the derivatives, results in:

$$\ddot{x}_0 + \varepsilon \ddot{x}_1 + \omega_0^2 x_0 + \varepsilon \omega_0^2 x_1 = (\varepsilon \cos \omega_f t)(1 - \gamma(x_0 + \varepsilon x_1)^2)(\dot{x}_0 + \varepsilon \dot{x}_1), \quad (18)$$

keeping the terms ε^0 , and ε^1 only, then left and right terms of (18) are:

$$\text{left term} = D_0^2 x_0 + \omega_0^2 x_0 + \varepsilon (D_0^2 x_1 + \omega_0^2 x_1 + 2D_0 D_1)x_0 + \dots, \quad (19.1)$$

$$\text{right term} = (\varepsilon \cos \omega_f T_0)(D_0 x_0 - \gamma D_0 x_0^3) + \dots \quad (19.2)$$

Equating the coefficients of like powers, ε^0 , and ε^1 on both sides (left and right terms) of (19), we have:

$$D_0^2 x_0 + \omega_0^2 x_0 = 0, \quad (20)$$

$$D_1^2 x_1 + \omega_0^2 x_1 = -2D_0 D_1 x_0 + (\cos \omega_f T_0)(D_0 x_0 - \gamma D_0 x_0^3). \quad (21)$$

The solution of (20) is written as:

$$x_0 = A(T_1) \exp(i\omega_0 T_0) + \bar{A}(T_1) \exp(-i\omega_0 T_0) + \dots, \quad (22)$$

where $\bar{A}(T_1)$ is the conjugate of the $A(T_1)$. Substitute of equation (22) into (21), equation (22) becomes:

$$\begin{aligned} D_1^2 x_1 + \omega_0^2 x_1 = & \exp(i\omega_0 T_0)(-i\omega_0 2A' + i\omega_0 A \cos \omega_f T_0 - i\omega_0 3\gamma A^2 \bar{A} \cos \omega_f T_0) \\ & - \exp(i3\omega_0 T_0) i\omega_0 3\gamma A^2 \cos \omega_f T_0 + \dots \end{aligned}$$

where,

$$A' = \frac{dA}{dT_1}. \quad (23)$$

Because the secular term $\exp(i\omega_0 T_0)$, the motion of $x(t)$ will grow without bound as the time increases, thus, x_1 does not always provide a small correction to x_0 ,

and (17) is not uniformly valid as time increases. Eliminating the term from (23) that produces secular terms in x_1 gives:

$$-i\omega_0 2A' + i\omega_0 A \cos \omega_f T_0 - i\omega_0 3\gamma A^2 \bar{A} \cos \omega_f T_0 = 0. \quad (24)$$

Expressing A in the form of:

$$A(T_1) = a(T_1) \exp(i\phi(T_1)), \quad (25)$$

where both a and ϕ are real functions of T_1 . Substituting (25) into (24) and separating the real and the imaginary parts, we obtain:

$$A \cos \omega_f T_0 - 3\gamma a^3 \cos \omega_f T_0 - 2 \frac{da}{dT_1} = 0, \quad (26.1)$$

$$2a \frac{d\phi}{dT_1} = 0. \quad (26.2)$$

Eq. (26.2) giving $\dot{\phi} = 0$, $\phi = \text{constant}$. Letting $a = a_0$, at $T_1 = \epsilon t = 0$, then:

$$a(t) \cong \sqrt{c_1} \exp(\delta x_f), \quad (27)$$

where $c_1 = a_0^2 / (1 - 3\gamma a_0^2) \cong a_0^2$, $\delta = \epsilon / 2\omega_f$, and $x_f = \omega_f t$. Keeping in mind that γ is much smaller than 1 and a_0 is also small at $t = 0$. Therefore, the first approximation to the solution of equation (15) is:

$$x(t) \cong a_0 \exp(\delta x_f) \cos(\omega_0 t), \quad (28)$$

where since δ is smaller than 1, (28) can be written as:

$$\exp(\delta x_f) = 1 + \delta \text{Sin} x_f + \frac{\delta^2 \text{Sin}^2 x_f}{2!} + \frac{\delta^3 \text{Sin}^3 x_f}{3!} + \dots \quad (29)$$

Substituting (29) into (28), with some straight forward but tedious manipulation, yields:

$$\begin{aligned}
x(t) &\equiv a_0 \exp(\delta x_f) \cos(\omega_0 t) \\
&= a_0 \{k_0 \cos(\omega_0 t) + k_1 \sin(\omega_0 + \omega_f)t + k_1 \sin(\omega_0 - \omega_f)t \\
&\quad - k_2 \cos(\omega_0 + 2\omega_f)t + k_2 \cos(\omega_0 - 2\omega_f)t \\
&\quad - k_3 \sin(\omega_0 + 3\omega_f)t + k_3 \sin(\omega_0 - 3\omega_f)t \\
&\quad + \dots\},
\end{aligned} \tag{30.1}$$

where,

$$k_0 = (1 + \frac{\delta^2}{4} + \dots), k_1 = (\frac{\delta}{2} + \frac{\delta^3}{16} \dots), k_2 = \frac{\delta^2}{8} + \dots, \text{ and } k_3 = \frac{\delta^3}{48} + \dots \tag{30.2}$$

From the presented solution of equation (15), we can clearly state that if one wants to observe oscillation of a transistor with external ramping bias in frequency domain, one should expect to see multiple spectra of the oscillation. The spacing of the spectral sidebands to the resonant frequency is equal to the harmonics of the modulation frequency $\pm n\omega_f$, and the ratio of the amplitude of these sidebands contains the information of ϵ . Since δ is smaller than 1, higher order terms for term with δ^3 and higher can be neglected. Upon substituting $\delta = \epsilon / 2\omega_f$ into (30) and some simple manipulation yields the VDP parameter ϵ ,

$$\epsilon = \frac{8\omega_f k_2}{k_1}. \tag{31}$$

where ϵ has dimension of $1/t$ which comes from the scaling of gain with the resonant frequency of $1/\omega_0$, therefore, the value of ϵ calculated from Eq. (32), should also scale by the $1/\omega_0$. The absolute value calculated ϵ from the experiment is:

$$\epsilon = \frac{8\omega_f k_2}{\omega_0 k_1}. \tag{32}$$

The formulation used to obtain the parameter ϵ is in a simple form even though the derivation process is tedious.

5.4. Results and Discussion

To further verify the accuracy of the approximate solution of Eq. (32), the results from direct numerical calculation of Eq. (15) with the analytical solution obtained by the method of multiple scale are compared. Figure 5.7 shows the power spectrum of a direct numerical solution in the frequency domain. The resonant frequency, ω_0 , used in the simulation is 1 Hz and the external modulation frequency, ω_f , is 0.1 Hz. In the numerical calculation, Eq. (15) is converted into a set of nonlinear first order differential equations and are solved numerically in the time domain. The power spectrum of the solution is obtained by discrete fast Fourier transform. From Figure 5.7, one should see that the center frequency of the oscillation is close to the resonant frequency of the circuit, ω_0 . Many sidebands are generated from the external modulation frequency of ω_f . The frequency displacement of the sidebands from the center frequency is $\pm n\omega_f$. Thus, there are nine sidebands in the frequency range of 1 Hz shown in the plot. Figure 5.8, shows the power spectrum of the approximate solution of Eq. (15) derived from the method of multiple scales. Comparing Figure 5.8 with Figure 5.7, it shows reasonable agreement with the direct numerical calculations. In particular, the magnitudes of the first and the second sidebands from two calculations are in better agreement than the higher order sidebands. The error introduced in the higher order sidebands

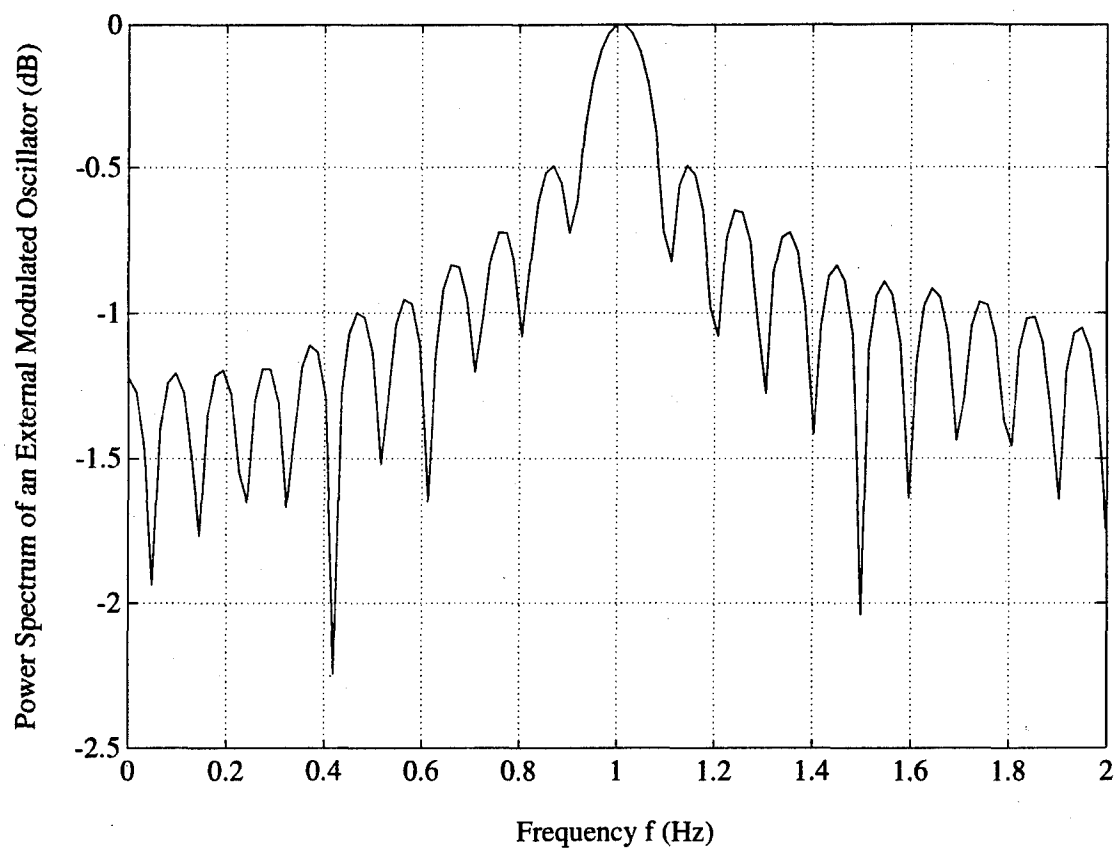


Figure 5.7. Power spectrum of the VDP equation with a periodic coefficient calculated from a numerical simulation. Simulation parameters $\epsilon = 0.01$, $\gamma = 0.01$, $\omega_o = 1$ Hz, $\omega_f = 0.1$ Hz.

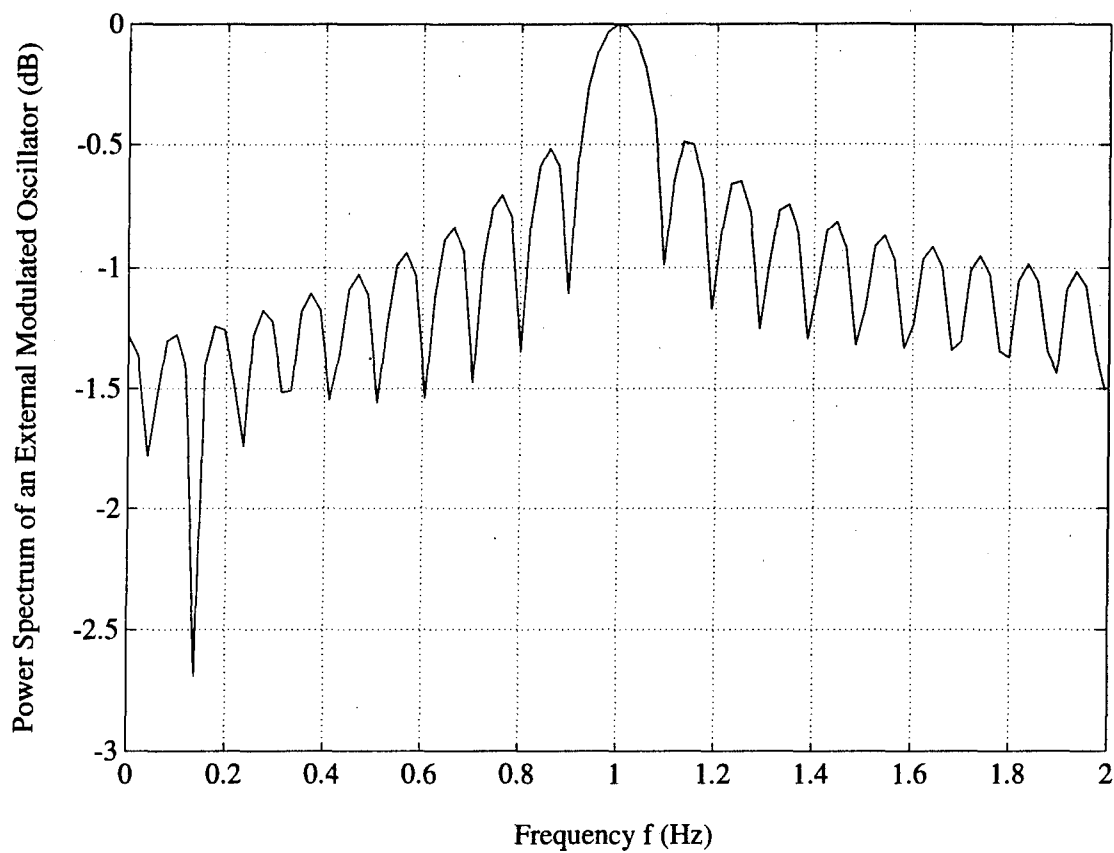


Figure 5.8. Power spectrum of the VDP equation with a periodic coefficient calculated from analytical solution. Simulation parameters $\varepsilon = 0.01$, $\omega_0 = 1$ Hz, $\omega_f = 0.1$ Hz.

originates mainly from the neglect of the higher order terms in the approximate solution. Results of Figures 5.7 and 5.8, indicate that equation (32) provides an accurate approximated solution for practical applications.

The experimental set-up to verify the theory is shown in Figure 5.9. The transistor is biased with two independent power supplies, the drain-source terminal is connected to a d.c. power supply, and the gate-source terminal is connected with a signal generator. As the transistor starts oscillation, the output power of the active antenna is detected by a horn antenna located about 35 cm away. Then the detected signal is sent to a spectrum analyzer. With only d.c. bias voltages used, the VDP parameter γ can be determined by using Eq. (14) using the measurement data of Figure 5.6. When a modulated signal is added to the gate-source bias voltage of the transistor, the power spectrum of the oscillator is shown in Figures 5.10a and 5.10b, where modulated frequencies ω_f are at 7.5 MHz and 11.7 MHz respectively. As we can see, as the frequency ω_f increases, the displacement of the sidebands from the center frequency increases, and the frequency offsets are exactly in the form of $\omega_o \pm n\omega_f$. These phenomena are in agreement with those predicted from our theory. By measuring the ratio of the magnitude of the first and the second sidebands, the value of ε can be calculated from Equation (32).

It is important to note, that when we solved equation (15), which is in the form of, $\ddot{x} - \varepsilon \cos\omega_f t \cdot (1 - \gamma x^2)\dot{x} + \omega_0^2 x = F_n(t) + F_{ext}(t) + \dots$, where $F_n(t)$ are noise terms, $F_{ext}(t)$ is external injection locking signal, etc., we considered the equation to be source free. That is, the terms in the right side of the equation are set to zero.

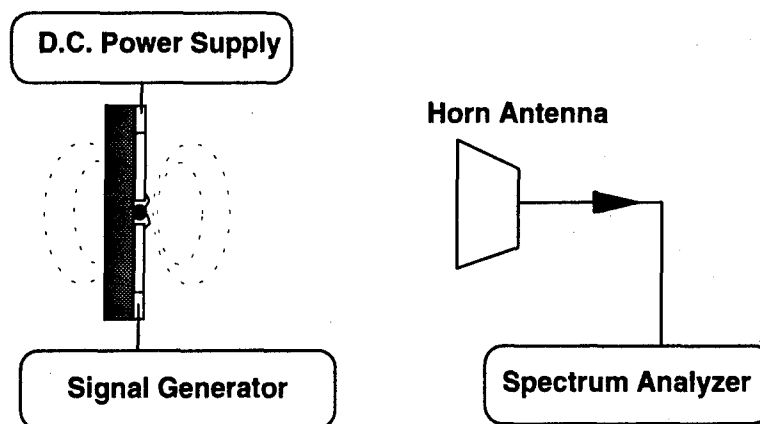
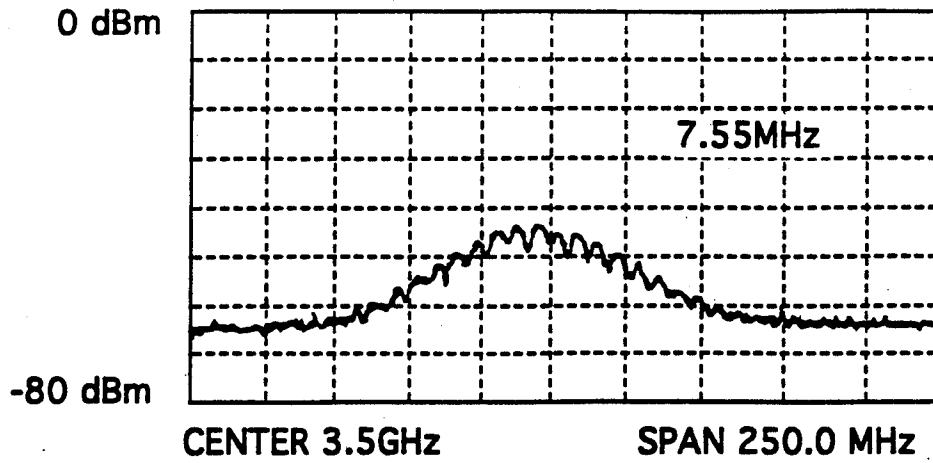
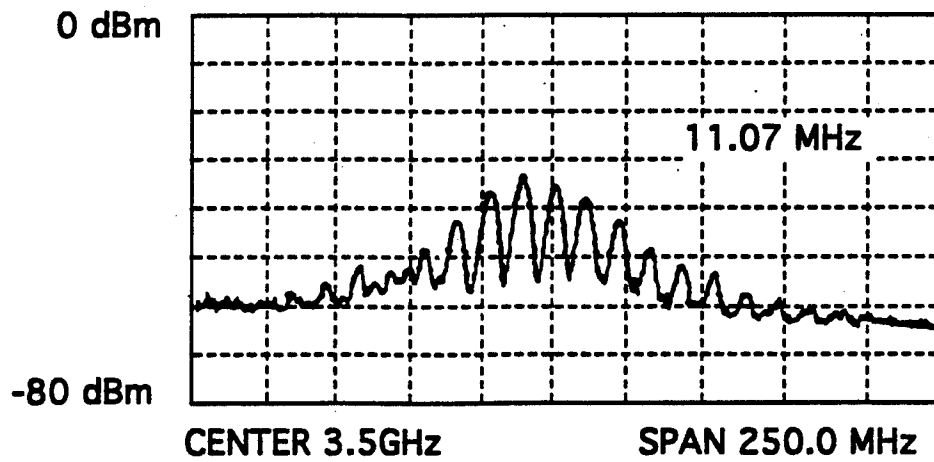


Figure 5.9. Experimental set-up for a measurement of the VDP parameter.

Therefore, the linewidth of the spectrum calculated from the approximate solution is zero. Theoretically, the VDP parameter ε can be determined from the experiment as long as the modulation frequency, ω_f , is larger than zero. However, practically speaking, the transistor oscillator is not noise free, and the spectrum of the oscillator has a certain spectral width. It is well known that GaAs MESFETs have excess low-frequency noise at frequencies below 10 kHz due to electrons trapping in the semi-insulating substrate. These deep trapped states cause d.c. current fluctuations in the source-drain channel, and hence, introduce noise to the oscillator. The behavior of this type of noise will decrease as $f^{-3/2}$ above 10 kHz [23, 24]. This $f^{-3/2}$ -like noise is the fundamental noise in GaAs field effect transistors. If such a noise source is considered in the VDP equation, the phase of the oscillation in the transistor oscillator



(a)



(b)

Figure 5.10. Power spectra of a self-sustained active antenna at different external modulation frequencies. Center oscillation frequency $\omega_0 = 3.5$ GHz; (a), $\omega_r = 7.5$ MHz; (b), $\omega_r = 11.07$ MHz.

will have a time dependent term, which we call the phase noise of the oscillator. The linewidth of the oscillator is directly proportional to the bandwidth of the phase noise. Therefore, if the external modulation frequency ω_f is less than the linewidth of the oscillator, the result of the external modulation in the bias line will only broaden the linewidth of the VDP oscillator, and the multiple spectra can not be resolved from the measurement (shown in Figure 5.11). It is necessary that the modulation frequency of ω_f be larger than the linewidth for the proposed measurement.

5.5 Summary

We have shown that the transistor oscillator can be described by the VDP oscillator equation. It has been demonstrated that the VDP parameters are related to the large signal circuit parameters of an oscillator. By applying an external modulated signal to the bias voltage of a transistor oscillator, a simple approach to determine VDP parameters from the experiments has been developed. Analysis of the motion of a modulated oscillator indicates that the magnitude of the spectral sidebands of the oscillator are strongly dependent on the VDP parameters. An analytical expression to determine both of the VDP parameters from the experiment are given. Results of the experiment agree with the theoretical prediction, which further justifies the theory. The procedure can be summarized as follows: Step 1, the power spectrum of an oscillator under normal bias voltages is measured. By measuring the amplitude of the oscillation, the parameter γ can be calculated from Eq. (14). Step 2, a sinusoidal modulated signal is added to one of the bias voltages of the oscillator. By measuring

the amplitude of the main oscillation frequency and the first sideband, parameter of ϵ can be extracted from the formula provided in Eq. (32). Comparing the amplitude of the main oscillation frequency in step 2 with the one in step 1, the effect of the modulation depth can be calibrated. Notice that this technique is only valid for the oscillator with a single oscillation frequency. The VDP oscillator model has advantages for predicting the dynamic behavior of an oscillator under the influence of external injection signals, and analysis of coupled oscillator arrays. If one needs to use the VDP equation for a transistor oscillator, the presented technique provides an alternative and effective means to determine the VDP parameters experimentally.

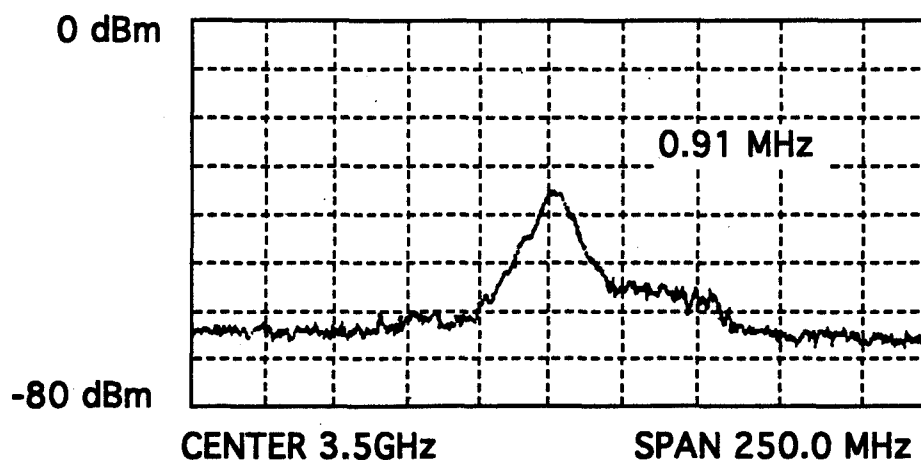


Figure 5.11. Power spectrum of a self-sustained active antenna with external modulation frequency $\omega_f = 0.91$ MHz; which is less than the bandwidth of the phase noise.

References

1. W. R. Curtice, "A MESFET Model for Use in the Design Integrated Circuit," IEEE Tran. Microwave Theory Tech., vol. 28, 1980, pp. 448-456.
2. W. R. Curtice, M. Ettenberg, "A Nonlinear GaAs FET Model for Use in the Design of Output Circuit for Power Amplifiers," IEEE Tran. Microwave Theory Tech., vol. 33, 1985, pp. 1383-1394.
3. W. R. Curtice, "GaAs FET Modeling and Nonlinear CAD," IEEE Tran. Microwave Theory Tech., vol. 36, 1988, pp. 220-230.
4. Y. Hu, J. Obregon and J. Mollier, "Nonlinear Analysis of Microwave FET Oscillators Using Volterra Series," IEEE Tran. Microwave Theory Tech., vol. 37, 1989, pp. 1689-1963.
5. M. Miller, M. Golio, B. Bechwith, E. Arnold, D. Halchin, S. Ageno, and S. Dorn, "Choosing an Optimum Large Signal Model for GaAs MESFETs and HEMTs," IEEE Microwave Theory Tech. Symp. Digest, 1990, pp. 1279-1282.
6. I. Smith, "Dynamic Modeling of Nonlinear Microwave Devices," Electronics Letters, Vol. 25, Aug., 1989, pp. 1237-1239.
7. A. Madjar, "A Fully Analytical A.C. Large-Signal Model of the GaAs MESFET for Nonlinear Network analysis and Design," IEEE Tran. Microwave Theory Tech., vol. 36, 1988, pp. 61-67.
8. H. S. Statz, P. Newman, I. Smith, R. A. Pucel, and H. Haus, "GaAs FET Device and Circuit Simulation in SPICE," IEEE Tran. Electron Devices, vol. 43, 1987 pp. 160-169.
9. J. M. Dorto and J.E. Muller, "Accurate Large-Signal GaAs MESFET Modeling for a Power MMIC Amplifier Design," Microwave J., 1993, pp. 74-84.
10. Van der Pol, B. "Forced Oscillations in a System with Nonlinear Resistance," Phil. Mag., 1927, pp. 65-80.
11. M. Sargent, M.O. Scully, and W.E. Lamb, Jr., "Laser Physics," Addison-Wesely Publishing Company, Inc., 1974.
12. J. J. Stoker, "Nonlinear Vibrations in Mechanical and Electrical Systems," Interscience Publishers, INC., New York, 1950.
13. C. Hayashi, "Nonlinear Oscillations in Physical Systems," McGraw-Hill Book Company, 1964.

14. K. Kurokawa, "Some Basic Characteristics of Broadband Negative Resistance Oscillator Circuits," *Bell Syst. Tech. J.*, vol. 48, 1969, pp. 1937-1955.
15. R. Adler, "A Study of Locking Phenomena in Oscillators," *Proc. IRE*, vol. 34, 1946.
16. R. A. York, "Nonlinear Analysis of Phase Relationship in Quasi-Optical Oscillator Arrays," *IEEE Trans. Microwave Theory Tech. Special Issue on Quasi-Optical Techniques*.
17. J. M. Golio, "Microwave MESFETs and HEMTs," Artech House, Inc. 1991.
18. R. Anholt, "Investigation of GaAs MESFET Equivalent Circuit Using Transient Current-Continuity Equation Solutions," *Solid -State Electronics*, vol. 34, 1991, pp. 693-700.
19. L. J. Sevin, Jr., "Field-Effect Transistors," McGraw-Hill Book Company, 1965.
20. K. Y. Chen, P. D. Biernacki, A. R. Mickelson, Z. B. Popovic, "Optical Measurement of Microwave Grid Oscillator Power Combiners," *IEEE International Microwave Symposium*, June 14-18 1993.
21. A. H. Nayfeh, D.T. Mook, "Nonlinear Oscillations," A Wiley-Interscience Publication, 1979.
22. N. Minorsky, "Nonlinear Oscillations," D.Van Nostrand Company, Inc., 1962. Interscience publishers, Inc., 1950.
23. J. Day, M, Trudeau, P. Maclister and C.M. Hurd, "Instability and Gate Voltage in GaAs Metal-Semiconductor Field-Effect Transistors," *Can. J. Physics*. 67, 1989, pp. 238-241.
24. B. K. Ridley, J. J. Criso, and F. Shishiyanu, "Slow Domains and Negative Resistance via the Enhanced Capture of Transferred Electrons in n Type GaAs," *J. Phys. C; Solid State Phys.*, vol. 5 1972, pp. 187-198.

CHAPTER 6

CONCLUSION AND SUGGESTIONS FOR FUTURE WORK

Various active antennas have been successfully fabricated on GaAs substrates, and the microwave characteristics of the antennas were tested. A non-invasive, in-situ optical sampling technique has been used to obtain the potential distributions on these active antennas. The results of optical sampling reveal some unique characteristics of active antenna arrays. To overcome the uncertainty which arises by noise levels, simulations on a two dimensional active antenna were performed to reconstruct the true potential distribution on the electrode of the antenna. This is important for a meaningful interpretation of the operational state of an active device.

Our measurements clearly indicate that the stability condition of the oscillator is determined from the circuit geometry within each period of the structure. Sampling measurements showed that the form of potential distribution in each elementary cell is similar, and is not effected by the presence of the neighbor cell or the mirror. Furthermore, we found that the actual potential distribution on the electrode had larger fields near the active devices. It is this near field that determines the stability of the active devices. For the first time, single antennas with the same geometry were built and successfully demonstrated the above prediction. It is also shown that the presence of bias lines can alter the relations between the active element and the passive circuit parameter. Replacing the bias lines with shielded wire changes the unstable condition of the active antenna, which then becomes stable.

A linear decay of potential along the radiating lead of the short active antenna was extracted, which was consistent with the distributed conductance that we calculated in the circuit analysis. The potential value on the gate radiating leads was measured at about 5dB lower than the one in the drain leads. This indicates that the active antenna was always excited asymmetrically in both radiating leads.

The results of the phase measurements were informative for understanding the active device. Large phase shifts across the active device (about 180 degrees) were detected from the experiment. This explains the reason why the antenna always resonates at the antenna length much smaller than half the wavelength.

The working mechanism of active antennas with periodic structures evidently can be analogous to the grating surface emitting laser. Like the gain section in the GSEL, the transistor provided the gain for the oscillation. Each elementary cell can be viewed as an individual oscillator, the coherent operation of the array was achieved by the mutual coupling of the radiation field from the near antenna or the mirror. The far-field pattern was determined by the array factor of the antenna array.

To describe a transistor oscillator, the Van der Pol(VDP) oscillator model was adopted in our analysis. A circuit analysis of a single active antenna in the large signal limit was qualitatively described. The calculation was based on the nonlinear interaction between the d.c. drain-source channel current with the amplitude of the a.c. voltage. For our circuit configuration, the calculation shows that the magnitude of the negative impedance decreased as the a.c. voltage increased. As a result, the active antenna can be described by the VDP equation. A new experimental technique

to determine the linear net gain of the VDP oscillator and the underlying theory was developed. This technique was examined by preliminary experiments. The experimental results agree well with the theory. By incorporating this technique, the two VDP parameters can be determined from a simple experimental set-up, using only a spectrum analyzer and a signal generator.

The size of a finite array was found not to effect the oscillation of the active antenna, but it will determine the general performance of the array. An example of this would be in the case of the far-field pattern, locking bandwidth and the degree of coherence of the output beam.

Application of the knowledge we gained from this investigation can be applied to the optimization of the device. Since the antenna array is a coupled oscillator array, the important circuit parameters can be defined from the optimization of a single active antenna. This will simplify the prior expensive and time consuming device fabrication processes.

With the new understanding of an active antenna array, the possibility of self-phase locking for beam steering arrays can be investigated by the VDP coupled oscillators and parameters can be determined experimentally from the procedures developed in chapter 5.

Due to the radiative nature of the antenna and the thin substrate that we used in the experiment, processing of optical sampling results became more laborious and uncertain than we expected. This can be improved in the near future with two procedures. First, the power of a single active antenna can be increased by optimizing

the active element and corresponding geometry. Secondly, the thickness of the substrate can be increased up to the limit that there will be no surface wave excitement inside the substrate. By optimizing the power and increasing the substrate thickness, we should get a better signal and noise ratio in the optical sampling measurement. The process to recover the potential distribution on the electrode can then be calculated directly from the inversion of the equations in chapter 3.

BIBLIOGRAPHY

R. Adler, "A Study of Locking Phenomena in Oscillators," Proc. IRE, vol. 34, 1946.

A. H. Al-Ani, A. L. Cullen and J. R. Forrest, "A Phase-Locking Method for Beam Steering in Active Array Antenna," IEEE Trans. Microwave Theory Tech., vol. 22, pp. 698-703, June, 1974.

A. P. Anderson, W. S. Davies, M. M. Dawond and P. E. Galanakis, "Note on Transistor-Fed Active-Array Antennas," IEEE Trans. on Antennas Propagat., vol. 19, pp. 537-539, July, 1971.

A. P. Anderson and M. M. Dawond, "The Performance of Transistor Fed Monopoles in Active Antennas," IEEE Trans. on Antennas Propagat., vol. 21, pp. 371-374, May, 1973.

R. Anholt, "Investigation of GaAs MESFET Equivalent Circuit Using Transient Current-Continuity Equation Solutions," Solid State Electronics, vol. 34, 1991, pp. 693-700.

J. A. Arnaud, and F. A. Pelow, "Resonant-Gird Quasi-Optical Diplexers," The Bell Sys. Tech. J. pp. 263-283, Feb., 1975.

C. A. Balanis, "Antenna Theory-Analysis and Design," John Wiley & Sons, 1982.

A. Bangert, and M. Ludwig, "A Direct Optical Injection Locked 8-GHz MMIC Oscillator," IEEE MTT-S Int. Microwave Sym. Dig., pp. 499-502, 1992

A. Bangert, J. Rosenzweig, A. Hulsmann, G. Kaufel, K. Kohler, and J. Schneider, "Optical Control of Pseudomorphic HEMT-Based MMIC Oscillators," Microwave and Optical Lett., vol. 6, pp. 36-38, Jan., 1993.

J. Birkeland and T. Itoh, "A 16 Element Quasi-Optical FET Oscillator Power Combining Array with External Injection Locking," IEEE Trans. Microwave Theory Tech., vol. 40, pp. 475-481, March, 1992.

N. Camilleri, and B. Bayraktaroglu, "Monolithic Millimeter-Wave IMPATT Oscillator and Active Antenna," IEEE Trans. Microwave Theory Tech., vol 36, no12, pp. 1670-1676, Dec., 1988.

K. Chang, and C. Sun, "Millimeter-Wave Power Combining Techniques," IEEE Trans. Microwave Theory Tech., vol. 31, pp. 91-107, Feb. 1983.

K. Chang and K. Hummer, J. L. Klein, "Experiments on Injection Locking of Active Antenna Elements for Active Phased Arrays and Spatial Power Combiners," *IEEE Trans. on Microwave Theory Tech.*, vol. 37, pp. 1078-1084, July, 1989.

W. Charczenko, "Coupled Mode Analysis, Fabrication, and Characterization of Microwave Integrated Optical Device," Ph.D. Thesis, University of Colorado at Boulder, see also Guided Wave Optics Lab., report #27, 1990.

K. Y. Chen, P. D. Biernacki, A. R. Mickelson, Z. B. Popovic, "Optical Measurement of Microwave Grid Oscillator Power Combiners," *IEEE International Microwave Symposium*, June 14-18 1993.

W. R. Curtice, "A MESFET Model for Use in the Design Integrated Circuit," *IEEE Tran. Microwave Theory Tech.*, vol. 28, 1980, pp. 448-456.

W. R. Curtice, M. Ettenberg, "A Nonlinear GaAs FET Model for Use in the Design of Output Circuit for Power Amplifiers," *IEEE Tran. Microwave Theory Tech.*, vol. 33, 1985, pp. 1383-1394.

W. R. Curtice, "GaAs FET Modeling and Nonlinear CAD," *IEEE Tran. Microwave Theory Tech.*, vol. 36, 1988, pp. 220-230.

J. P. Daniel, "Mutual Coupling Between Antennas for Emission or Reception--Application to Passive and Active Dipoles," *IEEE Trans. on Antennas Propagat.*, vol. 22, pp. 347-349, March, 1974.

J. P. Daniel and C. Terret, "Mutual Coupling between Antennas--Optimization of Transistor Parameters in Active Antenna Design," *IEEE Trans. on Antennas Propagat.*, vol. 23, pp. 513-516, July, 1975.

M. Dawond and A. P. Anderson, "Calculations Showing the Reduction in the Frequency Dependence of a Two-Element Array Antenna Fed by Microwave Transistors," *IEEE Trans. Antennas Propagat.*, vol. 20, pp. 497-499, (1972).

J. Day, M. Trudeau, P. Maclister and C.M. Hurd, "Instability and Gate Voltage in GaAs Metal-Semiconductor Field-Effect Transistors," *Can. J. Physics*. 67, 1989, pp. 238-241.

J. M. Dorto and J.E. Muller, "Accurate Large-Signal GaAs MESFET Modeling for a Power MMIC Amplifier Design," *Microwave J.*, 1993, pp. 74-84.

This 1928 work is referenced in J. H. Dunlavy and B. C. Reynolds, "Electrically Small Antennas," in 23rd Ann. USAF Antenna Symp., (Oct., 1972).

R. D. Esman, and L. Goldberg, and, J. F. Weller, "Optical Phased Control of an Optically Injection-Locked FET Microwave Oscillator," *IEEE Trans. Microwave Theory Tech.*, vol. 37, pp. 1312-1518, Oct., 1989.

P. L. Fanson and Ku-Mu Chen, "Instabilities and Resonances of Actively and Passively Loaded Antennas," *IEEE Trans. on Antennas Propagat.*, vol. {22}, pp. 342-347, March, 1974.

R. Fralich and J. Litva, "Beam-Steerable Active Array Antenna," *Electron. Lett.*, vol. 28, no.2, pp. 184-185, Jan., 1992

L. Goldberg, C. Rauscher, J. F. Weller, and H. F. Taylor, "Optical Injection Locking of X-Band FET Oscillator Using Coherent Mixing of GaAS Lasers," *Electron. Lett.*, vol. 19, no.20, pp. 848-850, Sept., 1983.

J. M. Golio, "Microwave MESFETs and HEMTs," Artech House, Inc. 1991.

R. C. Hall, R. Mittra, and K. M. Mitzner, "Analysis of Multilayered Periodic Structures Using Generalized Scattering Matrix Theory," *IEEE Trans. Microwave Theory Tech.*, vol. 36, no. 4, pp. 511-517, April, 1988.

C. Hayashi, "Nonlinear Oscillations in Physical Systems," McGraw-Hill Book Company, 1964.

C. H. Henry, R. F. Kazarinov, and R. A. Logan, "Observation of Destructive Interference in the Radiation Loss of the Second-order Distributed Feedback Lasers," *IEEE J. Quantum Electron.*, vol. 21, pp. 151-154, 1985.

D. R. Hjelme and A. R. Mickelson, "Voltage Calibration of the Direct Electrooptic Sampling Technique," *IEEE Trans. on Microwave Theory and Tech.*, vol. 40, pp. 1941-1950, Oct., 1992.

D. R. Hjelme, M. J. Yadlowsky, and A. R. Mickelson, "Two-Dimensional Mapping of Microwave Potential on MMIC's Using Electrooptic Sampling," *IEEE Trans. on Microwave Theory and Tech.*, vol. 41, pp. 1149-1158, June/July, 1993.

Y. Hu, J. Obregon and J. Mollier, "Nonlinear Analysis of Microwave FET Oscillators Using Volterra Series," *IEEE Tran. Microwave Theory Tech.*, vol. 37, 1989, pp. 1689-1693.

R. F. Kazarinov, and C. H. Henry, "Second-order Distributed Feedback Lasers with Modes Section Provided by First-Order Radiation Loss," *IEEE J. Quantum Electron.*, vol. 21, pp. 144-151, 1985.

G. Koepf, "Optical Processor for Phased-Array Antenna Beam Forming," SPIE, vol. 477, Opt. Tech. for Microwave Applications, pp. 75-81, May, 1984.

I. Kontorovich and N. M. Lyapunova, "Active Antennas," Radio Eng. Electron. Phys., vol. 19, pp. 126-127, 1974.

J. D. Kraus, "Antennas," McGraw-Hill Book Company, Second edition, 1988.

K. Kurokawa, "The Single -Cavity Multiple-Device Oscillator," IEEE Trans. Microwave Theory Tech., vol. 19, pp.793-801, Oct., 1971.

K. Kurokawa, "Some Basic Characteristics of Broadband Negative Resistance Oscillator Circuits," Bell Syst. Tech. J., vol. 48, 1969, pp. 1937-1955.

W. W. Lam, C. F. Jou, N. C. Luhmann, Jr., and D. B. Rutledge, "Diode Grids for Electronic Beam Steering and Frequency Multiplication, " Int. J. Infrared and Millimeter Waves, vol. 7, no. 1, pp. 27-41, 1986.

S. W. Lee, and T. T. Fong, "Electromagnetic Wave Scattering from an Active Corrugated Structure," J.Appl. Phys., Vol. 43, pp. 388-396. Fed., 1972.

W. K. Leverich, X. Wu, and K. Chang, "FET Active Slotline Notch Antenna for Quasi-Optical Power Combining," IEEE Trans. on Microwave Theory Tech. vol. 41, Sept. 1993.

S. Liao, "Microwave Device & Circuits", third edition, Prentice Hall, 1990.

M. G. Li, and C. H. Lee, "Intermixing Optical and Microwave Signal in GaAs Microstrip Circuit and Its Applications," Microwave and Optical Tech. Lett. vol.6, pp. 27-32, Jan. 1993.

T. S. M. Maclean and P. A. Ransdale, "Short Active Aerials for Transmission," Int. J. Electron, vol. 36, pp. 261-269, Feb., 1974.

A. Madjar, A. Paolletta, P. R. Herczfeld, " Light Interaction With GaAS-MESFET and Its Applications-A Review," Microwave and Optical Lett., vol. 6, pp. 22-27, Jan., 1993.

A. Madjar, "A Fully Analytical A.C. Large-Signal Model of the GaAs MESFET for Nonlinear Network analysis and Design," IEEE Tran. Microwave Theory Tech., vol. 36, 1988, pp. 61-67.

R. J. Mailoux, P. R. Caron, and F. J. LaRussa, "An Array Phasing Device which Uses Only One Phase Shifter for Each Direction of Scan," *IEEE Tans. on Antenna propagat.* vol. 16, pp. 258-260., March, 1968.

H. H. Meinke, "Active Antennas," *Nachrichtentech. Z.*, vol. 19, pp. 697-705, Dec. 1966.

M. Miller, M. Golio, B. Bechwith, E. Arnold, D. Halchin, S. Ageno, and S. Dorn, "Choosing an Optimum Large Signal Model for GaAs MESFETs and HEMTs," *IEEE Microwave Theory Tech. Symp. Digest*, 1990, pp. 1279-1282.

J. W. Mink, "Quasi-Optics Power Combining of Solid-State Millimeter-Wave Sources," *IEEE Trans. Microwave Theory Tech.*, vol. 34, pp. 273-279, Feb., 1986.

N. Minorsky, "Nonlinear Oscillations," D. Van Nostrand Company, Inc., 1962. Interscience publishers, Inc., 1950.

A. H. Nayfeh, D.T. Mook, "Nonlinear Oscillations," A Wiley-Interscience Publication, 1979.

R. J. Noll, and S. H. Macomber, "Analysis of Grating Surface Emitting lasers," *IEEE J. Quantum Electron.*, vol. 26, pp. 456-466, 1990.

A. Pance, M. J. Wengler, "Microwave Modeling of 2-D Active Grid Antenna Arrays," *IEEE Trans. Microwave Theory Tech.*, vol. 41, Jan. 1993.

Pocklington, "Electrical Oscillation in Wires," *Proceeding of the Cambridge Philosophical Society*, pp. 324-333, 1897.

Van der Pol, B. "Forced Oscillations in a System with Nonlinear Resistance," *Phil. Mag.*, 1927, pp. 65-80.

Z. B. Popovic, M. Kim, D. B. Rutledge, "Grid Oscillator," *Int. J. Infrared and Millimeter Waves*, vol. 9, no. 7, pp. 647-654, 1988.

Z. B. Popovic, R. M. Weikle, II, M. Kim, and D. B. Rutledge, "A 100-MESFET Planar Grid Oscillator," *IEEE Trans. Microwave Theory Tech.*, vol. 39, pp. 1930-200. Feb., 1991.

P. K. Rangole and S. S. Midha, "Short Antenna with Active Inductance," *Elec. Lett.*, vol. 10, pp. 462-463, Oct., 1974.

J. E. Raue, "Power Amplification at 55-65 GHz with 18 GHz Gain-bandwidth Product," *Proceedings of IEEE G-MTT International Microwave Sym.* pp. 60-62, 1973.

D. B. Rutledge, S. E. Schwarz, "Planar-Multimode Detector Array for Infrared and Millimeter-Wave Applications," *IEEE J. of Quantum Electronics* vol. 17, pp. 407-414, March, 1981.

V. Radisic, D. Hjelme, A. Horrigan, Z. Popovic and A. R. Mickelson, "Experimentally Verifiable Modeling of Coplanar Waveguide Discontinuities," *IEEE Trans. on Microwave Theory and Tech.*, vol. 41, pp. 1524-1533, Sept., 1993.

B. K. Ridley, J. J. Criso, and F. Shishiyanu, "Slow Domains and Negative Resistance via the Enhanced Capture of Transferred Electrons in n Type GaAs," *J. Phys. C; Solid State Phys.*, vol. 5 1972, pp. 187-198.

A. De Salles and J. R. Forrest, "Initial Observation of Optical Injection Locking of GaAs Metal Semiconductor Field Effect Transistor Oscillators," *Appl. Phys., lett.*, vol. 38, pp. 392-3944, 1981.

M. Sargent, M.O. Scully, and W.E. Lamb, Jr., "Laser Physics," Addison-Wesely Publishing Company, Inc., 1974.

P. S. Sarma, and S. Venkateswaran," Simulated Inductance with A Transistor and R. C. Elements," *Electronics letters*, vol. 5 No. 26, Dec. 1969.

L. J. Sevin, Jr., "Field-Effect Transistors," McGraw-Hill Book Company, 1965.

H. Shigesawa, and M. Tsuji, "A Completely Theoretical Design Method of Dielectric Image Guide Grating in the Bragg Reflection Region," *IEEE Trans. Microwave Theory Tech.*, vol. 34, pp. 420-426, April, 1986.

I. Smith, "Dynamic Modeling of Nonlinear Microwave Devices," *Electronics Letters*, Vol. 25, Aug., 1989, pp. 1237-1239.

R. Smyth, "Static and Dynamic Electricity," Hemisphere Publishing, New York 1989.

I. Stakgold, "Boundary Value Problems of Mathematical Physics," vol. 1 and 2, The Macmillan Company, London, 1972.

H. S. Statz, P. Newman, I. Smith, R. A. Pucel, and H. Haus, "GaAS FET Device and Circuit Simulation in SPICE," *IEEE Tran. Electron Devices*, vol. 43, 1987 pp. 160-169.

J. J. Stoker, "Nonlinear Vibrations in Mechanical and Electrical Systems," Interscience Publishers, INC., New York, 1950.

W. Streifer, R. D. Burnham, and D. R. Scifres, "Analysis of Grating Coupled Radiation on GaAs:GaAlAs Lasers and Waveguides," *IEEE J. Quantum Electron.*, vol. 12, pp. 422-428, 1976.

W. Streifer, D. R. Scifres, and R. D. Burnham, "Analysis of Grating Coupled Radiation on GaAs:GaAlAs Lasers and Waveguides-Part II," *IEEE J. Quantum Electron.*, vol. 12, pp. 494-499, 1976.

D. J. Sturzebecher, X. Zhou, X. S. Zhang, and A. S. Daryoush, "Optically Controlled Oscillators for Millimeter-Wave Phased-Array Antennas." *IEEE Trans. Microwave Theory Tech.*, vol. 41, pp. 998-1003, June/July, 1993.

H. J. Sun, R. J. Gutmann, and J. M. Borrego, "Optical Tuning in GaAs MESFET Oscillators," *MTT-S Int. Microwave Sym. Dig.*, PP. 40-42, 1981.

S. Tiwari, "Compound Semiconductor Device Physics," Library of Congress cataloging-In-Publication Data, 1992.

E. M. Turner, "Subminiature Integrated Antenna," *Proc. 18th Ann. Conf. IEEE Veh. Group*, Dec. 1967.

R. M. Weikle, "Quasi-Optical Planar Grids for Microwave and Millimeter-wave Power-Combining," Ph. D. dissertation, CALTE, Pasadena, 1991.

H. A. Wheeler, "Small Antenna," *IEEE Trans. on Antenna and Propagat.*, vol. 23, pp. 462-469, (1975).

W. C. Wong, "Single and Noise Analysis of a Loop-Monopole Active Antenna," *IEEE Trans. on Antennas Propagat.*, pp. 574-632, July, 1974

R. A. York and R. C. Compton, "Quasi-Optical Power Combining Using Mutually Synchronized Oscillator Arrays," *IEEE Trans. Microwave Theory Tech.*, vol. 39, pp.1000-1009, June, 1991.

R. A. York, "Nonlinear Analysis of Phase Relationship in Quasi-Optical Oscillator Arrays," *IEEE Trans. Microwave Theory Tech. Special Issue on Quasi-Optical Techniques.*